DOE/ET/13323--2

MASTER

Catalytica
ASSOCIATES, INC.

DISCLAIMER

Master

DISTILLATE FUEL-OIL PROCESSING FOR PHOSPHORIC ACID FUEL-CELL POWER PLANTS

Submitted to

Department of Energy
Germantown, MD 20545

Contract No. EC-77-C-03-1384

Prepared by

CATALYTICA ASSOCIATES, INC.
3255 Scott Blvd., Suite 7-E
Santa Clara, CA 95051

Principal Investigator
Ken K. Ushiba

Catalytica File No. 1036
February, 1980

THIS PAGE

WAS INTENTIONALLY

LEFT BLANK

TABLE OF CONTENTS

TABLE OF CONTENTS (cont)

1. INTRODUCTION

This is a continuation of Catalytica's effort to assess various synthesis-gas generating technologies for their applicability to fuel-cell power generation. In a preceding report, we covered a broad spectrum of syngas technologies ranging from naphtha steam reforming to residual oil and coal gasification processes (*Catalytica*, 1978). In this report, we have focused on syngas generation from distillate fuel oil and reviewed the status and the research and development needs of those emerging technologies which are potentially applicable to fuel cells.

Electric power generation by a phosphoric acid fuel cell integrated with a naphtha reformer has reached the demonstration stage with the 4.8-MW unit soon to be completed at Consolidated Edison's plant in New York (Handley, 1979). The naphtha-based plant is expected to achieve a heat rate of 9300 Btu/kwh or better through its 40,000 hours of service. In the meantime, efforts are continuing in order to improve various aspects of the fuel-cell power plant.

One of the current efforts is to expand the fuel processor's capability to process distillate fuels as efficiently as the naphtha reformer. At present, no commercial process is capable of reforming distillate fuels into synthesis gas. However, a number of companies are engaged in the development of such processes, and these processes are discussed in this report.

Case studies of a phosphoric acid fuel-cell power plant based on distillate fuel are presented. In one case, an autothermal reformer is featured as the fuel processor while in the other case, a combination of a high-temperature steam reformer and an autothermal reformer is featured. The objective of the study is to estimate the range of heat rates obtainable when the autothermal reformer or the high-temperature steam reformer is integrated in the power plant.

The phosphoric acid fuel cell tolerates certain levels of H_2S and CO which are common contaminants in the synthesis gas generated from distillate fuel. Efforts are made to examine how much of these gases can be tolerated by the cell. Since the information has an important bearing on the extent of syngas cleaning required, the pertinent test results are reviewed in this report.

It is recognized that key problems confronting the development of the distillate process are catalyst deactivation by sulfur and carbon formation. A literature review presented in the appendix covers recent studies addressing these critical areas of steam reforming. The review was made by Professor Calvin H. Bartholomew of Brigham Young University.

2. SUMMARY

This report reviews the current efforts to develop distillate oil-steam reforming processes and discusses the applicability of these processes for integration with the fuel cell. The development efforts can be grouped into the following processing approaches:

- High-temperature steam reforming (HTSR)
- Autothermal reforming (ATR)
- Autothermal gasification (AG)
- Ultra desulfurization followed by steam reforming

Sulfur in the feed is a key problem in the process development. A majority of the developers consider sulfur as an unavoidable contaminant of distillate fuel and are aiming to cope with it by making the process sulfur-tolerant. Average sulfur in commercial distillate fuel is in a 0.15-0.25 wt % range.

In the HTSR development, the calcium aluminate catalyst developed by Toyo Engineering represents the state of the art. This catalyst is unaffected by sulfur but becomes active only at higher than normal reforming temperatures, e.g., above 900°C. This is an economic concern since a greater amount of fuel is required by the furnace as the reforming temperature is increased. United Technology (UTC), Engelhard, and Jet Propulsion Laboratory (JPL) are also involved in the HTSR research.

The ATR of distillate fuel is investigated by UTC and JPL. Soot formation is a major problem as it causes reactor plugging. It can form in the feed preheater where fuel is heated to about 1400°F and in the catalyst bed. Soot in the preheater is formed as a result of thermal cracking and can be minimized by reducing the residence time of hydrocarbons. For example, JPL noted a major decline in thermal cracking when the residence time was reduced from 6.6 to 2.5 milliseconds. In the reactor, there is always a potential of carbon

formation as the ATR is operated under fuel-rich conditions (low O_2/C rates). Therefore, an ATR catalyst must be able to gasify carbon as soon as it is formed. Furthermore, the catalyst must maintain the gasification activity in the presence of sulfur. Thus far, the lowest O_2/C ratios achieved in the ATR of distillate fuel oil are in a range of 0.38 to 0.40 mole of O_2 per atom of carbon in the feed. An immediate goal of current research is to lower this ratio to about 0.35 mole O_2/atom C so that the thermal efficiency approaches that of conventional steam reforming.

The autothermal gasification (AG) of distillate fuel is being investigated by Engelhard and Siemens AG. As in the ATR, the fuel is catalytically gasified utilizing the heat generated by *in situ* partial combustion of feed, however, the goal of the AG is to accomplish the initial breakdown of the feed into light gases and not to achieve complete conversion to CO and H_2. Engelhard's test results indicate that a soot-free gasification of distillate fuel can be accomplished with the O_2/C ratios as low as 0.3 mole O_2/atom C and gas space velocities in a 100,000 hr^{-1} range. Monolithic catalysts containing Rh, Pt, and Pd showed good activities. For the fuel-cell integration, a secondary reforming of the light gases from the AG step is required. Engelhard is currently testing a system in which the effluent from the AG section enters the steam-reforming section, all housed in a single vessel.

The AG process by Siemens employs a nonnoble metal catalyst which is sulfur-resistant. The process can gasify distillate fuels using surprisingly low O_2/C ratios. In a series of tests, Siemens gasified a diesel fuel at an O_2/C ratio of 0.125 mole/atom. They indicate that the space velocity in this test was about 12 times larger than that used in conventional steam reforming. There was no sign of soot formation; however, the gasification conversion was about 61%, and the gaseous effluent contained high concentrations of light olefins.

Unlike the majority of the developers, Topsøe uses a feed pretreatment approach and has shown that when the level of sulfur is reduced to below 0.1 ppm, a distillate fuel oil can be steam-reformed at conditions very similar to those for naphtha reforming. The reduction in sulfur content is achieved in a two-stage hydrotreatment.

To evaluate the thermal efficiencies of a 5-MW dispersed fuel-cell power plant, we conducted case studies that feature as the fuel processor an ATR in one case and an HTSR combined with an ATR unit in the other case. No. 2 fuel oil was used as the only energy source for the power plant. In the case based on the use of the ATR unit alone, the heat rate of the power plant was evaluated with respect to air-to-fuel ratios and methane leakages in the ATR effluent. The feed preheating was assumed at 1400°F. The results for a 5-MW plant are shown below:

O_2/C ratio, moles O_2/atom C	CH_4 in ATR Exit lb-moles/hr	vol%	Heat rate, Btu/kwh
0.35	3.48	0.33	9,513
	2.48	0.24	9,410
	1.48	0.14	9,300
	0.48	0.05	9,200
0.30	3.34	0.34	9,100
	2.34	0.24	9,000

The O_2/C ratio of 0.35 mole/atom represents an immediate goal of the research efforts. At this ratio, the power plant may achieve a heat rate of about 9500 Btu/kwh or better, depending on how far the ATR catalyst can reform the residual methane. If the O_2/C ratio can be reduced to 0.30, a 9000-Btu/kwh heat rate becomes possible.

In the case with HTSR/ATR, the reforming temperature in the HTSR was assumed at 820°C, and a thermal efficiency of 71% was assumed for the reformer furnace. In the ATR, an O_2/C ratio of 0.18 mole O_2/atom C was estimated to be sufficient to reform methane in the HTSR effluent. A heat rate of 8930 Btu/kwh has been estimated for this power plant. The residual methane in the ATR effluent was assumed as 1.70 lb mole/hr (0.21 vol%).

3. REVIEW OF TECHNOLOGIES

At present no commercial processes are capable of steam-reforming distillate or heavier fuels. However, a number of companies are engaged in the development of such a process. In this section, the status of these development efforts is summarized. Among the active companies are:

- Toyo Engineering (Japan)
- United Technology Corp. (U.S.)
- Jet Propulsion Laboratory (U.S.)
- Engelhard (U.S.)
- Haldar Topsøe (Denmark)
- Siemens AG (Germany)
- Mitsui Toatsu (Japan)
- Others

3.1 Toyo Engineering

The Total Hydrocarbon Reforming (THR) process, a high-temperature steam-reforming process being developed by Toyo Engineering, is capable of gasifying a wide range of hydrocarbons, including crude oil, atmospheric and vacuum residues, gas oils, naphtha, LPG, and natural gas. The principal catalyst, called T-12, is a calcium aluminate consisting of CaO, 51 wt%; Al_2O_3, 48 wt%; SiO_2 less than 0.1 wt%; and FeO_3, MgO, Na_2O for the balance (Tomita, 1979). Among the various chemical species possible in a $CaO \cdot Al_2O_3$ solid system, the most desirable species for use as a catalyst is $12CaO \cdot 7Al_2O_3$. Other possible solid phases include $CaO \cdot Al_2O_3$ and $3CaO \cdot Al_2O_3$. Compared with these, $12CaO \cdot 7Al_2O_3$ possesses superior properties as a catalyst, namely, good steam reforming activity, resistance to carbon deposition, and high mechanical strength (Yoshida, 1977).

To supplement the moderate steam-reforming activity of the T-12 catalyst, Toyo also developed a high-temperature reforming catalyst called T-48, which consists of Ni, CaO, and Al_2O_3. The CaO loading is smaller than in the T-12, but much greater than in the conventional Ni-based catalyst. It is claimed that the high CaO loadings minimize spinel formation between Ni and Al_2O_3. It apparently also minimizes carbon formation (*Catalytica*, 1977). In the THR process, the T-48 catalyst bed is situated downstream of the T-12 bed and completes the reforming of the residual light hydrocarbons in the effluent of the T-12 section. Despite the presence of Ni, T-48 is apparently sulfur-tolerant because it is operated at high temperatures, usually above 900°C (1650°F), and in the presence of substantial amounts of hydrogen.

Table 3-1 lists the properties of T-12 and T-48. Toyo is developing three types of THR for syngas generation. These are described in Table 3-2. Toyo indicates that a distillate oil can be completely gasified without carbon formation by the THR-HD process. The THR-R process with a special feed atomization provision can also gasify residual oils containing sulfur and heavy metals. However, the residual oil gasification results in the formation of soot, 3-5 wt%, which passes through the catalyst bed. Toyo notes that heavy metals in the feed are found in the soot and do not plug the reactor (Tomita, 1979).

For fuel-cell applications, the THR-HD version is pertinent. In fact, Toyo is currently conducting a series of tests for EPRI to identify suitable operating conditions for gasifying No. 2 fuel oil. Preceding these tests, Catalytica Associates and Kinetics Technology International evaluated the Toyo THR-HD as integrated in a 5-MW acid fuel-cell power plant (Tio/Ushiba, 1979). The study included calculation of heat and mass balances for the integrated power plant, equipment sizing, and capital and operating cost estimates. The major findings of this study are presented later in this report. Table 3-3 lists the THR-HD test data (bench scale), that served as the design basis in the study. It is clear from the listed product gas composition that THR-HD cannot complete the steam-reforming of a gas oil at temperatures below, say

TABLE 3-1

CATALYSTS FOR THR PROCESS

	T-12		T-48	
	Cylinder	Raschig Ring	Cylinder	Raschig Ring
Crushing strength (kg/cm^2)	200	400	150	300
Water absorption (vol%)	50		55	
Particle density (g/cm^3)	4		4.6	
Bulk density (g/cm^3)	1.3		1.4	
Chemical species	$Ca_{12}Al_{14}O_{33}$ $Ca_3 Al_2 O_6$		---	

Source: (Tio/Ushiba, 1979)

TABLE 3-2

THR Process Types

Feedstock	Type	Developmental Status
Natural gas-naphtha	THR-LH	Basic research completed Semipilot tests underway
Kerosene, gas oil Vacuum gas oil Cracked oil	THR-HD	Basic research completed Semipilot tests underway
Crude oil, atom. residue Vacuum residue	THR-R	Pilot test completed

Source: (Tio/Ushiba, 1979)

TABLE 3-3

EXPERIMENTAL DATA OF GAS OIL REFORMING - THR-HD

1) Gas Oil Specification

C/H	6.19
Sulfur	0.5 wt %
Specific gravity	0.835 (15/4°C)
Distillation	
IBP	220°C
50 vol %	282°C
EP	340°C

2) Reforming Data

Temperature (°C)	950	900	850	900*
Pressure	Ordinary	Ordinary	Ordinary	Ordinary
S/C (moles/atom)	2.99	2.99	2.99	3.04
Composition				
H_2 (vol %)	64.89	63.50	59.24	68.91
CO	21.16	19.08	17.00	19.10
CO_2	9.46	11.69	13.88	10.96
CH_4	4.41	5.29	6.46	0.96
C_2H_4	-----	0.36	3.01	-----
C_3H_6	-----	-----	0.31	-----
H_2S	0.08	0.08	0.10	0.07

*Low Space Velocity Reforming.

Source: Toyo Engineering.

900°C (1652°F). For example, the approaches to methane reforming equilibrium for the four cases in Table 3-3 have been estimated to be:

	Approach to Methane Reforming Equilibrium			
Temperature (°C)	950	900	850	900 (low SV)
ΔT, Equil. approach (°C)	326	293	282	215

In the above, some improvement is noted for the low-space-velocity case. Still, these approach temperatures are an order of magnitude greater than the usual 25-50°C approaches available in conventional naphtha reforming.

3.2 United Technology Corporation

UTC is well known for its naphtha reformer specifically developed for use in fuel-cell power plants. This reformer is the heart of the 4.8-MW fuel cell unit soon to be demonstrated in New York City. UTC is also developing distillate fuel reforming technology, both high-temperature steam reforming and autothermal reforming (Houghtby et al., 1978).

3.2.1 UTC Naphtha Reformer

The UTC naphtha reformer has high thermal efficiency, fast load-following capability, routine shutdown and cold start capability, etc., which are features not found in conventional reformers. With some innovative modifications, these unique features may be applicable to distillate reforming. The UTC reformer has been disclosed by several patents (U.S. 4,071,330, 4,098,587, 4,098,588, 4,098,589).

Figure 3-1 describes the flow patterns around a given reformer tube in the New York demonstration unit. The catalyst is loaded in the outer of the two

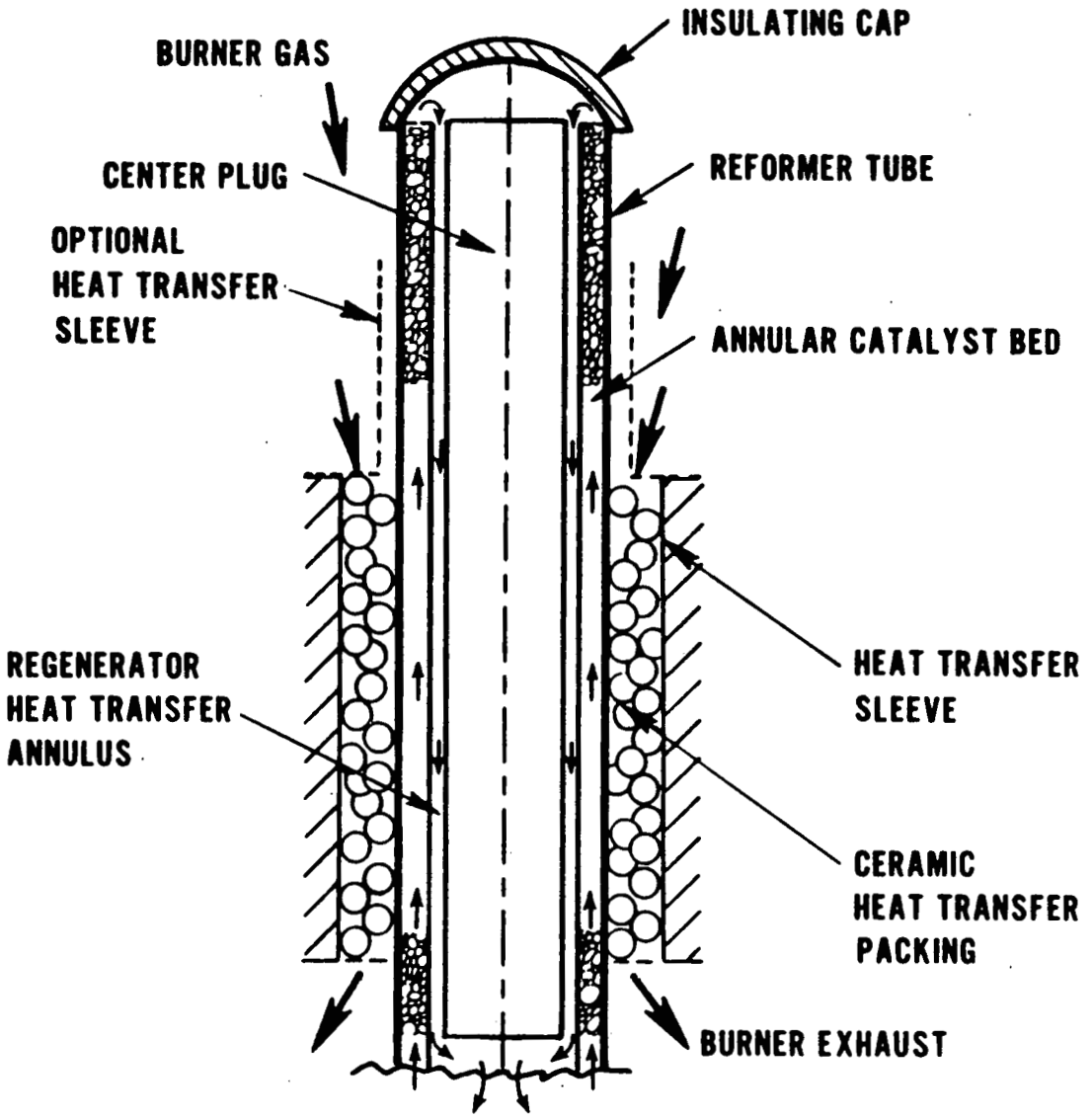

Fig. 3-1. 4.8-MW reformer tube (Olesen and Sederquist, 1979).

annular spaces created by three concentric tubes. The inner space serves as the passageway for hot product gases. The main function of the innermost tube, which is closed at both ends, is to support the tubular assembly and to maintain the annular dimensions. Hydrocarbon feed enters at the base of the tube structure and rises through the catalyst bed. The catalyst section is heated by flue gas travelling countercurrently and outside of the tube. Hot reformed gases emerge at the top of the catalyst space and are immediately directed downward through the annular space just inside the catalyst bed. In this manner, waste heat in the product gases is transferred across the tube wall and utilized in the reforming zone. The compactness of the unit and the effective use of heat energy are the two outstanding features of the UTC reformer. Furthermore, the tube bundle is encased in a sealed vessel which, in the case of the New York unit, is pressurized to 50 psia (Olesen and Sederquist, 1979). This enhances the compactness and the thermal efficiency.

The New York demonstration unit (Fig. 3-2), which contains 37 tubes in a single vessel 112 in. in diameter and 138 in. tall, generates about 3.0 million scf/d of H_2. The reformer tubes operate at an inlet bed pressure of 80 psia and exit bed pressure of 66 psia with an external burner pressure of 50 psia (Olesen and Sederquist, 1979).

In tests, UTC carried out 72 cycles of full operation – shutdown – cooling to room temperature – cold start to full operating. They reported no mechanical damage nor any evidence of catalyst deactivation (Olesen and Sederquist, 1979). In the New York demonstration unit, the reformer is fired with the fuel-cell purge gas. Thus, an increase in power demand increases the feed rate, which in turn produces a proportionate increase in the volume of purge gas to the furnace as the fuel cell is controlled to consume a constant percentage of hydrogen in the anode feed. It is reported that the residence time in the combined fuel-processing and fuel-cell system is only about 5 sec. This accounts for the extremely quick response of the UTC naphtha reformer. In the hot standby mode of operation, feed is required at about 15% of full load. This is primarily to maintain the turbocompressor at an acceptable speed and ΔP. From this standby mode, the unit can achieve full output within 15 sec (Sederquist, 1978).

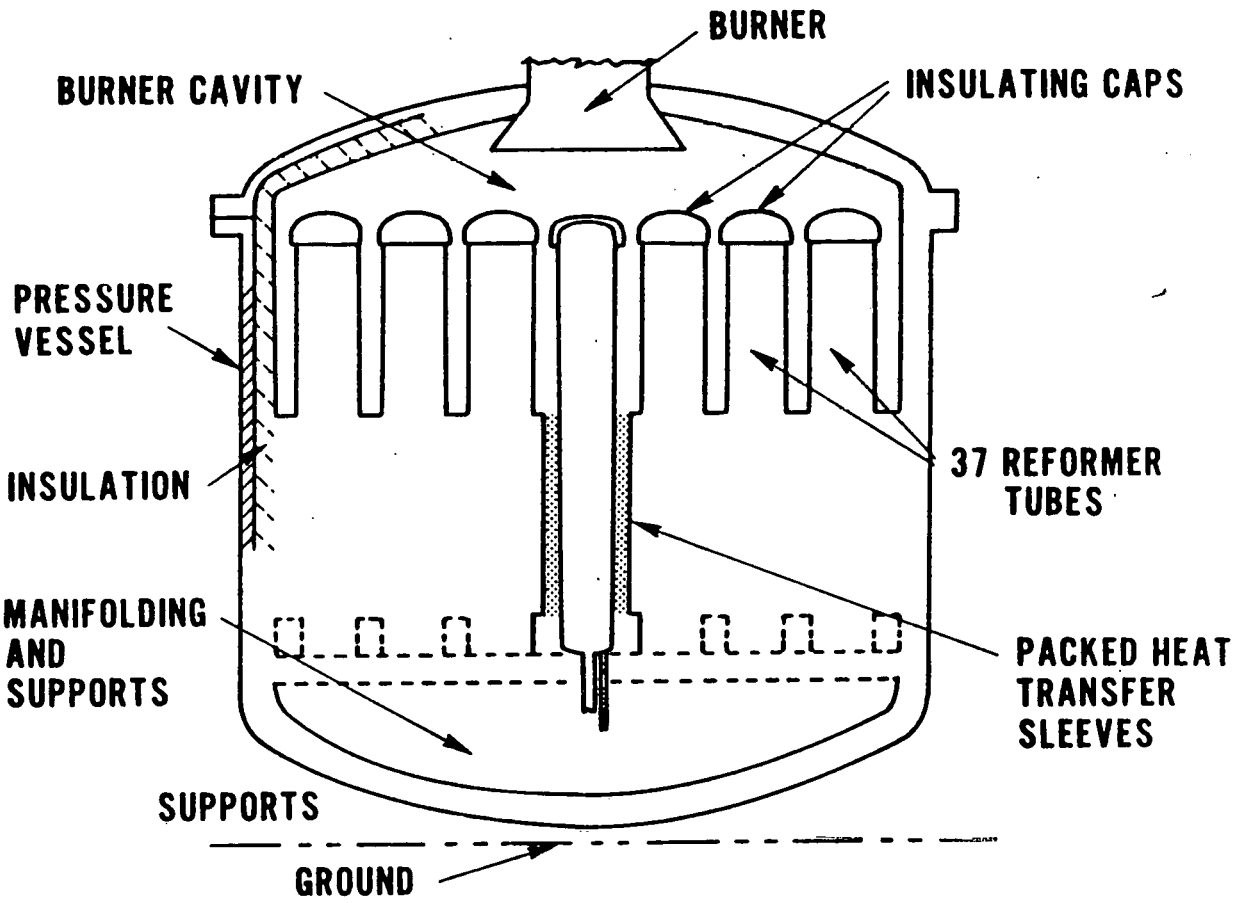

Fig. 3-2. 4.8-MW reformer assembly (Olesen and Sederquist, 1979).

3.2.2 Autothermal Reforming of Distillate

In its work on autothermal reforming (ATR) of distillate fuel (Houghtby et al., 1978; Bett, 1978, 1979), UTC has found that soot formation is the most critical factor limiting the thermal efficiency of this mode of steam reforming. To operate soot-free, an excess of feed must be combusted; the amount of excess depends on several key design variables, including the catalyst, preheating temperature, feed mixer design, and steam-to-carbon ratio. Figure 3-3 shows the soot-forming characteristics of a UTC bench-scale unit. In this correlation, the extent of carbon formation is expressed in terms of ΔP across the reactor as the O_2/C ratio is varied. Feed preheating was set at a constant temperature. The plot shows that a less than 10% change in the air feed rate can cause sufficient precipitation of soot to double the reactor pressure-drop.

Currently, the ATR development at UTC is centered around reducing the O_2/C ratio. As shown in Fig. 3-4, UTC has achieved the value of 0.4 mole/atom. This may be further reduced by the combination of a better reactor design and a higher preheating temperature. UTC has set target values as:

O_2/C	0.35 mole/atom
Preheating	1400°F (760°C)

A higher preheating temperature would be desirable, but distillate fuel at temperatures approaching 1400°F is very unstable. This requires that the heating be done very quickly with a precisely controlled heat flux.

3.2.3 High-Temperature Steam-Reforming of Distillate Fuel

UTC has tested steam-reforming of a No. 2 fuel oil desulfurized to 100-200 ppm S. In one series of tests, the feed was reformed at temperatures of 1500°F to 1800°F, a WHSV of 0.4 lb/lb-hr, and an H_2O/C ratio of 5 mole/atom. In the best endurance run, a 99.9% hydrocarbon conversion was maintained for 410 hr with only 50 ppm methane in the effluent. However, a steady accumulation of soot was

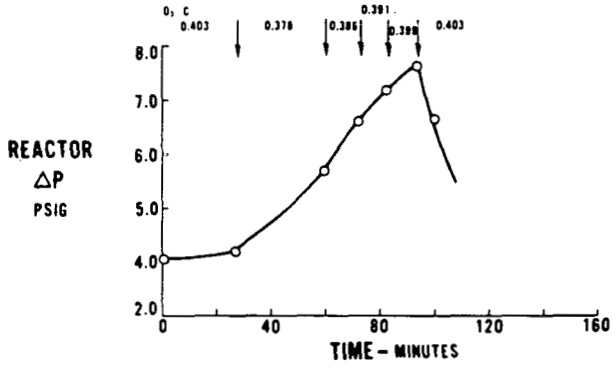

Fig. 3-3. Adiabatic reformer locating the carbon boundary (Bett, 1979).

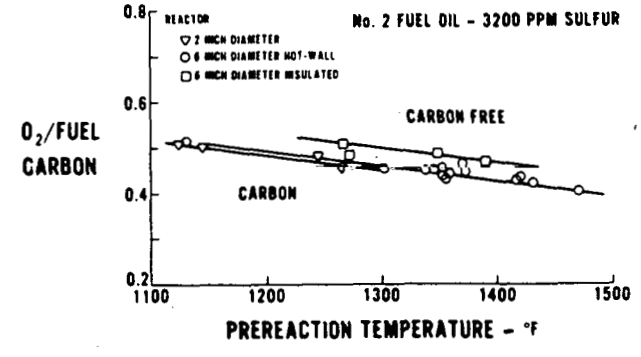

Fig. 3-4. Operating line for various reactors with similar mixer configuration (Bett, 1979).

revealed in terms of pressure-drop increases (King, 1977). Carbon formation within the pores of the catalyst caused the catalyst to powder (Houghtby et al., 1978).

In high-temperature reforming tests (1900°F), on the same desulfurized No. 2 oil and the same WHSV and H_2O/C ratio, UTC found no catalyst powdering, but the soot that formed in the preheating zone plugged the inlet to the catalyst bed. Subsequently, however, a trap was installed ahead of the catalyst bed, and carbon-free reforming was maintained for 190 hr. Later attempts to repeat this performance have failed. UTC attributes the failure to inconsistencies in feed mixing (Houghtby, 1978).

3.3 Jet Propulsion Laboratory

For autothermal reforming of a No. 2 oil, JPL has constructed a 3-3/4-in. i.d. stainless steel reactor as shown in Fig. 3-5. JPL found that successful gasification is dependent on achieving a high feed preheating in less than 10 ms (Houseman, 1979). To accomplish this, vaporized fuel at 700°F is injected into a mixture of air and steam which is preheated to above 1400°F. Before entering the catalyst bed, the three components are mixed as they flow through a zone packed with helical coils. JPL achieved feed mixing within 3-7 ms.

For the ATR of a No. 2 oil containing 0.35 wt% sulfur and 22 vol% aromatics, JPL achieved a minimum O_2/C ratio of 0.40 mole/atom (Houseman, 1979). The preheat temperature was 1400°F and H_2O/C ratio was 3.0 moles/atom. For this run, JPL used three commercial catalysts packed as shown in Fig. 3-6. Approximate compositions of these catalysts are:

Norton	NC-100:	1/2-in. sphere, 5-6% Ni on zirconia
ICI	46-1:	11/16-in. o.d. x 5/16-in. long hollow cyl., 17% Ni, 7% K_2O, 7% Mg, 7.9% Ca on silica alumina
Girdler	G56B:	1/8-in. x 1/8-in. tablets, 24% Ni on silica-free alumina

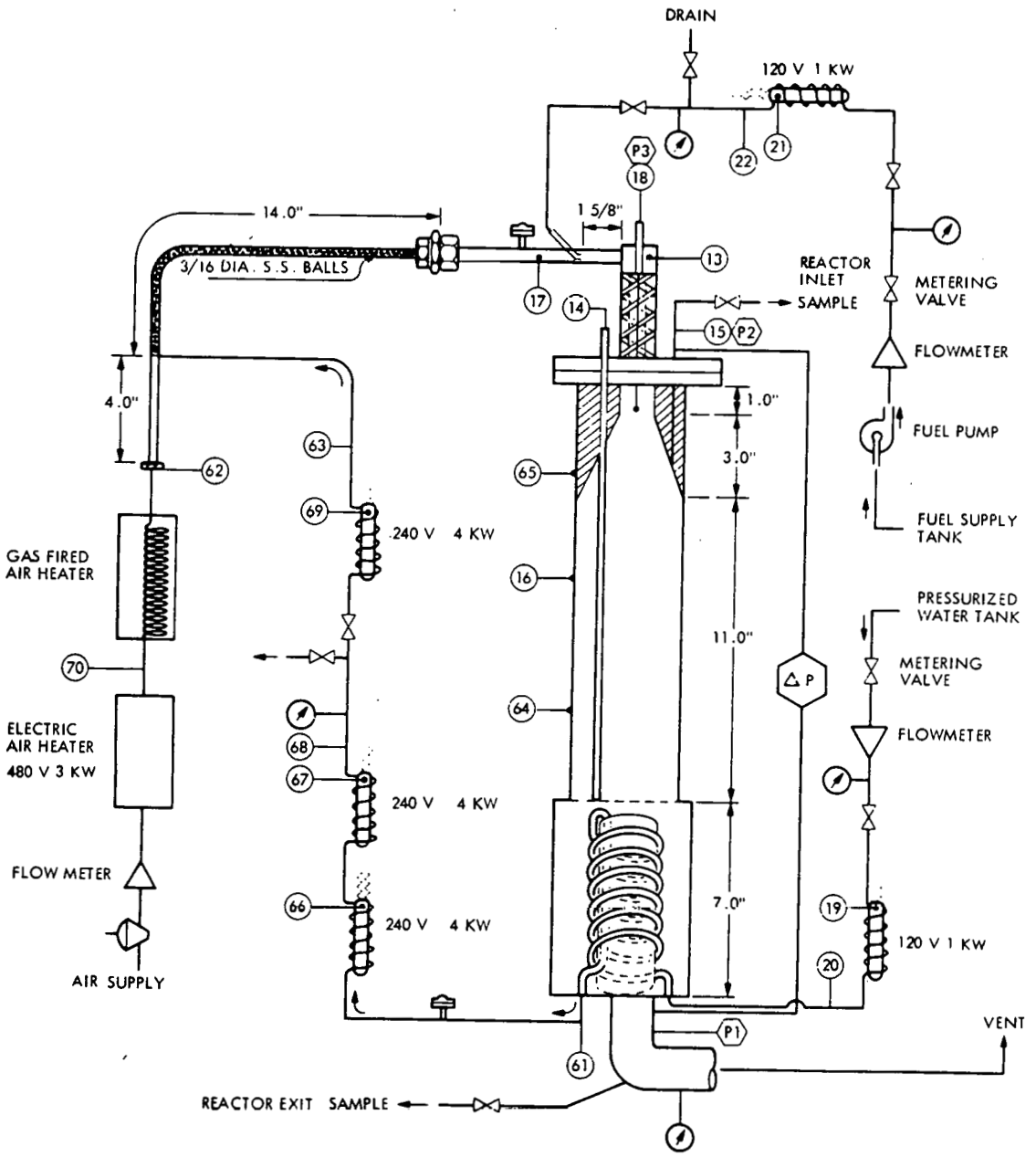

Fig. 3-5. Schematic of JPL catalytic partial oxidation reactor A (Houseman, 1979).

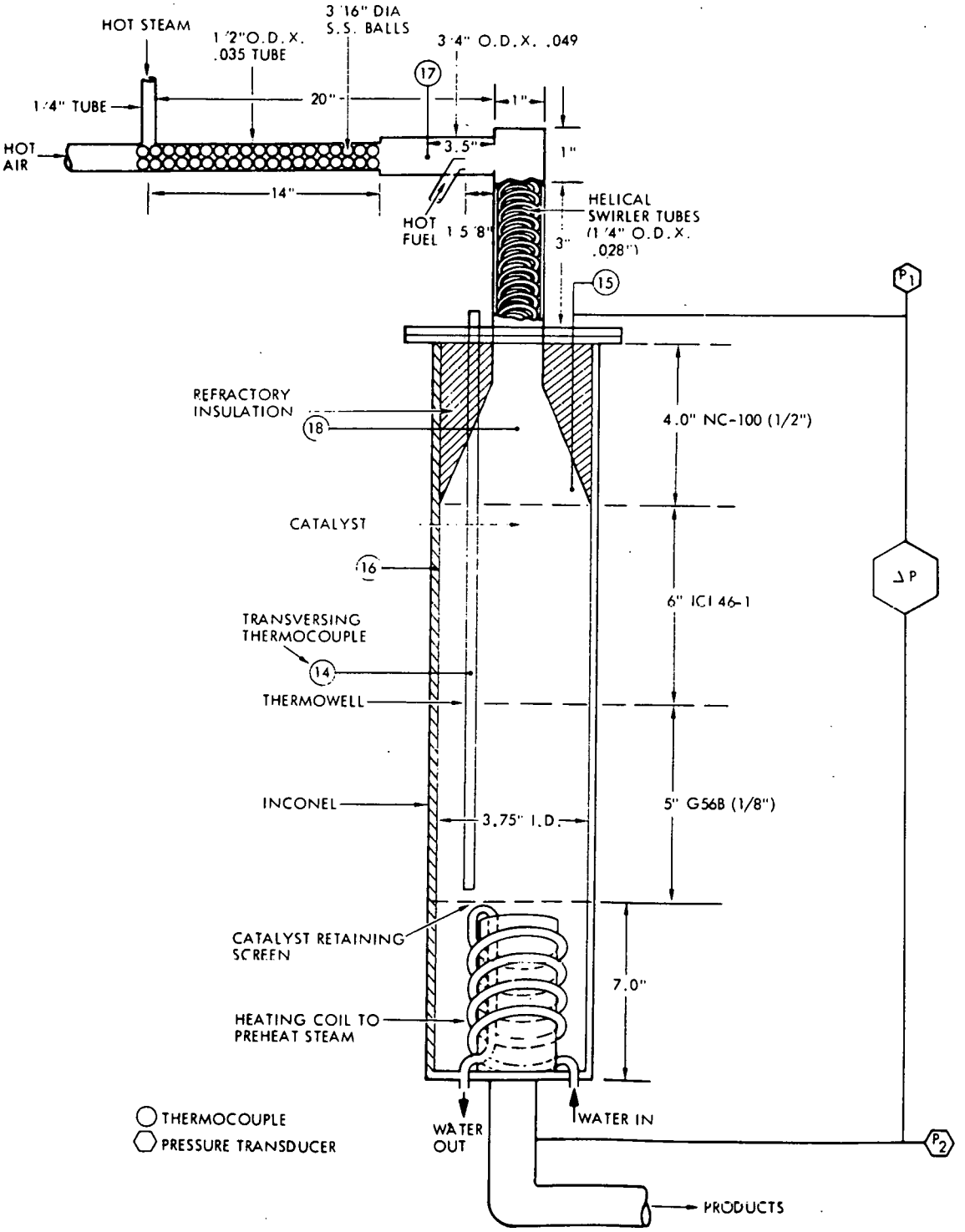

Fig. 3-6. Schematic of JPL catalytic partial oxidation reactor B (Houseman, 1979).

In one comparative test, JPL examined the extent of thermal cracking occurring in two preheaters having different residence time (Houseman, 1979). The results are shown below:

Preheater design	Residence time, ms	Preheater exit, dry vol%			
		H_2	CO	CO_2	HC gases
A	6.6	2.58	8.12	6.55	13.01
B	2.5	0.99	3.22	3.19	1.72

O_2 / C = 0.40 mole/atom, H_2O/C = 3.0, GHSV = 7000 hr^{-1}
T(air + steam) - 1520°F

The preheater A represents an older design having a longer residence time, while B is an improved version in which the hydrocarbon preheating space has been reduced to about 38% of A. In both tests, thermal cracking is noted but to a much greater extent in A. JPL noted no soot formation in both tests. They did not compare these two designs under soot-forming conditions; therefore, it is difficult to assess the impact on soot-forming tendency of one design over the other.

3.4 Engelhard Industries and Siemens AG

Under DOE funding, Engelhard has been investigating two types of catalytic syngas generation from No. 2 fuel oil (Yarrington, 1979):

- Hydrogen-assisted steam reforming
- Catalytic partial oxidation (autothermal gasification)

In hydrogen-assisted reforming, recycle H_2 is mixed with hydrocarbon feed and steam. The objective here is to reduce the poisoning effect of sulfur by having a sufficient hydrogen partial pressure at the inlet to the reformer catalyst bed. Preliminary test results indicate coke formation to be an over-riding problem.

The most interesting developments have been in the catalytic partial oxidation. The process may be more aptly called autothermal gasification since the feed is primarily gasified to light hydrocarbons and a relatively small extent to CO and H_2. For the gasification of a No. 2 oil containing 0.17% sulfur, Engelhard prepared a cordierite monolith catalyst having Pt, Pd, and Rh as active metals. The following is one of the experiments obtained with this catalyst:

O_2/C ratio*:	0.308 mole/atom
H_2O/C ratio:	0.46 mole/atom
Inlet temperature:	358°C (676°F)
GHSV:	106,000 hr^{-1}
Product composition, vol%	(dry)
H_2	13.5
CO	>1.7
CO_2	3.5
C_3 gases	5.6

*Air was used

Although the data are incomplete, the above test points out that the process can achieve a favorably low O_2/C ratio and operates under an extremely high space velocity. Upon removal of the catalyst after the test, Engelhard noted some sign of soot downstream of the reactor but no carbon deposits in the monolith catalyst.

Earlier, Siemens AG reported a successful catalytic gasification of a diesel fuel under a very low O_2/C ratio and a very high space velocity (Henkel, 1977). It may be interesting to compare some of the test results by this process with the Engelhard process. The following is a summary of one of the tests conducted by Siemens.

O_2/C ratio:	0.125 mole/atom
H_2O/C ratio:	0.44 mole/atom
Catalyst temperature:	799°C (1470°F)
LHSV:	32 hr^{-1}
Conversion:	60.7 wt%
Product composition, vol%	
H_2	11.3
CO	31.4
CO_2	24.6
CH_4	10.7
C_2H_6	2.1
C_2H_4	18.7
O_2	1.8

The test was conducted using oxygen instead of air. Space velocity is shown in terms of liquid charge rate. Siemens indicates that the feed rate used in the test is about 12 times larger than the usual loading in conventional steam reformers. The O_2/C ratio is extremely low, and yet it is indicated that soot was not formed. However, it is noted that the gasification did not achieve a complete conversion and the product contained high concentrations of olefins. A rather significant amount of oxygen in the gasifier effluent is noted.

The catalytic gasification processes by Engelhard and Siemens produce significant quantities of light hydrocarbon gases including olefins. For the fuel-cell applications, these gases must be steam-reformed in a secondary unit. Engelhard is currently testing candidate catalysts for such a reforming step. To be effective, the catalyst must be able to withstand sulfur and to achieve a near-equilibrium conversion of the light gases.

3.5 Haldor Topsøe A/S

Rostrup-Nielsen and Tottrup of Topsøe have recently studied steam reforming of distillate fuel containing various concentrations of sulfur (Rostrup-Nielsen, 1979).

Described here are the results of three reforming experiments in which (1) a light gas oil containing 20ppm sulfur was reformed over a commercial nickel-based catalyst, (2) a heavy gas oil containing 6600 ppm sulfur was reformed over a nonmetal catalyst, and (3) a No. 2 fuel oil containing 8500 ppm sulfur was hydrotreated in stages to reduce sulfur to 0.07 ppm and was reformed over a commercial nickel-based catalyst.

Of the three experiments, the third is the most interesting. Topsøe has demonstrated that a distillate fuel with an ultra-low sulfur level can be reformed at conditions applicable to naphtha.

3.5.1 Light Gas Oil with 20ppm Sulfur

A light gas oil having a boiling range of 143°C/314°C and containing 20ppm sulfur was reformed over Topsøe's commercial catalyst RKNR. Table 3-4 describes the test. The RKNR catalyst is a nickel catalyst having magnesia and alumina as the support and is widely used for naphtha reforming.

When the inlet portion of catalyst bed is poisoned by sulfur, the most severe poison for a nickel-based reforming catalyst, unconverted feed may pass to the hotter part of the bed, where coking may become critical and the extent of thermal cracking may become significant.

As shown in the table, good reforming activity was maintained for 2.5 hr. However, the authors indicate that by the third hour on stream, a breakthrough of feed was observed. The test was conducted at an exit temperature of 660°C. This relatively low reforming temperature was chosen in order to minimize thermal cracking. The deactivation of a nickel catalyst by sulfur however, is more severe at this lower temperature.

3.5.2 Heavy Gas Oil with 6600 ppm Sulfur

One way of dealing with the problems of sulfur is to employ a catalyst that is

TABLE 3-4

Steam Reforming of Light Gas Oil (20 ppm)

Catalyst

RKNR: 25% wt nickel on alumina/magnesia; silica <0.2 wt %, alkali metals <0.3 wt %

Feed

IBP/FBP	134°C/314°C (273°F/597°F)
Sulfur	20 ppm

Reforming conditions

Time from start (hr)	1	2.5
H_2O/C (moles/atom)	8.5	3.9
H_2O/H_2 (moles/mole)	8.2	10.6
LHSV, hr^{-1}	0.84	1.8
Pressure (kg/cm^2g)	30	30
T_{inlet}/T_{exit} (°C/°C)	510/660	510/660

Product gas

CH_4(vol %, dry basis)	14.3	27.7
$C_2 - C_6$(vol %, dry basis)	<0.01	<0.01
ΔT (approach), CH_4 reforming (°C)	33	27

Source: Rostrup-Nielsen, 1979

not affected by it, or to use a nickel-free catalyst. Topsøe tested a nonmetal catalyst in the gasification of a heavy gas oil containing 0.66 wt % sulfur. Gasification was conducted at a T_{inlet} of 560°C and a T_{exit} of 820°C. The results are summarized in Table 3-5.

The Topsøe HPK catalyst, a K-ZrO_2, has a tendency to lose potassium during operation and as a consequence, carbon deposition may increase (Andersen, 1975). To minimize this problem, addition of a small quantity of an aqueous solution of potassium sulfate into the feed is recommended. However, even with a continuous addition of salt, the catalyst bed accumulates sufficient soot to require regeneration of the catalyst. The reference does not indicate whether potassium was added or how much carbon deposited during the test run reported in Table 3-5.

As indicated, the test lasted for 300 hours. Contrary to the exit gas in the steam reforming of light oil (data in Table 3-4), the exit gas in this case contained about 20 vol. % of C_2-C_6 components. Also, the feed was not completely gasified. Topsøe does not indicate whether the yield data represent average values or the result of a single sample.

The exit temperature of 820°C is rather low for a nonmetal catalyst. This is reflected in the incomplete conversion. In general, a temperature of at least 900°C is required to completely gasify a fuel oil over a nonmetal catalyst (Tomita, 1976).

3.5.3 Severely Hydrotreated No. 2 Oil

A third alternative studied by Topsøe was ultra-hydrodesulfurization of a No. 2 fuel oil, followed by steam reforming over the commercial naphtha reforming catalyst RKNR. A No. 2 fuel oil containing 0.85 wt % sulfur was desulfurized to less than 0.1ppm by two-stage hydrotreating. Table 3-6 describes the hydrotreating operation and steam reforming of the hydrotreated oil.

TABLE 3-5

Gasification of Heavy Gas Oil

(Bench-scale test with Topsøe (nonmetal) catalyst HPK)

Feedstock: HGO (Oman crude)
IBP/FBP - 195°C/405°C, 0.66 wt % S
0.856 g/ml

Process conditions

T_{inlet}/T_{exit}	560°C/820°C
P_{exit}	3.5 kg/cm^{2}g
LHSV	1.4
H_2O/C_nH_m	4.6 wt/wt
Duration	300 hr

Product

	Dry exit gas (vol %)	Yield (wt % of HC feed)
H_2	47.9	7.5
CO	1.6	3.6
CO_2	15.9	54.8
CH_4	14.8	18.6
Subtotal	80.2	
C_2H_6	1.9	4.7
C_2H_4	11.6	25.5
C_3H_8	0.1	0.4
C_3H_6	3.5	11.8
C_4-C_6	2.7	13.6
Total	100	
Liquids		7
		147*

* Incl. reacted H_2O.

TABLE 3-6

Two-Stage Desulfurization of No. 2 Oil Followed by Steam Reforming over Commercial Ni Catalyst

HYDRODESULFURIZATION

HDS in two stages over Topsøe catalyst MAG-42 AHF
LHSV = 1, 98 kg/cm^2g, 375°C, 0.5 Nm^3/kg oil

	Before HDS	After HDS
Specific gravity, 60/60°F	0.8350	0.8070
°API	38	43.8
C/H (wt/wt)	6.41	6.03
Aromatics (vol %)	11.3	4.7
Distillation, ASTM		
IBP	207°C	146°C
50 vol %	280°C	269°C
FBP	315°C	311°C
Sulfur (wt ppm)	8500	0.07
Nitrogen (wt ppm)	25	< 0.5

STEAM REFORMING

Bench scale on RKNR catalyst (Ni on magnesia and alumina)
Duration: 240 hr

H_2O/C	3.7 moles/atom
H_2-flow	0.3 Nm^3/kg oil
Pressure	30 kg/cm^2g
T_{inlet}/T_{exit}	500°C/680°C
SV_{Cl}	1400 vol/vol/hr
ΔT ref. equil.	< 5°C
C_nH_m in dry exit gas	< 0.01 vol %

Source: (Rostrup-Nielsen, 1979)

As one would expect, quite severe conditions are required to achieve the ultra-low sulfur. It can be seen that general chemical makeup of the fuel oil has been affected by this operation. In other words, a decrease in aromatics content, a decrease in gravity, and a decrease in IBP all point to the fact that substantial hydrocracking has occurred during desulfurization. Topsøe does not report the light gas make but in such a high severity operation, some formation of C_1-C_4 gases is expected.

The steam reforming reported in Table 3-6 is, in many respects, very similar to commercial naphtha reforming. The hydrogen recycle is higher by a factor of three than what is recommended for naphtha (Topsøe, 1979), but this is expected for a heavy oil. The most surprising aspect of the operation is that methane reforming is achieved very close to the equilibrium at a rather low reforming temperature of 680°C.

By this test, Topsøe has demonstrated that steam reforming of distillate oils can be accomplished with a conventional nickel catalyst at conditions very similar to those of naphtha reforming, when the feed sulfur is reduced below 0.1ppm. As indicated in Table 3-6, the reforming test lasted 240 hours, and, according to one of the authors, no catalyst deactivation nor carbon formation was observed during this test period (Rostrup-Nielsen, 1979).

The importance of sulfur removal is clear when the reforming test on a gas oil containing 20ppm sulfur (Table 3-4) is compared with the present case (Table 3-6). With the same catalyst and under very similar operating conditions, one run was terminated after 3 hours because of sulfur deactivation, while the other, with a sulfur-free feed, continued to operate without deactivation for the duration of the test, 240 hours.

3.6 Mitsui Toatsu Chemical

Synthesis-gas generation from crude oil or residual feedstock containing sulfur is described in a patent assigned to Mitsui Toatsu (Mitsui Toatsu, 1979).

The reactor consists of a top catalyst zone to gasify heavy hydrocarbons, and a bottom catalyst zone to steam-reform these gases so that the methane concentration in the product is very low. The gasification is carried out autothermally.

The examples of the catalyst to be used in the first zone are: calcium aluminate, potassium aluminate, and sodium aluminate. The main constituent of the catalyst for the second zone is chromium oxide. Other components may be added to chromia as a diluent or to improve the physical properties.

Table 3-7 describes the test catalysts for both zones. Various combinations of these catalysts were used to generate syngas from Kuwait crude oil and residual oils.

Table 3-8 shows the gasification of Kuwait crude at 1000°C over catalyst A or B by itself or over various combinations of A with E. The operating conditions were:

Pressure	1 kg/cm^2
H_2O/C ratio:	1.5 mole/atom
O_2 stoichiometric ratio:	0.295
GHSV:	200 hr^{-1}

The O_2 stoichiometric ratio is defined as the amount of O_2 fed divided by the amount required for complete combustion of the feed hydrocarbon. The GHSV (gaseous hourly space velocity) was calculated on the basis of gases at standard conditions and on the empty reactor volume. From Table 3-8 it is clear that the two-catalyst system is required in order to achieve low methane slip. Also, a range of optimum volume ratios for catalysts A and E is indicated. Soot formation amounted to about 0.3 wt % of hydrocarbon feed, but it was not retained in the catalyst bed.

Table 3-9 shows the gasification of Kuwait crude over other catalyst combinations. For all tests, the catalyst volume ratio was set at 25%/75%. The operating conditions were essentially the same as those in Table 3-8. With

TABLE 3-7

Description of Gasification Catalysts

Designation	Composition (wt %)	Compressive Strength (kg/cm^2)	Water Stability
First Zone			
A	$12CaO\text{-}7Al_2O_3$ & small amount $3CaO\text{-}7Al_2O_3$	350	Good
B	KAl_5O_8 & small amount $K_2Al_{24}O_{37}$	300	Good
C	$NaAl_5O_8$ & small amount $Na_2Al_{24}O_{37}$	300	Good
Second Zone			
D	Cr_2O_3 100%	100-200	Good
E	Cr_2O_3 97%, MgO 3%	450	Good
F	Cr_2O_3 95%, Al_2O_3 5%	330	Good
G	Cr_2O_3 50%, Al_2O_3 50%	350	Good
H	Cr_2O_3 25%, Al_2O_3 75%	300	Good
I	Cr_2O_3 95%, CaO 5%	220	Good
J	Cr_2O_3 97%, ZrO_2 3%	400	Good
K	Cr_2O_3 95%, NiO 5%	320	Good
L	Cr_2O_3 95%, CoO 5%	380	Good

Source: (Mitsui Toatsu, 1979)

TABLE 3-8

Gasification of Kuwait Crude By Mitsui Toatsu Process

Test No.		1	2	3	4	5
Catalyst	Zone 1, vol %	A	B	A 10	A 25	A 75
	Zone 2, vol %			E 90	E 75	E 25
Pressure (kg/cm^2)		1.0	1.0	1.0	1.0	1.0
Temperature (^oC, exit)		1000	1000	1000	1000	1000
H_2O/C (moles/atom)		1.5	1.5	1.5	1.5	1.5
O_2 stoich. ratio		0.295	0.295	0.295	0.295	0.295
GHSV (hr^{-1})		200	200	200	200	200
Composition (%)	H_2	50.4	51.6	57.3	57.3	57.1
	CO	26.0	25.3	28.5	28.5	28.4
	CO_2	17.0	17.2	13.5	13.5	13.5
	CH_4	5.9	5.2	0.00	0.00	0.38
	C_2H_4	0.1	0.08	0	0	0
	C_2H_6	Trace	0	0	0	0
	H_2S	0.6	0.6	0.6	0.6	0.6
Soot	On catalyst	None	None	Small	None	None
	In exit gas (wt % HC feed)	0.40	0.52	0.30	0.28	0.30
Test period (hr)		5.0	5.0	5.0	5.0	5.0

Source: Mitsui Toatsu, 1979

TABLE 3-9

Gasification of Kuwait Crude (continued)

Test No.			6	7	8	9	10	11	12	13
Catalyst	Zone 1, 25%		A	A	A	A	A	A	A	A
	Zone 2, 75%		D	F	G	H	I	J	K	L
Pressure (kg/cm^2)			1.0	1.0	1.0	1.0	1.0	1.0	1.0	1.0
Temperature (^oC)			1000	1000	1000	1000	1000	1000	1000	1000
H_2O/C (moles/atom)			1.5	1.0	1.5	1.5	1.5	1.5	1.5	1.5
O_2 stoich. ratio			0.295	0.282	0.295	0.295	0.295	0.295	0.295	0.295
GHSV (hr^{-1})			200	200	200	200	200	200	200	200
Composition (%)		H_2	57.1	53.1	56.1	55.9	56.0	57.2	56.5	56.2
		CO	28.7	34.3	30.0	29.0	30.5	27.5	30.2	29.8
		CO_2	13.6	12.0	13.2	13.6	12.4	14.5	12.7	13.4
		CH_4	0.00	0.02	0.10	0.48	0.03	0.02	0.00	0.01
		C_2H_4	0.0	0.0	0.0	Trace	0.0	0.0	0.0	0.0
		H_2S	0.6	0.6	0.6	0.6	0.6	0.6	0.6	0.6
Soot	On catalyst		None	None	None	None	None	None	None	None
	In exit gas (wt% HC feed)		0.36	0.56	0.37	0.48	0.38	0.52	0.38	0.33
Test period (hr)			5.0	5.0	5.0	5.0	5.0	5.0	5.0	5.0

Source: Mitsui Toatsu, 1979

respect to methane slip and soot formation, none of the combinations shown in this table is better than that in test No. 4 in Table 3-8. Thus, the best catalyst combination among those tested is:

1st zone: 25 volumes of catalyst A (calcium aluminate)
2nd zone: 75 volumes of catalyst E (97% Cr_2O_3, 3% MgO)

Table 3-10 shows longer test runs with combinations of catalysts A/E and B/E. As feed, Kuwait crude, atmospheric resid, and vacuum resid were used. For test Nos. 14 and 15, no oxygen is indicated in the feed; therefore, the gasification was presumably carried out in an externally heated reactor. It is noted that soot formation in these two tests was considerably lower than in the other runs. This is probably because of the use of a higher H_2O/C ratio, which reduced the CO concentration.

Test Nos. 15 and 18 are 10-day and 30-day runs, respectively. Judging from the soot level and methane leak in the product gases, the catalysts appear to have maintained good activities during the test.

Test No. 14 represents the only run made at 950°C. In this 30-hour run, Kuwait crude was steam-reformed with only a trace of methane slip. Also the soot level was the lowest among all tests. Interestingly, this run was made at a higher space velocity than were most of the runs, but this did not increase the methane slip nor the soot level.

In summary, the Mitsui Toatsu process described here has potential for fuel-cell application because:

- The catalysts can tolerate very high feed sulfur.
- The dual catalyst system can achieve high reforming conversion with methane slip less than 1%.
- A very small amount of soot is formed, an average of about 0.5 wt % of hydrocarbon feed
- The process has been demonstrated with Kuwait crude and its residual oils.

TABLE 3-10

Gasification of Kuwait Crude and Residual Oils (Continued)

Test No.			14	15	16	17	18
Catalyst	Zone 1, 25%		B	A	A	A	A
	Zone 2, 75%		E	E	E	E	E
HC feed			Crude	Atm Resid	Atm Resid	Vac Resid	Vac Resid
Pressure (kg/cm^2)			6	1	9	50	1
Temperature (^oC)			950	1000	1000	1000	1000
H_2O/C (moles/atom)			3.8	3.8	1.0	1.5	1.5
O_2 stoich. ratio			0	0	0.282	0.305	0.325
GHSV (hr^{-1})			900	300	1350	1350	200
Composition (%)		H_2	68.8	68.4	53.0	52.5	30.2
		CO	17.0	17.9	34.1	34.5	14.6
		CO_2	12.0	12.9	12.1	11.4	9.6
		N_2	0	0	0	0	45.0
		CH_4	0.3	0.18	0.2	0.8	0
		H_2S	0.3	0.42	0.6	0.9	0.6
Soot	On catalyst		None	None	None	None	None
	In exit gas (wt % HC feed)		0.05	0.10	0.6	1.0	0.8
Test period (hr)			24	240	30	30	720

Source: Mitsui Toatsu, 1979

3.7 Waseda University, Tokyo

Kikuchi, et al., tested steam reforming of atmospheric and vacuum resid in the presence of nickel-on-dolomite catalysts in a fluidized reactor (Kikuchi, 1979). The purpose of using the dolomite support was to desulfurize by the reaction:

$$CaO + H_2S \rightleftharpoons CaS + H_2O \qquad (1)$$

This lowers the H_2S concentration so that poisoning of nickel by the following reaction is minimized:

$$Ni + H_2S \rightleftharpoons NiS + H_2 \qquad (2)$$

Kikuchi, et al., found that the reactions (1) and (2) are rapid enough to approach equilibrium at 900°C.

The catalyst was prepared by first calcining dolomite at 700°C and then impregnating it with a solution of nickel nitrate. Finally, the impregnated dolomite was calcined at 1200°C. The composition of finished catalyst was:

NiO	5.0%
CaO	62.2%
MgO	31.7%
SiO_2	0.7%
Al_2O_3	0.1%
Fe_2O_3	0.1%

This catalyst was used in a fluidized reactor (42 mm i.d. x 400 mm) to gasify various heavy oils. The results are shown in Table 3-11. The gas yield in the table represents conversion of feed carbon to gaseous compounds including CO, CO_2, and C_1-C_4 hydrocarbons. Atmospheric residual feeds were almost totally gasified, but about 4-10% of the vacuum residues remained unconverted. This is not surprising since gasification of residual feed usually requires temperatures above 950°C (Tomita and Kitagawa, 1976).

TABLE 3-11

Gasification of Heavy Feeds

	Topped Residues		Vacuum Residues		
Feed Oil	Arabian Light	Iranian Heavy	Berri	Arabian Light	Arabian Medium
Sulfur, wt %	2.81	2.71	3.46	3.24	5.30
Con. carbon, wt %	7.8	10.7	14.9	17.7	18.3
Product gas volume (l/g)	3.94	3.85	3.50	3.57	3.73
Gas yield (%)	100	99	90	93	96
Gas composition (%)					
H_2	59.3	60.1	59.8	59.9	59.9
CO	28.7	27.7	27.7	26.8	30.5
CO_2	6.7	6.0	5.7	6.4	4.8
CH_4	4.8	5.1	5.6	5.3	4.3
C_2H_6	0.1	0.1	0.2	0.2	0.1
C_2H_4	0.4	0 9	1.3	1.3	0.5
H_2S	0.027	0.024	0.027	0.027	0.025
Desulfurization (%)	94.9	95.6	95.9	96.4	97.6

Reaction conditions: Temperature = 900°C; steam ratio = 1.1-1.2 (H_2O moles/C mole); residence time = 0.38-0.42 sec; product gas volume = liter per gram feed oil; gas yield = % conversion of feed carbon to gaseous compounds (CO, CO_2, and C_1-C_4 gases).

Source: Kikuchi, 1979

In the gasification of Arabian light topped crude, the gasification activity started to decline after 4 hours on stream, corresponding to 11.5% conversion of CaO to CaS. The activity was measured in terms of product gas volume per unit weight of hydrocarbon feed. The decline in activity was attributed to carbon deposition, as the original activity could be restored by treatment in flowing O_2. It is speculated that conversion of CaO to CaS enhances carbon formation.

In summary, the dolomite-supported nickel catalyst can sustain fresh activity for short periods of time but it is easily coked. This coking tendency increases as a small fraction of CaO component is sulfided. This suggests that such a reforming catalyst requires frequent regeneration. The authors do not explore the method of regeneration. However, it should entail the key chemical reactions of burning of carbon and calcining of CaS. Deactivation of dolomite from repeated regeneration is well recognized in the development of the CO_2 acceptor process for coal gasification and the fluid-bed coal combustion process. For these reasons, the steam reforming process using a nickel-dolomite catalyst faces a formidable job of overcoming process engineering and perhaps economic obstacles.

4. CASE STUDIES

A naphtha-based fuel-cell power plant can now achieve a heat rate of 9300 Btu/kwh or better. Thus, in order to be competitive, a distillate fuel-based power plant is required to match this heat rate. In this section, case studies of a phosphoric acid fuel-cell power plant featuring two promising distillate fuel reforming schemes are presented. In one case, the power plant features an autothermal reformer. In another case, it features a combination processing consisting of a high-temperature steam reforming followed by an ATR step. The objective of the study is to provide a perspective for the distillate-based power plant to achieve the target heat rate using the selected fuel processors.

The first case study evaluates the influence of key ATR parameters such as the O_2/C ratio, reforming conversion, and feed preheating on the heat rate. The energy and mass balance and calculation of heat rate for the whole power plant were made for two O_2/C ratios: 0.35 and 0.30 mole/atom. The feed preheating was set at 1400°F. As indicated earlier, the ATR process can currently operate with the O_2/C ratios in a range 0.39-0.41 mole/atom, and efforts are being made to achieve a near-term target of 0.35. The lower value of 0.30 selected in the study may be regarded as the ultimate ATR goal. The study also examines the sensitivity of heat rate to changes in methane concentration in the ATR effluent. The methane slip is an important parameter, since the fuel cell cannot utilize methane, whereas each additional mole of methane reformed in the ATR makes four moles of hydrogen available for electric conversion by the fuel cell.

The second case study evaluates a high-temperature steam reforming with a secondary reforming (ATR) in an acid-cell power plant. This is the result of a recent EPRI project in which Catalytica Associates and Kinetics Technology International, with the cooperation of Toyo Engineering, evaluated the Toyo's high-temperature steam reforming process as integrated with a phosphoric acid fuel cell (Tio/Ushiba, 1979).

The key parameter in the case study is the methane slip from the HTSR. The Toyo process tends to emit rather significant methane slip. As a means of achieving a higher methane conversion, the study investigated an idea of placing an autothermal reforming downstream of the HTSR.

4.1 A 5-MW Acid Fuel-Cell Power Plant with ATR of No. 2 Fuel Oil

4.1.1 Base Case ($O_2/C = 0.35$)

The process flow of the base-case power plant is shown in Figure 4-1. The only energy input to this plant is the No. 2 fuel oil charged to the ATR unit. Table 4-1 lists key design parameters. Mass balance is given in Table 4-2.

No. 2 oil is heated to 700°F in a fired heater, which also preheats the ATR air to 1400°F. These two preheated streams are mixed with superheated steam at 1600°F at the ATR inlet. The net feed mixture is estimated to be at 1400°F. In the ATR unit, partial combustion of the fuel provides the thermal energy needed to promote the steam reforming. At an O_2/C ratio of 0.35, the combustion heat is more than enough to support the endothermic reforming reactions. Thus, the ATR effluent is hotter than the inlet stream. The methane slip was arbitrarily chosen.

The hot ATR effluent is used to superheat the ATR steam to 1600°F (871°C). The remaining sensible heat is used to preheat various process streams. Cooled to 662°F, the ATR product enters a high-temperature shift reactor, where the CO content is reduced to 2%. This residual CO is further shifted in a low-temperature shift reactor to less than 0.5%. After condensate recovery, the gas stream is charged to the anode compartments of the fuel cell, where 90% of the hydrogen is electrochemically consumed.

The anode exhaust is at 60 psia; when preheated to 1050°F (>66°C), it is capable of driving the turboexpander (T-2), which in turn provides power for the ATR air compressor (C-2). After the power recovery, the anode exhaust is used as the sole fuel in the fired heater (H-1).

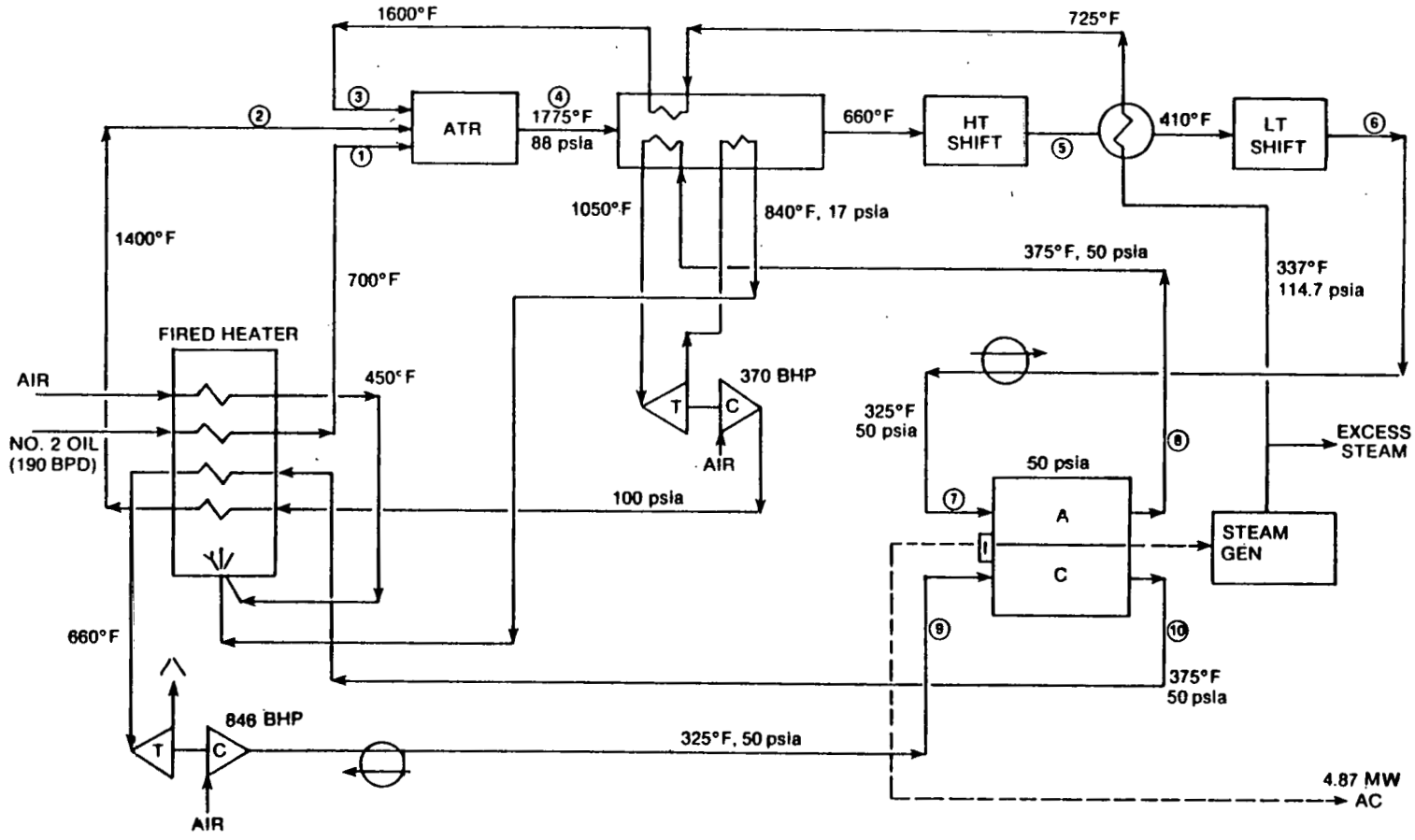

Fig. 4-1. 5-MW fuel-cell power plant with ATR of no. 2 fuel oil (O_2/C = 0.35 mole/atom).

TABLE 4-1

Design Basis for 5-MW Power Plant with ATR

No. 2 Oil	
Feed rate	13.38 lb moles/hr (189.7 barrels/day)
Molecular formula	$C_{12.75}H_{22.6}$, MW = 175.6
Sulfur	0.2 wt %
Higher heating value	19,700 Btu/lb
Lower heating value	18,200 Btu/lb
ATR unit	
O_2/C ratio	0.35 mole/atom
H_2O/C ratio	3.0
Feed preheat	1400°F (fuel, air, and steam combined)
Methane in effluent	0.33 vol %
Fuel cell	
Cell voltage	0.65 v
H_2 utilization	90%
O_2 utilization	70%
Cell temperature	375°F
Waste heat release	50,000 Btu/lb mole H_2
DC-AC inverter loss	4% of gross DC

TABLE 4-2

5-MW Acid Cell Power Plant
with ATR-Base Case ($O_2/C = 0.35$)

Streams: lb moles/hr

	Reformer Feed 1	ATR Air 2	ATR Steam 3	ATR Exit 4	HT Shift Exit 5	LT Shift Exit 6	Anode Feed 7	Anode Exit 8	Cathode Air 9	Cathode Exit 10
H_2				275.59	338.59	356.10	356.10	35.61		
CO				83.63	20.63	3.02	3.12	3.12		
CO_2				83.49	146.49	164.00	164.00	164.00		
H_2O			511.69	380.53	317.53	300.02	11.2	11.2		320.74
CH_4				3.48	3.48	3.48	3.48	3.48		
N_2		224.48		224.48	224.48	224.48	224.48	224.48	861.86	861.86
O_2			59.66						229.10	68.73
H_2S	0.02 wt %			140 ppm	140 ppm	140 ppm	192 ppm	332 ppm		
No. 2 oil	13.38									
Total	13.38	284.14	511.69	1051.21	1051.21	1051.21	762.62	441.88	1090.96	1251.33
T, °F	700	1400	1600	1775	774	440	325	375	325	375
p, psia	95	95	95	88	71	60	50	50	50	50

The fired heater (H-1) preheats the feed oil and the oxygen-containing streams, such as ATR air, cathode exhaust, and furnace air. Major power-consuming items are the cathode air compressor (C-1, 846 bhp), ATR air compressor (C-2, 370 bhp) and miscellaneous process drives (C-3, 107 bhp). As shown in Figure 4-1, these power requirements are all met by either the process stream turboexpander or a steam turbine. Thus, all the electricity generated by the fuel cell is exported.

In summary, the described power plant consumes 2,351 lbs/hr or 190 barrels/day of No. 2 fuel oil and in turn generates 5.07MW of DC electricity. With a 4% loss in the DC-AC inverter, a net 4.87MW of AC is exported. The heat rate, based on the net AC and the higher heating value of the fuel oil, is 9,513Btu/kwh.

4.1.2 Sensitivity of Heat Rate to Methane Leakage

Since autothermal reforming of sulfur-containing fuel oil is not yet well understood, parameters such as preheat temperature and methane slip for the base case were assumed. The methane slip was assumed at 3.48 lb-moles/hr or 0.33 vol. %. In terms of methane reforming reaction:

$$CH_4 + H_2O \rightleftharpoons CO + 3H_2,$$

the assumed methane slip represents an equilibrium approach temperature of 380°F (193°C). This approach is an order of magnitude greater than what is achievable in conventional naphtha reforming. On the other hand, preliminary test data indicate that an approach temperature of as high as 580°F (304°C) may have to be anticipated when methane reforming is attempted in the presence of sulfur (Tio/Ushiba, 1979).

We evaluated the sensitivity of the base case heat rate against methane slips at 2.48, 1.48, and 0.48 lb-mole/hr. As shown in Table 4-3, for each mole decrease in CH_4 slip, the heat rate improves by about 100 Btu/kwh. Thus, at the lowest assumed value of 0.48, the heat rate is 9,200 Btu/kwh.

TABLE 4-3

Heat Rate of Acid Power Plant With
ATR Operating at 0.35 Mole O_2/Atom C
= Sensitivity with ATR Methane Slip

CH_4 in ATR Exit, lb-moles/hr	Approach to CH_4 Reforming Equil., $^oF(^oC)$	Heat Rate, Btu/kwh
3.48 (Base Case)	380 (193)	9,510
2.48	344 (173)	9,410
1.48	290 (143)	9,300
0.48	184 (84)	9,200

Note: Base Case as represented by Figure 4-1 and Table 4-2.

One negative effect of improved methane conversion in ATR is the decreased heating value of the anode exhaust. Since the anode effluent is the only fuel source for the fired heater (H-1), a large drop in heating value may create a heat imbalance in some parts of the integrated system. This is what happens when the methane slip is reduced to 0.48 lb-mole/hr, while the heat balance is still feasible at the methane slip above 1.48 lb-mole/hr. Compared with the base case, about one million Btu/hr less heat will be available from the combustion of anode gas. As a result, the feed preheating as shown in the base case(Figure 4-1)will no longer be feasible, unless some additional fuel is supplied. Also, because the reforming reaction is endothermic, each additional percent of methane reformed decreases the ATR effluent temperature by about 15°F.

4.1.3 Modified Base Case with $O_2/C = 0.30$

In the following case study, the ATR unit operates with an O_2/C ratio of 0.30. The feed preheating is the same as in the base case, 1400°F. The H_2O/C ratio is also the same, 3 moles/atom.

The process flow diagram for this modified power plant is shown in Figure 4-2. Table 4-4 shows the mass balance. Compared with the base case, the major differences are as follows:

- ATR air requirement is lower by about 14%;
- ATR effluent temperature is lower by about 230°F;
- ATR effluent can no longer preheat ATR steam to 1600°F; therefore, the final heating is done in fired heater.

The remainder of the system is essentially the same as in the base case.

As shown in Figure 4-2 and Table 4-4, the power plant consumes 2,249 lb/hr or 182 barrels/day of No. 2 oil and, as in the base case, generates 4.87MW of AC electricity for export. The heat rate is 9,100 Btu/kwh, a 4.3% improvement

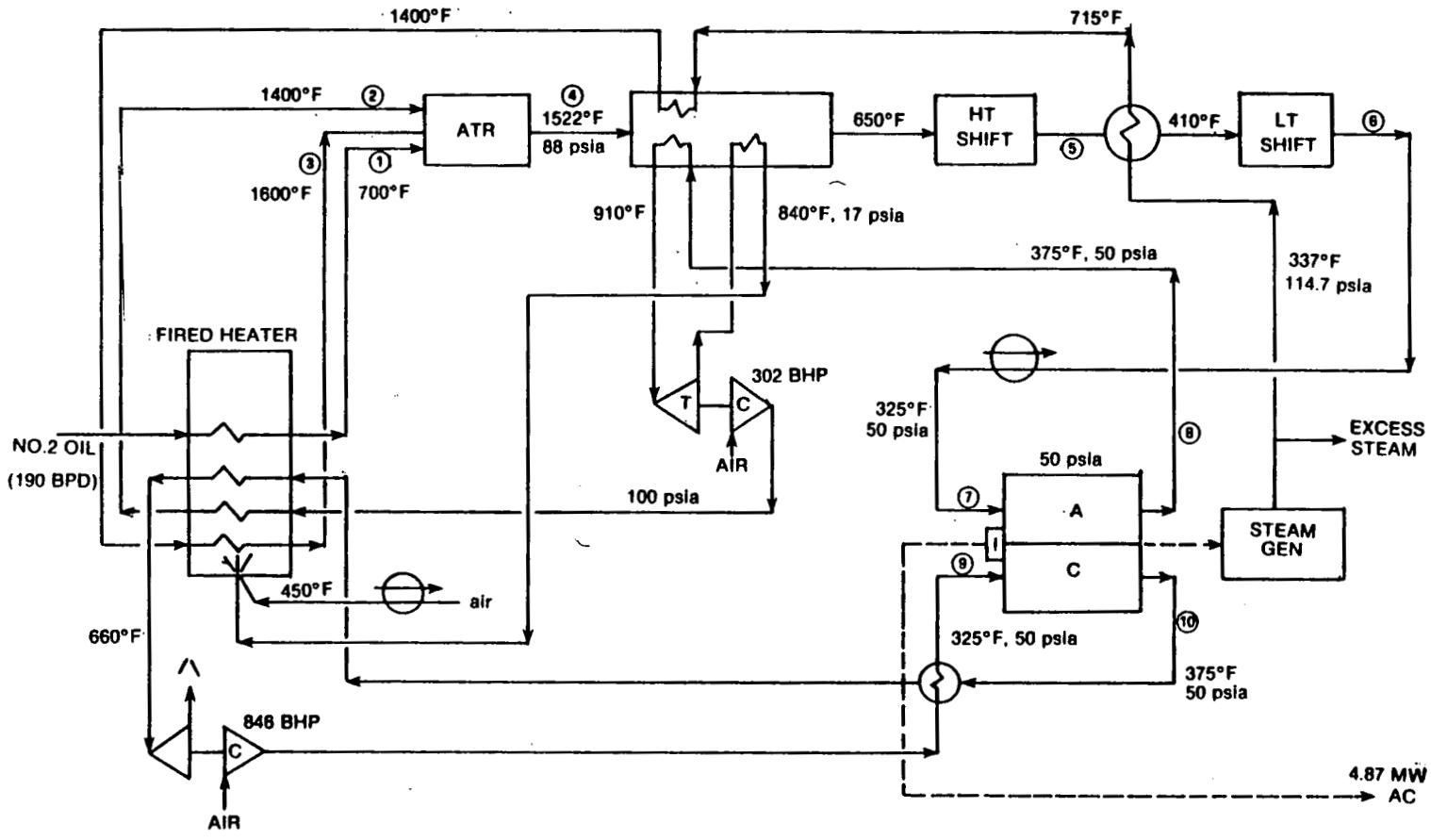

Fig. 4-2. 5-MW acid fuel-cell power plant with ATR of no. 2 fuel oil - modified (O_2/C = 0.30 mole/atom).

TABLE 4-4

5-MW Acid Cell Power Plant
with ATR-Modified (O_2/C=0.3)

Streams: lb-moles/hr

	Reformer Feed 1	ATR Air 2	ATR Steam 3	ATR Exit 4	HT Shift Exit 5	LT Shift Exit 6	Anode Feed 7	Anode Exit 8	Cathode Air 9	Cathode Exit 10	11	Furnace Air 12	Export Steam 13
H_2				280.85	340.30	356.38	356.38	35.64					
CO				78.95	19.50	3.42	3.42	3.42					
CO_2				80.92	140.37	156.45	156.45	156.45					
H_2O			489.60	346.72	287.27	271.19	10.52	10.52		320.74			340.21
CH_4				3.34	3.34	3.34	3.34	3.34					
N_2		184.18		184.18	184.18	184.18	184.18	184.18	861.86	861.86		108.46	
O_2		48.96							229.10	68.73		28.83	
H_2S													
No. 2 Oil	12.80												
Total	12.80	233.14	489.69	974.96	974.96	974.96	714.29	393.55	1090.96	1251.33		137.29	340.21
^oF	700	1400	1600	1522	768	442	325	375	325	375			
Psia	95	95	95	88	71	60	50	50	50	50			

over that in the base case. The target value of 9,000 Btu/kwh is not achieved, even with the optimistic O_2/C ratio chosen for the case.

The key differences between this case and the base case is that here less of the fuel is combusted in the ATR. On the one hand, this leaves more hydrocarbon feed to be reformed into hydrogen, which should result in a better heat rate. On the other hand, the ATR exit temperature is significantly lower, because less heat is generated by partial oxidation of the feed. For example, in the base case, the ATR steam was preheated to 1600°F by the ATR effluent, but this is not feasible in the present case, as shown in Figure 4-2. The final heating is done in a fired heater.

The lower ATR exit temperature also may adversely affect the reforming activity of the ATR catalyst, since deactivation of normal reforming catalyst by sulfur increases with decreasing temperature.

In the present case, the methane concentration was arbitrarily set at 3.34 lb-mole/hr (0.34 vol %), very similar to that in the base case. In terms of methane reforming reaction, this concentration corresponds to an approach temperature of 200°F (93°C), compared with 380°F (193°C) in the base case.

Reducing the O_2/C ratio in ATR will impose rather severe performance requirements on the catalyst. Perhaps such a high-performance ATR catalyst as assumed in the present case study will emerge from the current developmental efforts.

4.2 A 5-MW Acid-Cell Power Plant with HTSR/ATR of a No. 2 Fuel Oil

One of the near-term fuel-oil gasification technologies suitable for fuel-cell integration is Toyo Engineering's Total Hydrocarbon Reforming (THR) process, a form of high-temperature steam reforming (HTSR) (Bett, 1979; Houseman, 1979; Yarrington, 1978). Recently, Catalytica Associates and Kinetics Technology International, with the cooperation of Toyo Engineering, evaluated the THR process as integrated with a phosphoric acid fuel cell (4). The major findings of this study are described below.

The evaluation was based on a hypothetical 5-MW acid fuel-cell power plant with the THR process as the primary fuel processor to gasify a No. 2 fuel oil. The fuel processor also featured an autothermal reforming (ATR) section downstream of the THR unit, to reform the methane slip. At the present state of development, the THR process cannot achieve a high methane conversion at the reforming conditions employed in the study. Consequently, an unusually high concentration of methane exists in the THR effluent, and the power plant would have a poor heat rate, if the ATR unit was not added. For example, the heat rate without the ATR unit was estimated to be more than 10,000 Btu/kwh, whereas with the ATR unit, the system can potentially achieve 9,000 Btu/kwh or better, as is shown below.

4.2.1 Process Description

A process flow diagram for the optimized HTHR/ATR system is shown in Figure 4-3. The material balance associated with this case is shown in Table 4-5.

The No. 2 fuel oil is mixed with superheated steam at 804°C (1480°F) and reformed by the Toyo HTSR process. The product gases exit the reformer at 820°C (1508°F) and 84.7 psia and directly enter the ATR unit. Air to the ATR unit is preheated to 520°C (968°F). In the ATR unit, the residual methane exiting the primary reformer is reformed to increase the net H_2/CO content of the process stream.

The product gases from the ATR unit are cooled by exchanging heat with other process streams and then pass through two-stage CO shift converters to maximize the hydrogen content in this stream. The condensate is recovered before the stream is charged to the fuel cell.

In the anode compartment of the fuel cell, 90% of the hydrogen in the feed stream is converted to electricity at a cell voltage of 0.65.

The anode exhaust, at 191°C (375°F) and 50 psia, is subsequently heated to 538°C (1000°F) by heat exchanging with the ATR product stream, and is then expanded through a turboexpander, T-2. Here, 189 kW of power is recovered. The exit stream from T-2 is heated to 450°C (842°F) and burned in the reformer furnace.

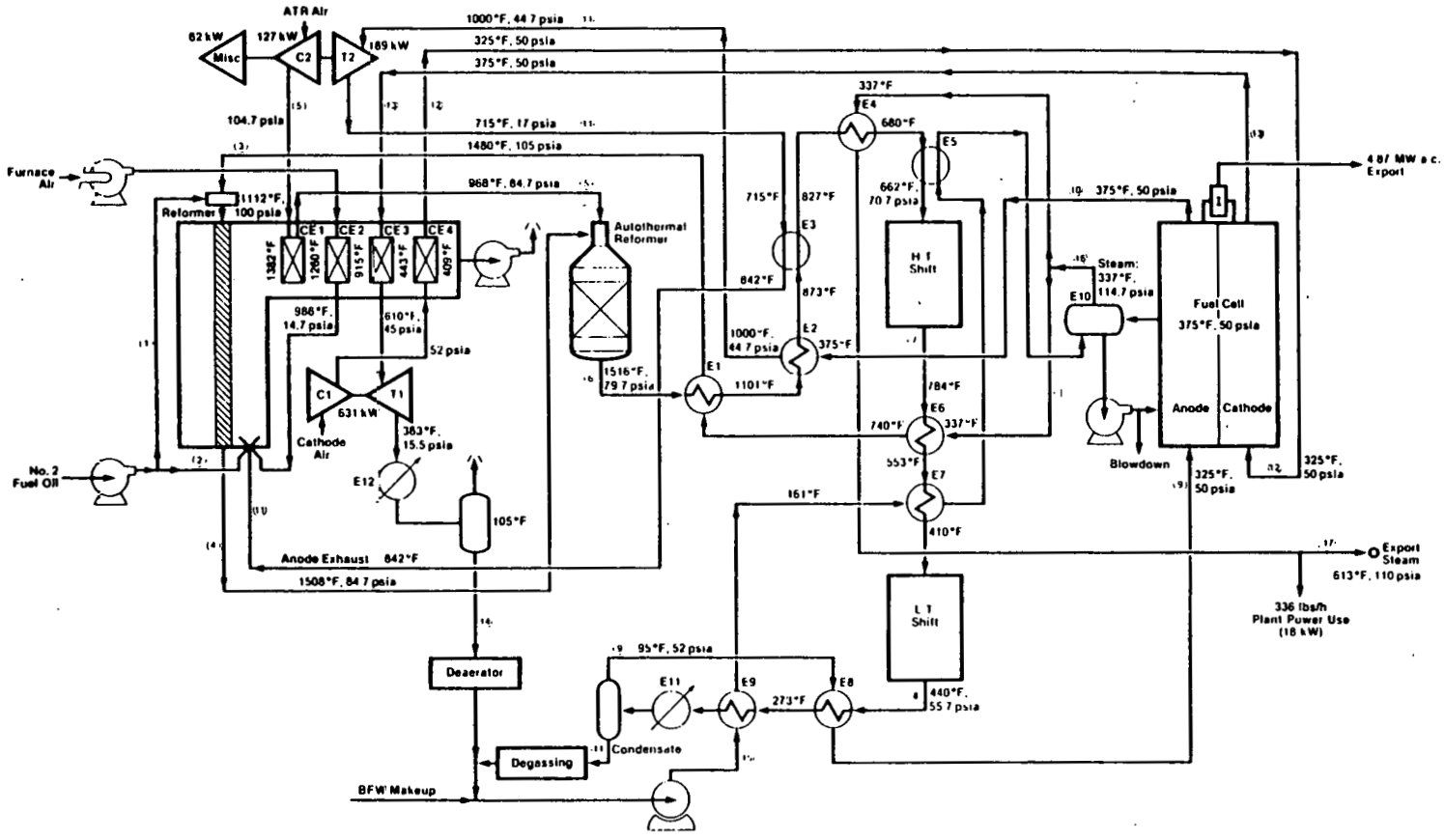

Fig. 4-3. Process flow diagram for a 5-MW acid-cell power plant, HTSR/ATR.

TABLE 4-5

A 5-MW Acid Cell Power Plant, HTSR/ATR

Steam Flows (lb-moles/hr)

Component	Reformer Feed 1	Fuel 2	Super-heated Steam 3	Reformer Exit 4	ATR Air 5	ATR Exit 6	HT Shift Exit 7	LT Shift Exit 8	Anode Feed 9	Anode Exit 10	Conden-sate 11	Cathode Feed 12	Cathode Exit 13	Conden-sate 14	BFW 15	Net Steam Make 16	Export Steam 17
H_2				169.33		287.68	336.65	356.38	356.38	35.64							
CO				33.83		72.58	23.60	3.87	3.87	3.87							
CO_2				57.53		71.34	120.32	140.05	140.05	140.05							
H_2O			436.87	287.98		274.76	225.78	206.05	9.11	9.11	196.94		320.74	250.65	866.62	841.38	385.86
CH_4				54.26		1.70	1.70	1.70	1.70	1.70							
N_2					100.30	100.30	100.30	100.30	100.30	100.30		861.86	861.86				
O_2					26.58							229.10	68.73				
No. 2 Oil	11.42	1.12															
Total	11.42	1.12	436.87	602.93	126.88	808.35	808.35	808.35	611.41	290.66	196.94	1090.96	1251.33	250.65	866.62	841.38	385.86

Exchangers	E-1	E-2	E-3	E-4	E-5	E-6	E-7	E-8	E-9	E-10	E-11	E-12	CE-1	CE-2	CE-3	CE-4
Duty, 10^6 Btu/hr	2.75	1.47	0.30	0.95	0.12	1.50	0.93	1.08	0.87	15.9	3.73	6.98	0.60	1.60	2.21	0.21

The cathode air is supplied by compressor C-1. It is preheated to 163°C (325°F) by an exchanger in the convection section of the reformer furnace and is charged to the cathode, where 70% of the O_2 is consumed to support the overall electrode reaction ($H_2 + \frac{1}{2}O_2 \rightarrow H_2O$). The water produced is carried out in the cathode exit stream. To recover power from this stream, it is preheated to 321°C (610°F) and expanded through T-1. This provides just enough power to compress the cathode air.

The fuel cell converts a net 320.74 lb-mole/hr of hydrogen, and generates about 16 million Btu/hr of waste heat. In the present scheme, this heat is utilized to generate 100-psig saturated steam. As shown in the diagram, part of this steam is superheated in E-1 and used for reforming. The steam flow rate suffers some pressure drop as it flows from the fuel cell to the reformer inlet.

Total plant power requirements include two air compressors, which need a combined power of 805 kW, and miscellaneous power consumers such as the furnace air blower and the induced draft fan, which use about 33 kW.

To meet the power requirements, two turboexpanders supply a total of 820 kW, which leaves a surplus of 15 kW after supplying the power for both air compressors. It was assumed that this surplus power could be used to meet part of the miscellaneous requirements, and the balance (~18 kW) would be met by a steam turbine using a small portion of the export steam. The amount of this steam needed to generate 18 kW shaft power is estimated at about 340 lb/hr.

In summary, the system has been designed such that all electricity generated by the fuel cell is exported, with the exception of the inverter losses, which amount to 4% of the gross DC output. This leaves a net AC export of 4,866 kW. To generate this amount of electricity the system consumes a total 12.54 lb-mole/hr of No. 2 fuel oil, or in terms of its heating value, 43.38 million Btu/hr. Thus, the heat rate of this power plant is 8,930 Btu/kwh.

4.2.2 Feedstock and Utilities Consumption

For operation at 100% of design capacity to produce 3.2×10^6 scf/d of H_2 the following consumptions are anticipated:

Fuel oil No. 2 feedstock ($x10^6$ Btu/hr HHV)	39.60
Fuel oil No. 2 fuel ($x10^6$ Btu/hr HHV)	3.86
Fuel cell off-gas ($x10^6$ Btu/hr HHV)	5.51
Boiler feed water (lb/hr)	9,145
Instrument air (scf/h)	3,500
N_2 for initial start-up (scf/h)	42,000

The production anticipated is as follows:

Fuel cell fuel ($x10^6$ Btu/hr HHV)	44.97
M.P. steam export (lb/hr)	7,880
Boiler blowdown (lb/hr)	880

The "overall heat rate" = $\frac{(39.60 + 3.86)10^6}{4,866}$ = 8,930 Btu/kwh

4.2.3 Discussion

Whether or not the power plant will perform as described here hinges strongly on how accurately the performance of the Toyo reformer has been predicted. Among the units in the power plant, this is the only unit whose performance is not well understood. The results of bench-scale tests published by Toyo Engineering show that a straight crude oil or even a vacuum residuum can be completely gasified by this process; therefore, a No. 2 oil should present no problems. An important concern in the design of the combined HTSR/ATR system is the temperature at which complete gasification is achieved.

Many of Toyo's tests were made at temperatures above 900°C (1652°F); even at these high temperatures, the product compositions are such that the corresponding equilibrium temperature is far below the actual reformer exit temperature. In other words, to achieve a practical reforming conversion, either a large volume of catalyst may have to be used or the reformer may have to be operated at a higher temperature.

In the detailed plant scheme presented in this report, the HTSR was designed with an exit temperature of 820°C (1508°F). The heat rate for this plant was calculated to be 8,930 Btu/kwh, a reasonably good rate for the first-generation fuel-cell system. It remains to be seen whether the assumed reforming temperature will be high enough to provide a reasonable conversion of the No. 2 fuel oil. If a higher reformer temperature is required, the heat rate will be higher than 9,000 Btu/kwh, since a higher reformer temperature requires a greater amount of fuel for the reformer furnace.

5. EFFECTS OF H_2S AND CO ON PHOSPHORIC ACID FUEL CELL

The phosphoric acid fuel cell tolerates certain levels of H_2S and CO which are common contaminants in the synthesis gas generated by the distillate oil reforming described in this report. Just how much of these gases can be tolerated by the cell is an important consideration from the standpoint of system optimization. Experimental results so far are not conclusive. One interesting indication is that there may be a synergism in the deactivating effects of H_2S and CO on the cell.

United Technology has run a long-term test to determine the cell tolerance to H_2S and CO. One cell was run for more than 2,400 hours with 130 to 200 ppm H_2S in the anode feed (King, 1977). This is shown in Figure 5-1. As it can be seen, the cell operated normally for up to 900 hours with anode gas containing CO and H_2S. UTC noted that the cell performance was restored by removing CO or H_2S, or by raising the cell temperature. For example, Figure 5-1 shows that a severe decay that occurred after ~650 hours was restored by removing CO while the flow of H_2S was maintained. UTC does not indicate how much CO was present before the performance decay. As far as could be determined by electrochemical measurements and transmission microscopy, the anode showed no permanent damages from the test.

In an earlier UTC test in which the anode gas contained 500 ppm H_2S, there was less than 1% performance loss (King, 1976).

At a more fundamental level, Binder, et al.,(1969) found that H_2S is more strongly adsorbed on Pt than CO is. Interestingly, when a Pt electrode was covered with S, its anodic oxidation of CO to CO_2 was much faster than that of the same electrode without S coverage. Binder, et al., also noted that under open-circuit conditions the shift reaction:

$$CO + H_2O \rightleftharpoons CO_2 + H_2$$

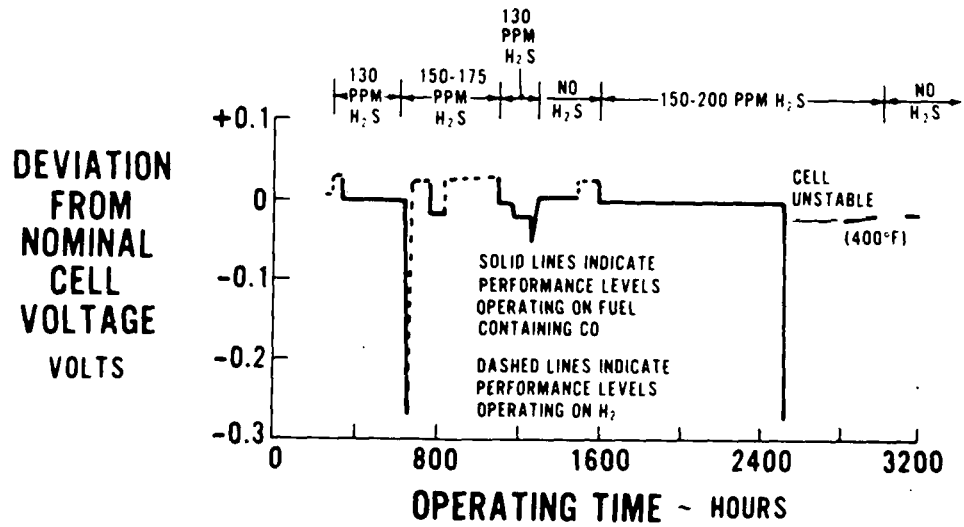

Fig. 5-1. H_2S tolerance of phosphoric acid cell.

occurred at a high rate on Pt covered with S, whereas on pure Pt, the reaction was very slow. The measurement was made at 90°C and in 3N H_2SO_4. Table 5-1 lists the results of this test. Since the equilibrium of the shift reaction at 90°C lies entirely on the side of $CO_2 + H_2$, the results imply that the shift reaction was far from being at equilibrium. Still, it is interesting to note the difference in H_2 generation between pure Pt and S-covered Pt; 1.3% of feed CO was converted to H_2 in the case of pure Pt, compared with 12% in the case of the S-covered Pt.

Stonehart and Ross (1975) measured potentiodynamically the competing adsorption of CO and H_2 on a Pt electrode in 1M H_2SO_4 and showed that CO is much more strongly adsorbed than H_2. This is in agreement with their previous findings that H atoms on Pt can be displaced by adsorption of CO, while displacement of adsorbed CO by gaseous H_2 does not occur. These authors note that, in an aqueous electrolyte, CO chemisorbed on Pt is not oxidized to CO_2 because the reversible hydrogen ionization:

$$H_2 \rightleftharpoons 2H^+ + 2e^-,$$

even on the few Pt sites available, is so rapid that the surface potential of the catalyst is controlled by this reaction and is maintained at a value below the oxidation potential of CO. These references do not provide enough clues to explain the abrupt cell performance decays observed in the UTC test. Nevertheless, they indicate that adsorption of H_2S or CO on Pt is quite fast and that, if these impurities are present in sufficient quantities in the anode gas, their surface coverages may reach equilibrium within a matter of hours. For example, it can be estimated that, at 200 ppm H_2S, the hourly flow of anode gas contains a number of H_2S molecules that is about equal to the number of the surface Pt atoms in the anode cell. In this respect, the behavior of the UTC test cell, which included periods of steady operation lasting 300-900 hours followed by rapid decays, cannot be explained in terms of competing surface coverages by CO and H_2S. Instead, the decays are likely to have been the results of secondary effects. To answer what these secondary effects are requires, first of all, understanding of interplays of adsorbed species existing on the electrode surface. A great deal of work is needed in this area.

TABLE 5-1

Gas Composition (vol %) Before and After Shift Reaction of CO with H_2O on Platinum Electrodes Under Open-Circuit Conditions in 3N H_2SO_4 at 90°C

	Gas Inlet		Gas Outlet after Shift Reaction		
	CO	CO_2	H_2	CO_2	CO
With sulfur adsorbate	100	--	12.1	12.1	75.8
	50	50	12.2	56.1	31.7
	10	90	5.9	90.6	3.5
Without sulfur adsorbate	100	--	1.3	1.3	97.4

REFERENCES

Anderson, K. T., Fischer, F., Rostrup-Nielsen, J. R., and Wrisberg, J., U. S. Patent 3,872,179 (1975).

Bett, J. A. S., Boswell, R. F., Lesieur, R. R., Meyer, A. P., and Preston, J. L., UTC, "Evaluation of Advanced Fuel Processing Systems for Fuel Cells," National Fuel Cell Seminar, June 26-28, 1979, Bethesda.

Bett, J. A. S., Lesieur, R. R., McVay, D. R., and Setzer, H. J., UTC, "Adiabatic Reforming of Distillate Fuels," National Fuel Cell Seminar, July 11-13, 1978, San Francisco.

Binder, H., Kohling, A., and Sandstone, G., "The Anodic Oxidation of Carbon Monoxide and Formic Acid on Platinum Covered with Sulfur," Advances in Chemistry Series No. 90, "Fuel Cell Systems-II, 1969," p. 128.

Boswell, R. F., Sederquist, R. A., and Snopkowski, D. J., UTC, U. S. Patent No. 4,098,588, July 4, 1978.

Boswell, R. F., Sederquist, R. A., and Snopkowski, D. J., UTC, U. S. Patent No. 4,098,589, July 4, 1978.

Catalytica Associates, "Assessment of Fuel Processing Alternatives for Fuel Cell Power Generation," EPRI Report, EM-570, September 1977.

Catalytica Associates, "Overview of Fuel Processing Technologies for Fuel Cell Power Generation," Interim Report for DOE Contract EC-77-C-03-1384, 1978.

Handley, L. M., "Status of 40-KW and 4.8-MW Fuel Cell Programs," National Fuel Cell Seminar, June 26-28, 1979, Bethesda.

Henkel, H. J., Kostka, H., and Michel, A., "Autothermal Gasification of Liquid Hydrocarbons by Partial Oxidation," EPRI Fuel Processing Meeting, April 13, 1977, Palo Alto.

Houghtby, W. E., King, J. M., and Thompson, R. A., UTC, "Advanced Technology Fuel Cell Program," EPRI Report, EM-956, December 1978.

Houseman, J., Voecks, G., and Shah, R., Jet Propulsion Lab., "Autothermal Reforming of No. 2 Fuel Oil," EPRI Report, EM-1126, July 1979.

Isogai, et al., Mitsui Toatsu, Japan Patent No. 79-20003 (1979).

Kerr, G. R., Olesen, O. L., Sederquist, R. A., and Szydlowski, D. F., UTC, U. S. Patent No. 4,098,587, July 4, 1978.

Kikuchi, E., et al., "Steam Reforming of Residual Oils in the Fluidized Bed of Nickel-Dolomite Catalyst," ACS Meeting, April 1-6, 1979, Honolulu.

REFERENCES

King, Jr., J. M., UTC, "Advanced Technology Fuel Cell Program," EPRI Report, EM-335, October 1976.

King, Jr., J. M., UTC, "Advanced Technology Fuel Cell Program," EPRI Report, EM-576, November 1977.

Olsen, O. L., and Sederquist, R. A., UTC, "The UTC Steam Reformer," KTI High Temperature Processing Symposium, October 1979, Santa Barbara.

Rostrup-Nielsen, J. R., and Tottrup, P. B., "Steam Reforming of Heavy Feedstocks," Symposium on Science of Catalysis and Its Applications in Industry, February 22-24, 1979, Sindri.

Rostrup-Nielsen, J. R., private communication, June 1979.

Sederquist, R. A., UTC, U. S. Patent No. 4,071,330.

Sederquist, R. A., UTC, "Evolution of Steam Reformers for Commercial Fuel Cell Power Plants," KTI Symposium for Reformers and Hydrogen Plants, March 1978, Santa Barbara.

Stonehart, P., and Ross, Phillip N., "The Commonality of Surface Processes in Electrocatalysis and Gas Phase Heterogeneous Catalysis," Catalysis Reviews - Science and Engineering, Volume 12, p. 1, Dekker, Inc., 1975.

Tio, T., Jones, R., and Minet, R., KTI Corporation, and Ushiba, K., Mahawili, I., and Levy, R., Catalytica Associates, "Assessment of Fuel Processing Systems for Dispersed Fuel Cell Power Plants, EPRI Report, EM-1010, March 1979.

Tomita, T., Kikuchi, K., Sakamoto, T., and Shinjo, T., "Gasification of Heavy Hydrocarbons with Calcium Aluminate Catalyst," ACS Meeting, April 1-6, 1979, Honolulu.

Tomita, T., "The THR Process by Toyo Engineering," High Temperature Processing Symposium, sponsored by Kinetics Technology International Corp., October, 1979, Santa Barbara.

Tomita, T., and Kitagawa, M., "A New Steam Reforming Process of Heavy Hydrocarbons," presented at European Meeting of Chemical Engineering, ACHEMA 76, 18th Chemical Congress and Exhibition, Frankfurt, 1976.

Topsøe, Haldor, A/S, "RKN Reforming," Hydrocarbon Processing, April 1979, p. 166.

Yarrington, R. M., "Catalytic and Process Development for the Hydrogen Preparation from Future Fuel Cell Feedstocks," DOE Fuel Cell Contractors Meeting, April 1979, Argonne National Lab.

Yoshida, et al., Japan Patent No. 52-138504 (1977).

APPENDIX A

I. INTRODUCTION

Poisoning of supported metal catalysts by sulfur compounds poses serious problems in a number of important processes, including steam reforming of sulfur-containing fuels. Sulfur apparently bonds strongly to metal surfaces, substantially reducing their catalytic activity. Even at sulfur impurity levels of only a few ppm, catalyst life may be reduced to only a few months or weeks. Because of the essentially irreversible adsorption of sulfur compounds on metals, regeneration is usually impossible or impractical.

In spite of its industrial importance, sulfur poisoning has received only moderate attention in previous scientific investigations and in the literature. The most recent comprehensive review of the literature dealing with poisoning of metals was Maxsted in 1951 (1). Madon and Shaw (2) reviewed the pre-1970 literature on the effects of sulfur in Fischer-Tropsch synthesis; some of this information is applicable to other reactions, including steam reforming.

In this section, we briefly review the more recent literature dealing with sulfur poisoning of metals, with the purpose of highlighting areas in which significant contributions have been made or could be made. The discussion is focused on several fundamental questions that emphasize the present lack of understanding and the need for further research:

- What is the nature of sulfur-metal bonding on surfaces? How is it affected by metal crystallite size, metal-support interactions, and metal or metal oxide promoters?
- How strong are surface metal-sulfur bonds? Under what conditions of temperature and partial pressure do sulfur compounds adsorb reversibly?
- What is the mechanism of sulfur poisoning in steam reforming and related reactions? Is it possible to predict catalyst life on the basis of such mechanisms or models?
- Is it possible to regenerate sulfur-poisoned catalysts?

II. THE NATURE OF METAL-SULFUR BONDS

Because sulfur has a lower electronegativity than oxygen (3), metal sulfides tend to be much more covalent than metal oxides; indeed,the sulfides occur often as nonstoichiometric phases, some with semimetallic behavior. Only the more electropositive elements, alkalies, and alkaline earths form sulfides that appear to be mainly ionic. Maxsted (1) suggested that sulfur compounds chemisorb on transition metals by forming bonds in which previously unshared electrons in the sulfur atom are shared in the d-orbitals of the metal. According to Kishi and Roberts (4) this diminishes the potential of the metal surface for back-bonding other molecules. That nonionic metal-sulfur bonding occurs on transition metal surfaces is suggested by recent *ab initio* calculations (5, 6) showing the net charge transfer between nickel and sulfur in two-dimensional sulfides to be 0.4 to 0.6 electron per sulfur atom. Such theoretical calculations appear to have considerable promise in revealing more about surface metal-sulfur bonds.

The thermodynamic properties of bulk metal sulfides are fairly well documented (7-13). The nickel-sulfur system, for example, shows many phase transitions and bulk phases, at high temperatures and large concentrations of H_2S (7-10). Data from Rosenquist in Figure A-1 show that, at temperatures of catalytic interest (400-600°C), nickel exists in the metallic state only at P_{H_2S}/P_{H_2} values of 10^{-3} to 10^{-4} and below. At higher H_2S concentrations, the bulk sulfide Ni_3S_2 is formed. Similar behavior is observed for iron-, cobalt-, and other metal-sulfur systems of catalytic interest. Thus, in steam reforming of fuels of high sulfur content, H_2S concentrations may be high enough to cause bulk sulfide formation in the metal catalyst. Generally the levels of H_2S encountered in processing of low sulfur fuels are in the ppm range; therefore, surface, rather than bulk, sulfides are formed.

Among the metals commonly used as catalysts, Co, Fe, Ni, Pt, Rh, and Ru have low free energies of formation of their bulk sulfides, indicating that relatively large gas-phase H_2S concentrations are necessary to maintain the bulk sulfides of

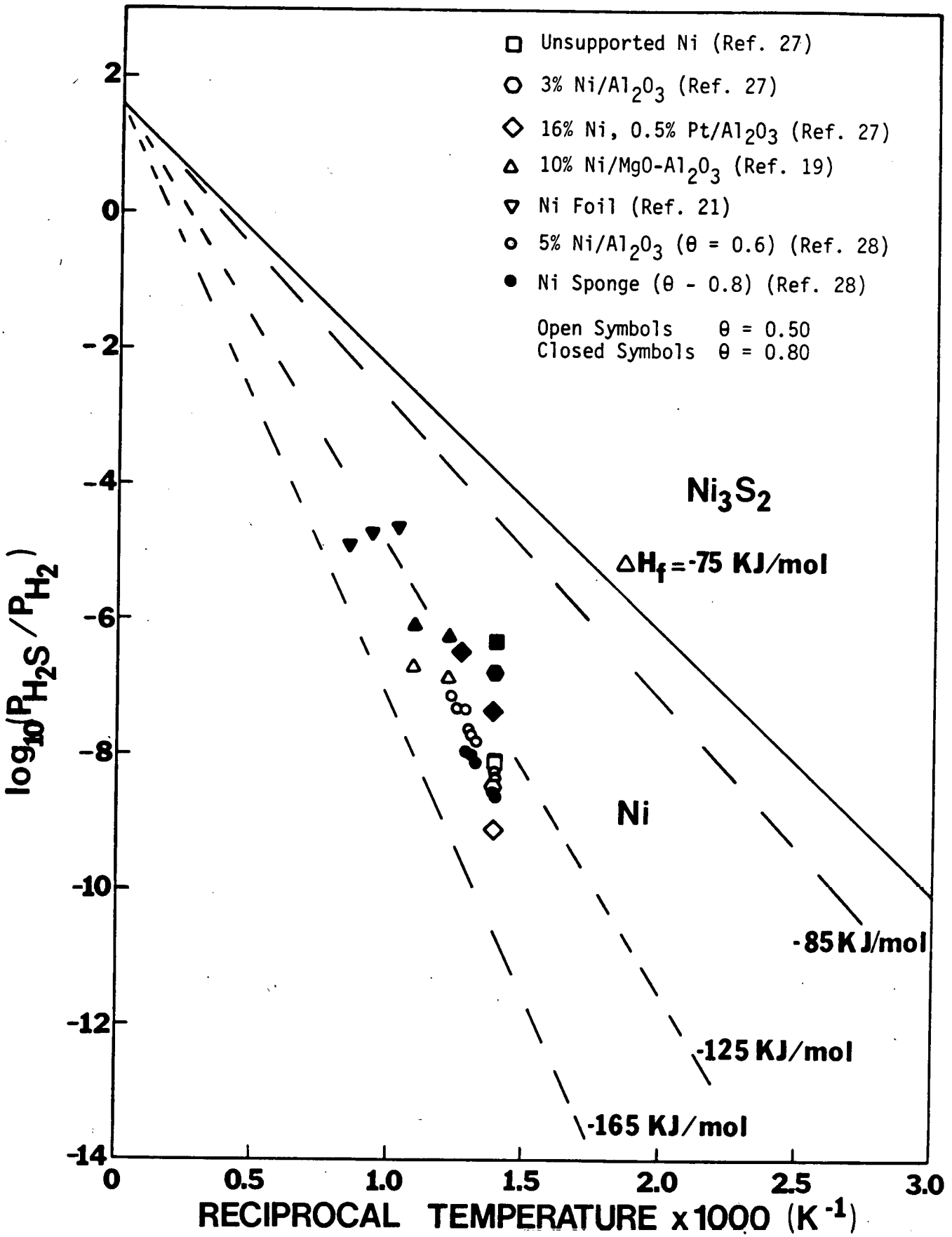

Fig. A-1. Equilibrium partial pressure of H_2S vs reciprocal temperature.

these metals. Sulfides of metals such as Cr, Mn, Mo, Re, Ti, V, W, Zn, and Zr have much higher free energies of formation. This suggests that sulfur-poisoning of one metal may be reduced by alloying it with another metal having a higher free energy of formation of the bulk sulfide. Indeed, Cr (14) and Mo (15) impart sulfur resistance to Ni.

III. ADSORPTION OF SULFUR COMPOUNDS ON METALS

A. Nickel

1. Stability of Adsorbed Sulfur

Nickel has been the most commonly studied metal for sulfur adsorption, and H_2S the most studied sulfur compound. Previous adsorption studies on polycrystalline films, powders, and supported nickel (16-29), and more recent studies on single crystal nickel (30-42), provide a great deal of insight into the fundamental mechanisms of surface nickel-sulfur compound interactions and of poisoning.

A number of early studies (5, 20, 27-29, 32, 33) suggest that the surface nickel-sulfur bond is more stable than the bulk nickel-sulfur bond. If so, the heat of adsorption should be larger than the heats of formation for bulk phases. In recent, definitive investigations, Oliphant et al. (27) and McCarty et al. (28) obtained heats of H_2S adsorption on polycrystalline Ni powders and on supported Ni from desorption isosteres and adsorption isosteres, respectively. Their two sets of data agree remarkably well, as shown in Table A-1. Since, according to these data, the heats of adsorption for H_2S on various forms of nickel may range from 130-160 kJ/mole, the enthalpy of adsorption is 55-85 kJ/mole more exothermic than is the enthalpy of formation of Ni_3S_2 of 75 kJ/mole.

The extent to which H_2S adsorption on Ni is reversible at various temperatures and concentrations, although a subject of obvious importance in regard to poisoning, has received only modest experimental scrutiny (19, 21, 27-29). Nevertheless, equilibrium adsorption and desorption isotherms at various temperatures (19, 27, 29) and isosteres (28) from these studies have established the concentrations at which less than saturation coverage is observed for a given temperature. For example, the isotherms of Oliphant et al. (27) in Figure A-2 reveal that, in the temperature range of 450-500^{o}C, less than saturation coverage (i.e., reversible adsorption) occurs on the Ni surface only at concentrations less than 1-2 ppm H_2S.

TABLE A-1

Experimental Heats of H_2S Adsorption on Metals
Compared with Heats of Formation for Bulk Sulfides

Metal	Temp., (°C)	Crystallographic plane	$-\Delta H_{ad}$[a] (kJ/mole S)	Method	Ref.	ΔH_f[b] (kJ/mole S)
Ag	300-450	(111)	114	Isotherms in H_2S/H_2	54	96 (Ag_2S)
	300-450	(100)	122			
	300-600	(110)	139			
Fe	850	Polycrystal	188	Isotherms in H_2S/H_2	63	150 (FeS)
Mo	1050-1150	(110)	215	Desorption	51	180 (Mo_2S_3)
Ni	450-500	Polycrystal	134	Desorption	27	75 (Ni_3S_2)
	450-500	16% Ni/Al_2O_3	150			
	450-500	Sponge	144	Ads. isostere	28	
	450-500	5% Ni/Al_2O_3	143			
Pt	900-1100	(111)	169	Desorption	72,73	138 (PtS)
		(100)	198			

[a] Per mole of H_2S.

[b] Per mole of S; corresponding to $(x/y)M + 1/2\ S_2 = (1/y)\ M_xS_y$.

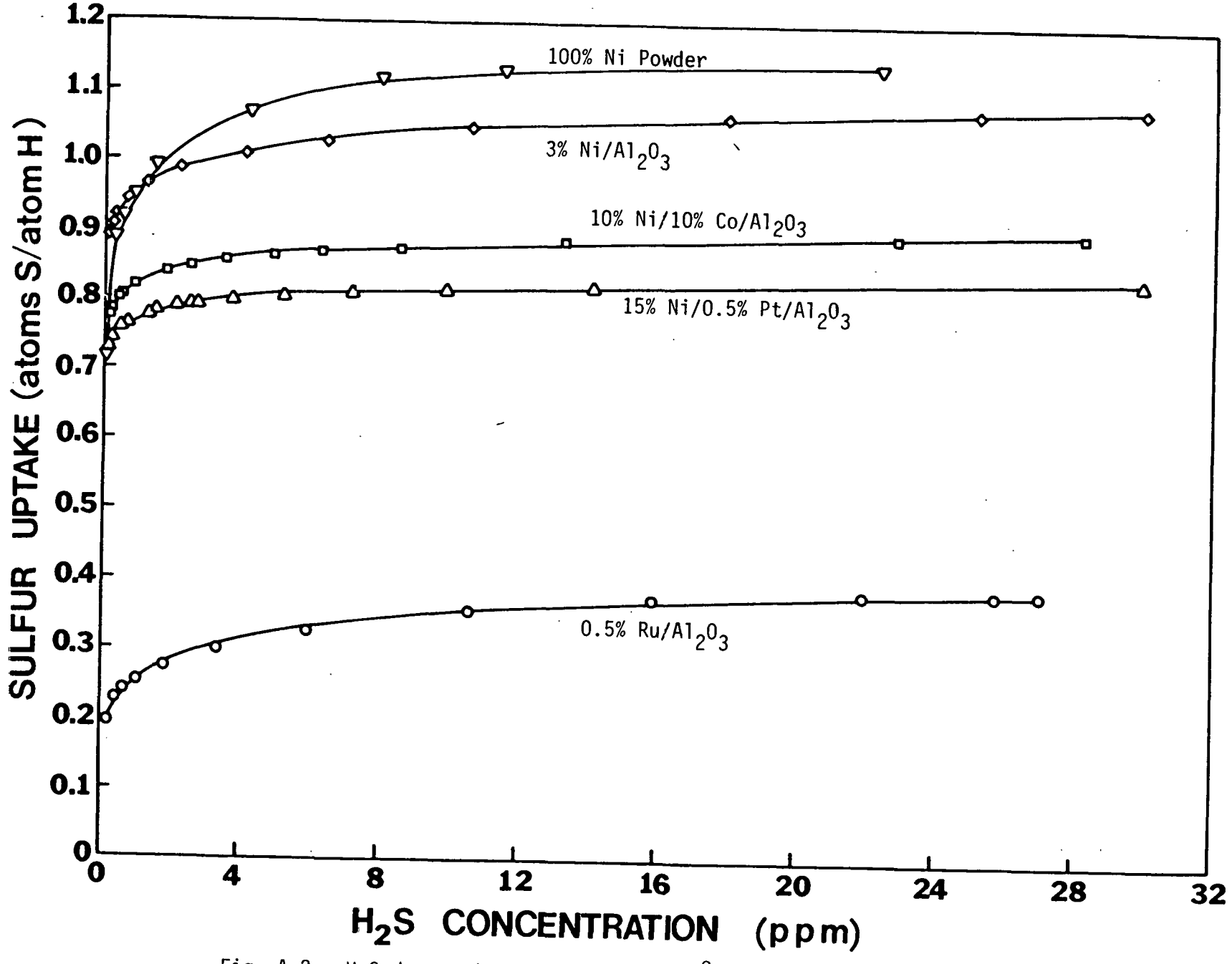

Fig. A-2. H_2S desorption isotherms at 450°C normalized to H_2 uptake.

The incredible stability of adsorbed sulfur is further demonstrated in Figure A-1, in which most of the early equilibrium adsorption data for Ni (19, 21, 27, 28) are represented on a single plot of ln (P_{H_2S}/P_{H_2}) as a function of reciprocal temperature. The solid line corresponds to the equilibrium data reported by Rosenqvist (7) for formation of Ni_3S_2 (in the temperature range 400 to 535°C). On the basis of equation

$$\Delta G^0 = RT \ln (P_{H_2S}/P_{H_2}) = H - T\Delta S \qquad (A\text{-}1)$$

the slope of this line is $\Delta H/R$, where ΔH = -75 kJ/mole and the intercept is a $-\Delta S/R$. The dashed lines in Figure A-1 represent equilibrium lines for chemisorbed sulfur with heats of adsorption of 85, 125, and 165 kJ/mole, assuming formation of Ni_3S_2 (i.e., the same intercept as the solid line for Ni_3S_2). Thus, according to these data, the enthalpy of adsorption of H_2S on Ni is 50-100 kJ/mole more exothermic than the enthalpy of formation of Ni_3S_2, depending on temperature and coverage. It is also apparent that the absolute value of the heat increases with decreasing coverage and that the equilibrium partial pressure of H_2S increases with increasing temperature.

From these data in Figure A-1 it is also possible to estimate the equilibrium partial pressure of H_2S at any given temperature for fractional coverages ranging from 0.5 to 0.8. For instance, at 450°C and θ = 0.5, the values of P_{H_2S}/P_{H_2} range from about 10^{-8} to 10^{-9}. In other words, half coverage obtains at 1 to 10 ppb H_2S, a concentration range at the lower limit of our present analytical capability! At the same temperature (450°C) almost complete coverage (θ = 0.9) obtains at values of P_{H_2S}/P_{H_2} of 10^{-8} to 10^{-6} (0.01 to 1 ppm) or in other words, at the H_2S concentrations encountered in many catalytic processes after the gas has been processed to remove sulfur compounds.

In view of the stability of adsorbed sulfur on Ni, it would be desirable to find modifiers (supports or additives) that would either (a) change nickel's sulfur adsorption properties in the direction of greater reversibility and/or (b) would enhance its sulfur adsorptive capacity substantially. Only two investigations thus far have directly explored these possibilities. Oliphant et al. (27) found that Pt- and Co-promoted Ni/Al_2O_3 evidenced slightly lower H_2S adsorptive capacities than did Ni/Al_2O_3 that was not promoted (see Figure A-2), although the adsorption isotherms for the bimetallics indicated about the same degree of reversibility as did those for Ni/Al_2O_3. Fowler and Bartholomew (29) found a significantly greater sulfur adsorption capacity for Mo-promoted Ni/Al_2O_3 than for nonpromoted Ni/Al_2O_3, although the adsorption of H_2S on the Mo catalysts was about as strong as that on Ni/Al_2O_3. Thus, these investigators were not successful in promoting more reversible adsorption of H_2S on Ni; however, the discovery of enhanced adsorption capacity in Ni/Mo catalysts is significant. Further investigation of the effects of metal and oxide promoters on adsorption properties of H_2S on Ni and other metals is an important area deserving further attention.

2. Adsorption Mechanisms

The interaction of H_2S (and organic sulfides) with metals may include a number of consecutive steps: reversible molecular adsorption of H_2S, dissociation, reconstruction of the metals surface to a two-dimensional metal sulfide, and incorporation into the bulk (at sufficiently high P_{H_2S}/P_{H_2} ratios) to form a three-dimensional metal sulfide. Unfortunately, little information is available, especially of a quantitative nature, regarding the kinetics of these various steps for the nickel/sulfur system. Apparently the incorporation of sulfur into nickel at $P_{H_2S} = 1$ atm occurs slowly at room temperature, diffusion through the sulfide layer controlling the rate (16). Rates of adsorption of H_2S on copper (28, 44, 45) are very rapid; the high sticking probability suggests that no barrier to adsorption and dissociation exists until the surface is saturated. Accordingly, sulfur poisoning of metals is not likely to be limited by rates of adsorption and reaction on the surface. Thus, surface coverages of sulfur can be predicted by equilibrium thermodynamics under most conditions of catalytic interest, although the same is not true of bulk sulfide formation, for which

the rate depends very much on the temperature and on the partial pressure of H_2S. In view of the lack of quantitative data for H_2S adsorption and absorption rates on Group VIII metals, additional research would be desirable.

Most of the early work (16-19, 21-29) suggests that H_2S completely dissociates on nickel surfaces, even below room temperature, although there is obvious disagreement regarding the number of nickel atoms per sulfur atom. Saleh et al. (16) suggested a three-site mechanism in the temperature range of 80-100°C:

$$H_2S_{(g)} + \text{-Ni-Ni-Ni} \rightarrow \begin{matrix} H & S & H \\ | & | & | \end{matrix} \text{-Ni-Ni-Ni-} \quad , \qquad \text{(A-2)}$$

whereas Den Besten and Selwood (17) inferred from magnetic measurements at 0-120°C that H_2S forms four bonds with the nickel surface:

$$G_2S_{(g)} + \text{-Ni-Ni-Ni-Ni} \rightarrow \begin{matrix} H & & S & & H \\ | & & / & \backslash & | \end{matrix} \text{-Ni-Ni-Ni-Ni} \, . \qquad \text{(A-3)}$$

They also found that, at high coverages, sulfur displaces hydrogen from the surface. In a more recent magnetic study of Ni/SiO_2, Ng and Martin (25, 26) also reported that H_2S adsorbs at room temperature,with initially four Ni surface atoms being involved in the bond formation for every H_2S molecule adsorbed; at P_{H_2S} of 1 atm, deeper layers of Ni are subsequently attacked. Rostrup-Nielsen (19) suggested a one-site mechanism at higher temperatures (550-650°C):

$$H_2S_{(g)} + Ni_{(s)} \rightarrow Ni\text{-}S_{(s)} + H_{2(g)} \qquad \text{(A-4)}$$

on the basis of obtaining a value of 1 for the power, n, in a Langmuir fit for his data. Oliphant et al. (27), on the other hand, obtained Langmuir exponents of 2.9 and 2.7 for Ni powder and 3% Ni/Al_2O_3, respectively, at 450°C, consistent with a three-site mechanism. The data of Oliphant et al. (27) are considered to be more reliable than those of Rostrup-Nielsen (19), since their desorption isotherms, each determined from a single sample, evidence considerably less scatter than does Rostrup-Nielsen's

adsorption isotherm, each point of which corresponds to a different sample. Accordingly, the three-site mechanism is favored, at least at high temperatures (400-600^{o}C).

Although infrared spectroscopy cannot provide direct information on metal-sulfur bonds, IR studies of the adsorption of sulfur compounds on supported Ni (18, 25, 47) and evaporated Ni films (23, 48) have supplied limited indirect mechanistic information. For example, the complete absence of S-H or C-S stretching frequencies when H_2S and CS_2 are adsorbed on Ni (23, 25) provides indirect evidence for the dissociative mechanism. Similarly, the absence of IR bonds for methyl mercaptan adsorption on Ni (23) is likewise interpreted in terms of dissociation of C-S and S-H bonds, consistent with the observations of Saleh et al. (49) of metal sulfide formation, accompanied by evolution of hydrogen, methane, and dimethyl sulfide. Mercaptans involving higher-molecular-weight hydrocarbons (23, 25, 47, 48) are generally believed to adsorb at room temperature as mercaptide structures, through dissociation of the H-S bond -- the C-C and C-S bonds remaining intact. Heating to 80^{o}C, however, decomposes the mercaptide, with formation of the corresponding olefin and a sulfided surface (48). IR data suggest that dimethyl sulfide adsorbs nondissociatively at room temperature (49), in accordance with the earlier results of Den Besten and Selwood (17). In the case of thiophene adsorption, the IR results are inconclusive, as the spectra for thiophene on SiO_2 and Ni/SiO_2 are the same (25).

3. Surface Structures

Significant advances during the past decade in surface-analysis techniques, such as low-energy electron diffraction (LEED) and Auger electron spectroscopy (AES), enable geometric structures of crystal faces and adsorbed atoms to be determined. A number of recent surface studies (21, 30-43) have provided useful information regarding structures of sulfur adsorbed on Ni. During the initial stages of sulfur adsorption on clean Ni single-crystal surfaces, sulfur atoms reside in high-coordination sites, i.e., the atomic hollows of the surface (21, 30-33). For example, on a Ni(100) surface, sulfur is adsorbed in an ordered layer with a p(2x2) overlayer, with each sulfur atom being bonded to four Ni atoms, up to θ = 0.25,

and from θ = 0.25 to 0.5, with a c(2x2) overlayer, with each sulfur atom being bonded to two Ni atoms. The adsorption of sulfur on Ni(111) and Ni(110) is apparently more complicated (21, 31, 36-38); the evidence suggests that sulfur restructures the nickel surface. For example, on clean Ni(111), a p(2x2) structure was observed at $\theta < 0.25$. At slightly higher coverages ($0.25 < \theta < 0.33$), the structure changed to a $\sqrt{3} \times \sqrt{3}$ R 30° pattern, with each sulfur atom being bonded to three Ni atoms in three coordination sites. As the surface coverage of sulfur increased beyond 1/3 monolayer, the surface of the Ni(111) was reoriented to a (100) layer, adsorbing more sulfur. Only surface Ni atoms underwent rearrangement, the bulk maintaining its (111) symmetry. It was found that sulfur is adsorbed on, and not incorporated into, the rearranged layer of surface Ni atoms. Edmonds and co-workers (36-38) speculate that the strong Ni-S interaction weakens the bonding between the surface and the next lower Ni layers, thereby permitting rearrangements of the surface Ni atoms. Indeed, the weakening of Ni-Ni bonds in cluster complexes by sulfur ligands does occur (39). The change from fourfold to twofold coordinated sulfur bonding as a function of increasing sulfur coverage implies that the adatom-adatom interactions are strong enough that subsequent adsorption requires modification of the bonding of preadsorbed atoms. The fact that the sulfur must modify its bonding to the Ni to allow further sulfur adsorption also implies that as one covers the surface, strong restraints are put on further adsorption of any sort.

Since poisoning by sulfur usually involves complete coverage, the surface structures under these conditions are of great interest. For all three low-index faces of Ni, the Ni surface saturated with sulfur corresponds to one sulfur atom for every two surface Ni atoms, and has a c(2x2) overlayer structure. A general conclusion is that the Ni-S bond lengths found on all surfaces are smaller than those occurring in stable Ni-S bulk compounds (5, 30, 32). This is further evidence that adsorbed sulfur is bonded to Ni more strongly than is sulfur in a bulk Ni sulfide. Indeed, ΔH_f is estimated to be -240 kJ/mole for sulfur bonded in a bridge position to Ni (5), compared with -74 kJ/mole for bulk Ni sulfide.

4. Adsorption Stoichiometries

There is apparently only fair agreement as to the stoichiometry of H_2S adsorption on Ni. The reasons for this are twofold: (1) the stoichiometry apparently depends on surface coverage, which in turn depends on P_{H_2S}, and (2) the stoichiometry varies with temperature, as desorption of hydrogen occurs more readily with increasing temperature, freeing sites for sulfur adsorption.

Evidence for the first observation was discussed in the previous subsection. Indeed, the studies of single-crystal Ni, obtained for the most part at very low P_{H_2S} values, show that the number of sulfur atoms adsorbed per Ni surface atom (S/Ni_s) ranges from 0.25 to 0.5. Based on adsorption studies at high P_{H_2S} (10 ppm - 1 atm) on polycrystalline or supported Ni, S/Ni_s values range from 0.25 to 0.33 at room temperature (16, 17, 25) to as high as 0.75-1.0 at 450-600°C (19, 27, 29). *A priori*, it is reasonable to expect that, at most, about 0.6 to 0.7 atom of sulfur chemisorbs on a clean Ni surface in view of the relative areas of about 0.10 and 0.065 $(nm)^2$/atom for S and Ni atoms, respectively.

These apparent discrepancies can be resolved as follows. First, the values of S/Ni_s of 0.25 and 0.33 (16, 17, 25) are observed at the lower temperatures (-78 to 25°C) because hydrogen atoms from the dissociative chemisorption of H_2S bond irreversibly with Ni sites, and thereby prevent further sulfur adsorption. Since at higher temperatures, the chemisorption of hydrogen is reversible, sulfur atoms can cover most or all of the Ni sites, and thus higher S/Ni_s ratios are possible.

The near-unity values of S/Ni_s observed by Oliphant et al. (27) for both supported and unsupported Ni on desorption after saturation at 25-30 ppm can be explained by a surface reconstruction at the higher concentration range. Accordingly, the authors hypothesized that, at H_2S concentrations less than 10 ppm, atomic sulfur is chemisorbed on the Ni surface up to a coverage of S/Ni_s = 0.7-0.8, consistent with Ni_3S_2 stoichiometry; however, saturation at 25-30 ppm with subsequent desorption is accompanied by a reconstruction of the surface to a surface sulfide of Ni, consistent with NiS stoichiometry.

This hypothesis is supported by the observation of a hysteresis effect for adsorption and desorption, characterized in part by a trend of increasing saturation coverage with increasing H_2S concentration for single equilibrium adsorption points.

B. Other Metals

The adsorption of H_2S on Group VIII and Ib metals (50,51) and in particular on Ag (52-54), Cu (44, 45, 55-58), Fe (23, 50, 59-64), Mo (51, 65-67), Ru (27, 68), and Pt (51, 69-75) results in surface metal sulfides having qualitatively similar structures and stability to those of Ni. Data showing that the metal-sulfur bond at the surface is generally more stable than in the corresponding bulk metal sulfide are summarized in Table A-1. Indeed, the heats of adsorption are 20-40% larger than the heats of formation of the most stable bulk sulfides. The data also show that sulfur is generally more strongly bonded on the more atomically rough metal planes. Dissociative adsorption of H_2S on metals (50, 59, 61, 68, 71, 74, 76) and restructuring of the metal surface by adsorbed sulfur (44, 45, 50, 51, 58, 61, 62, 69, 70) are also general phenomena. Kinetic studies (44, 71) reveal, in the case of Cu and Pt, two adsorption regimes; at $\theta < 0.5$-0.6 the adsorption occurs rapidly with a high sticking coefficient. However, at $\theta > 0.6$ the adsorption occurs slowly with a low sticking coefficient. This interesting behavior may result from surface reconstruction and/or a change in the mechanism of adsorption involving more weakly bound and less dissociated species at high coverages. Further investigation of this phenomenon would be worthwhile. Generally, further investigation of the kinetics and thermodynamics of H_2S adsorption on catalytic metals is needed. Since adsorption of H_2S on Co, Pd, Rh, and Ru has received very little or no attention, the investigation of these important catalytic metals should have a high priority.

IV. EFFECTS OF SULFUR ON ADSORPTION OF OTHER MOLECULES

Since one of the necessary steps in a heterogeneous reaction is the adsorption of one or more of the reactants, investigation of the effects of adsorbed sulfur on the adsorption of other molecules can reveal a great deal about the poisoning process. Particularly the effects of sulfur poisoning on CO and H_2 adsorption on metals are of interest, not only because these molecules participate in numerous reactions, but in addition, because they are used as selective titrants to measure metal surface area.

A. Nickel Catalysts

1. Effects on Hydrogen Adsorption

Results of previous investigations (15, 26b, 29, 77-84) show that hydrogen adsorption on nickel at room temperature is lowered by preadsorbed sulfur. Moreover, the fraction by which hydrogen adsorption is reduced is generally proportional to the fractional coverage of sulfur, although some of the data suggest a larger than linear reduction of metal surface area with increasing sulfur coverage during the initial stages of poisoning. This is illustrated by data in Figure A-3. Rendulic and Winkler (84) have shown a similar linear decrease in the initial sticking coefficient of hydrogen with increasing sulfur coverage. At maximum sulfur coverage, the sticking coefficient is virtually zero. Accordingly, H_2 adsorption at 25°C on partially sulfur-poisoned catalysts provides an accurate measure of the unpoisoned nickel surface.

2. Effects on Carbon Monoxide Adsorption

The effects of sulfur poisoning on the adsorption of CO on nickel (23, 26, 48, 77-81, 83, 85-91) are very complex; the nature of the adsorbed species and the adsorption stoichiometry vary considerably with changes in pressure, temperature, and sulfur coverage. For example, IR data (25) show that bridged bonding is diminished and subcarbonyl bonding enhanced by sulfur. Moreover, there are significant differences in the behavior of supported and unsupported Ni (80, 83). In fact, in the case of supported nickel catalysts, very significant increases in CO adsorption are observed at -80 to 25°C and moderate pressures (100-400 Torr) after treatment with

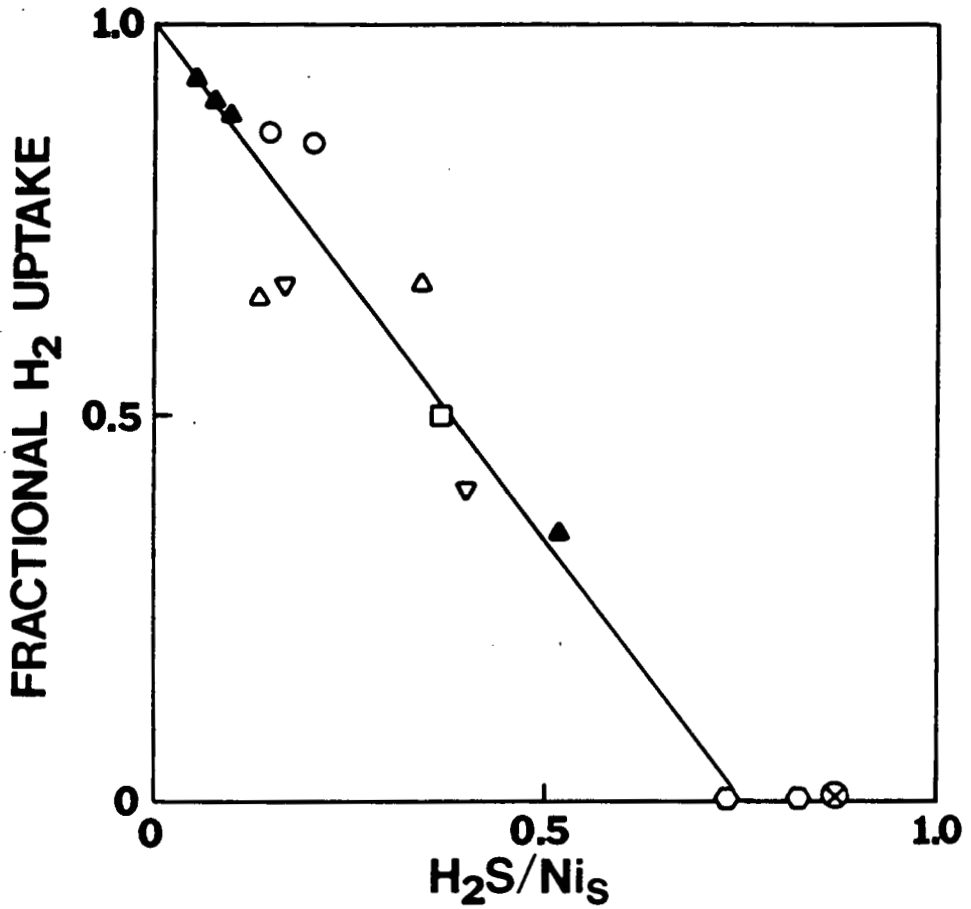

Fig. A-3. Fractional H_2 uptake vs H_2S coverage in molecules of H_2S per nickel surface atom. ▽Ni powder (INCO), ○14-16% Ni/Al_2O_3 washcoat/monolith, △3, 8, 14, and 23% Ni/Al_2O_3, □14% Ni/Al_2O_3, ⊗3% Ni/Al_2O_3, ⬡3% Ni/Al_2O_3. Open symbols: 5 or 10 ppm H_2S; closed symbols: 25 ppm H_2S; ⊗50 ppm H_2S.

H_2S (77-81, 83), apparently as a result of sulfur-catalyzed $Ni(CO)_4$ formation (83, 92). However, at low CO pressures (less than 1 Torr), sulfur completely inhibits room-temperature CO adsorption at $\Theta_S > 0.3$ (90). On the other hand, under high-temperature reaction conditions representative of methanation (200-400°C, 1 atm, P_{CO} = 5-10 kPa, $H_2/CO = 3$), dissociative adsorption of CO occurs on a completely poisoned Ni/Al_2O_3 catalyst, the extent of which is about 50% of that observed for an unpoisoned catalyst (91). These incredible differences in behavior at different pressures and temperatures emphasize the importance of investigating effects of sulfur poisoning under conditions representative of the particular process of interest.

3. Effects on Adsorption of Other Molecules

Since sulfur poisoning is known to modify selectivity properties in a number of hydrocarbon reactions, investigation of the effects of preadsorbed sulfur on the adsorption of organic molecules on metal catalysts may provide the basis for understanding this behavior. The only reported research on hydrocarbons is that of Ng and Martin (26b) dealing with acetylene and benzene adsorption on presulfided Ni/SiO_2. The volumetric, adsorption, and saturation magnetization data for these compounds reveal a more complex behavior than that of either H_2 or CO. Both acetylene and benzene adsorb on presulfided Ni/SiO_2 at room temperature; these results suggest interactions of the hydrocarbons with deeper nickel layers. Perhaps the most significant observation from this study is that preadsorbed H_2S inhibits the cracking of hydrocarbons on nickel.

That only one investigation (26b), so far, has considered the effects of sulfur poisoning on the adsorption of organic molecules, and only one study (93), poisoning of the adsorption of O_2 on nickel, strongly suggests the need for further research. A number of important molecules are suggested by considering some of the important reactions in which nickel catalysts are poisoned by sulfur, e.g., ethylene (hydrogeneration), methane (steam reforming), and cyclohexane (hydrocracking). Moreover, the study of poisoning of H_2 and CO adsorption by various sulfur compounds should be of high priority, since only one investigation (25) has considered such effects.

B. Other Metals

Relatively few studies (16, 67, 71, 77-79, 81, 84, 94-99) have examined the consequences of sulfur poisoning on the adsorption of other molecules on metals other than Ni. Generally, it appears that adsorptions of hydrogen, oxygen, and CO are prevented by adsorbed sulfur. For example, Bonzel and Ku (71a) reported a decrease in the binding energy of CO on the Pt(110) surface with increasing sulfur coverage; at Θ_S = 0.75, no CO was adsorbed. Bartholomew and co-workers (77-79, 81) reported that hydrogen uptakes for nickel bimetallics and ruthenium were generally decreased in proportion to sulfur coverage. Unfortunately, in most of the previous work, quantitative relationships between the coverage of sulfur and decrease in adsorption for a given adsorbate were not obtained. Thus, determination of the quantitative effects of sulfur on adsorption of reactants on metals is obviously a potentially fruitful area for further research.

V. EFFECTS OF SULFUR ON ACTIVITY/SELECTIVITY PROPERTIES OF METALS DURING REACTION

A. In Steam Reforming

Conventional nickel reforming catalysts are very sensitive to poisoning by sulfur compounds, suffering significant losses in activity at concentrations greater than 1-20 mg S/m^3 (100-105). Since organic sulfides are present in conventional reforming feedstocks such as natural gas and naphtha at levels as high as 300-500 ppm and at much higher levels in heavy oils and resids under consideration as potential feedstocks, desulfurization of the feed is essential before it is reacted over conventional catalysts. Organic sulfur compounds remaining in the feed after desulfurization are readily hydrogenated to H_2S under typical reforming conditions; thus, it is sufficient to consider poisoning by H_2S.

Adsorption studies of H_2S on nickel (summarized in Fig. A-1) indicate increasing reversibility of sulfur adsorption with increasing temperature. Since the reforming process is carried out at high temperatures (400-850°C), poisoning by sulfur should be somewhat reversible; indeed, the reversibility was demonstrated by Morita and Inoue (101-102), who found that nickel catalysts regained initial activity after removal of sulfur compounds in the feed. At any given temperature, there was a threshold concentration below which no detectable poisoning was observed.

Sulfur threshold concentrations determined by Morita and Inoue (101-102) and other workers (100-103) for outlet temperatures of 800-900°C are listed in Table A-2 and compared with equilibrium adsorption data from Figure A-1 for $\Theta_S = 0.5$. The agreement among experimental values, and of experimental values with predicted values from Figure A-1 at the same temperature, is generally good, which suggests that the reversibility of sulfur poisoning during reforming is a predictable consequence of equilibrium adsorption of H_2S. Accordingly, the poisoning effect of sulfur in reforming may be ascribed to blocking of the nickel surface.

This hypothesis is confirmed by the data of Rostrup-Nielsen (104, 105) listed in Table A-3, showing the effects of sulfur poisoning on the

TABLE A-2

Sulfur Threshold Levels[a] in Steam Reforming, ppm

Catalyst	Catalyst exit temp., °C			Ref.	Comments
	800	850	900		
14-25% Ni (ICI)	0.7	3.5	18	103	Full-scale reforming; catalyst temp., 400 to T°C
4.4% Ni	1.4	--	--	101,102	Isothermal bed
26% Ni	3	11	--		
Various Ni catalysts	7	14	21	100	Experimental concentrations based on equilibrium gas composition for: $CO + 3H_2 \rightleftharpoons CH_4 + H_2O$
Various Ni catalysts	3	7	16	Fig. A-1	P_{H_2S}/P_{H_2} values from Fig. A-1 based on extrapolation of equilibrium adsorption data at $\theta_S = 0.5$ for temperature shown.

[a]Threshold concentrations below which there is no measurable loss of activity at the temperature shown in ppm (V_{H_2S}/V_{CH_4}); 0.7 ppm (V/V) = 1 mg S/m^3 (STP).

TABLE A-3

Influence of Sulfur Poisoning on Specific Activity in Steam Reforming of Ethane on 25% Ni/Al_2O_3MgO (500°C, 31 atm, $H_2O/C = 4$)[a]

Sulfur content in wt, ppm	Sulfur coverage	Reaction rate, mole/g·h x 10	Reaction rate, mole/m^2 Ni·h x 10^3
80	<0.1	2.41	120
239	0.30	0.66	62
360	0.45	0.53	69
398	0.49	0.59	64
615	0.76	0.38	56
805	1.00	<0.01	--

[a]Data from Refs. 104 and 105.

specific activity of 25 wt % $Ni/MgOAl_2O_3$ in steam reforming of ethane at 500°C. The fact that the specific activities based on the remaining nickel surface area are reasonably constant over a wide range of sulfur coverage is evidence that chemisorbed sulfur poisons by blocking the metal surface for adsorption of reactants. At a sulfur coverage of 1.0, the rate is lowered by more than two orders of magnitude. Thus, the actual tolerance of conventional nickel catalysts toward sulfur poisoning during steam reforming at 500°C is very low.

Although the above-discussed studies have defined sulfur poisoning tolerances for conventional nickel catalysts used in steam reforming of natural gas and naphtha, they have not considered in sufficient detail the kinetics of poisoning at above-threshold concentrations nor the effects of catalyst and/or gas compositions on rate of deactivation and tolerance level. Nor is there any previous report on the effects of sulfur on product distribution (i.e., relative rates of production of H_2, CO, and CH_4) in steam reforming of hydrocarbons. Nevertheless, such studies have been conducted for nickel and nickel bimetallic catalysts in methanation of CO (15, 29, 82, 106), the reverse of methane steam reforming; the results suggest that catalyst and gas compositions are important in determining rates of deactivation. Moreover, sulfur poisoning significantly changes product selectivity in favor of hydrogen-poor products.

A recently announced Japanese process (107) for high-temperature steam reforming of high-sulfur, heavy-hydrocarbon feedstocks (such as resids), based on Ni/Ca aluminate catalysts, demonstrates the potential for developing sulfur-tolerant catalysts. Certainly, steam reforming of such high-sulfur, high-coking feedstocks will necessitate development of a new class of steam-reforming catalysts. The study of their sulfur tolerance should constitute an important, fruitful area of research.

B. General Poisoning Models

Realistic, accurate models of poisoning can serve two useful purposes: (1) provide insights into the mechanisms of poisoning and (2) enable

prediction of poison distribution and catalyst life. Unfortunately much of the previous work along this line has been based on unrealistic or inaccurate empirical models with very limited application. However, two recently described models (104, 108) appear to have more general application to poisoning processes, and specifically, sulfur poisoning in steam reforming.

Wise et al. (108) recently proposed a theoretical model of sulfur-poisoning kinetics in an isothermal fixed bed, assuming kinetically controlled poisoning conditions. In this model, the poisoning is considered to be an irreversible adsorption of a gaseous contaminant on nonporous particles at a rate $ds/dt = -kns$, where k is the deactivation rate constant, n the poison concentration, and s the poison site density. Simultaneous solution of the mass-balance and rate equations and integration over the bed leads to expressions relating outlet poison concentration and site density to time:

$$\ln[n_i/n_L - 1] = \ln[\exp(ks_0L/V) - 1] - kn_i[t - (L/V)] \qquad \text{(A-5)}$$

$$\ln[s_0/s - 1] = \ln[\exp(kn_i\ (t - L/V)) - 1] - ks_0(L/V)\ , \qquad \text{(A-6)}$$

where n_i and N_L are the inlet and outlet concentrations of poison, L/V is the space velocity, and s_0 is the initial site density. By plotting experimental breakthrough concentrations in the form of $\ln[n_i/n_L - 1]$ as a function of t, the values of the rate constant k and poison site density can be determined. Once k and s are known for a given catalyst and process, it is possible to estimate catalyst life for different space velocities and poison concentrations.

Bartholomew and co-workers (29, 82) extended this model to correlate activity as a function of time. Letting $a = s/s_0$ in Eq. A-6 simplifies the equation such that rate constants can be obtained from plots of $\ln[(1-a)/a]$ as a function of time. Fowler and Bartholomew (29) used this extended model to determine rate constants and site densities for Ni and Ni-Mo catalysts during methanation in 10 ppm H_2S. They were then able to estimate catalyst lifetimes in the methanation process for conditions

of 1 ppm and a space velocity of 3,000 hr^{-1}. For example, the process lifetimes of 14% Ni/Al_2O_3 and 10% Ni/20% Mo/Al_2O-SiO_2 catalysts were estimated to be 3 and 9 months, respectively, under these conditions. If activity-versus-time data could be generated for steam-reforming catalysts, it might be possible to use this model to estimate their lifetimes in the process, assuming that temperature profiles and concentration gradients through the reactor were taken into account. This model, however, is mainly useful for estimating the time of approach to equilibrium sulfur coverage at the relatively large poison concentrations and low temperatures, characteristic of the inlet to a steam-reforming reactor. However, the poisoning process would probably cause the temperature profile to move gradually through the reactor with time at sufficiently large inlet concentrations of H_2S.

Because of the large temperature gradients in steam reforming and the significant reversibility of H_2S adsorption at the high temperatures representative of the outlet conditions (800-850°C), the equilibrium distribution of sulfur in the catalyst and particles is of interest. Rostrup-Nielsen (104), has demonstrated how equilibrium sulfur coverage profiles through a steam-reforming reactor can be estimated for different inlet sulfur concentrations. His calculations assume that chemisorption equilibrium is readily established and depends only on P_{H_2S}/P_{H_2} and temperature. Axial profiles of hydrogen flow and temperature are represented by straight lines. Unfortunately, his calculations assume an unrealistically low value for the heat of chemisorption for H_2S on nickel of 42 kJ/mole; moreover, it is evident that poisoning influences the hydrogen and temperature profiles over a period of time. Thus the quantitative results of Rostrup-Nielsen are suspect. Qualitatively, however, they illustrate how overall sulfur coverages as a function of position in a fixed bed can be determined for different sulfur concentrations at any given time. Since sulfur apparently poisons by blocking the sites, it should be possible to link the sulfur profiles to changes in activity as a function of concentration.

In addition, the calculations of Rostrup-Nielsen consider the effects of

pore diffusion, the results suggesting that equilibrium coverage is attained rapidly at the external surface of the catalyst pellets in the entire bed; thus, the adsorption front moving gradually through the bed is not as sharp as it would be in the case of methanation at lower temperatures. This means that a large but short-term increase in the inlet sulfur concentration in the feed could significantly upset the entire process by causing a significant increase in the coverage of the external pellet layer throughout the reactor bed. It also means that accumulation in the interior of the pellet is a slow process. Indeed, Rostrup-Nielsen estimates overall inlet coverages for typical catalysts in naphtha reforming for an ammonia plant to be 10 and 70% of equilibrium coverage after 100 and 1,000 hours, respectively.

The work of Rostrup-Nielsen is very informative, but it also raises a number of important questions. It is clear that improvements could be made in his sulfur coverage profiles by using more realistic heats of adsorption for nickel and by using more realistic temperature and concentration profiles through the reactor. These more accurate data should be valuable in modelling the process at near-threshold concentrations of H_2S. Thus, the questions of how sulfur is <u>actually</u> distributed in the catalyst pellets and in the bed and how this distribution changes as a function of time at various H_2S concentrations merit further attention. Also, in the model by Wise and co-workers for steam reforming, it might be worthwhile to examine a modification in which pore diffusional resistance is considered, so as to account for the slow deactivation of the pellet interior.

VI. REGENERATION OF CATALYSTS

Relatively few studies of regeneration of sulfur-poisoned catalysts have been reported (44, 60, 104, 106, 109-115). Removal of sulfur by oxidation with air, oxygen, or water (44, 106, 109-113, 115) or by high-temperature desorption in H_2 (106, 114) have been proposed. Unfortunately,treatments in an oxidizing environment and/or at high temperature can cause severe thermal degradation of typical steam-reforming catalysts. Patents on the subject have not addressed these problems nor the rationale for such proposed procedures.

In the only previous, comprehensive study of regeneration, Rostrup-Nielsen (104, 110) found that significant removal of sulfur was obtained for nickel steam-reforming catalysts -- either unpromoted, or promoted with magnesium and calcium -- on treatment in steam at temperatures above 700°C, whereas removal was negligible for sodium- and potassium-promoted catalysts. This behavior suggests that promoters which bind sulfur strongly (such as K and Na) render the catalyst difficult to regenerate. Although the treatment in steam oxidized the nickel at high temperatures, the results indicate that steam does not influence the H_2S chemisorption equilibrium. However, when steam and air were used in regeneration, sulfates were formed; these were reduced back to H_2S in the subsequent reduction. Bartholomew et al. (106) observed similar behavior in regeneration of sulfur-poisoned Ni/Al_2O_3 in oxygen at 250°C, followed by reduction at 250 and 400°C,respectively. A moderate recovery of activity was observed following reduction at 250°C; however, after reduction at 400°C, the catalyst completely lost its activity again. Recent studies of the oxidation of sulfur adsorbed on well-defined Cu (44) and Ni (93, 115) surfaces suggest that it may be possible to remove sulfur as SO_2 at very low partial pressures of O_2, thereby avoiding the formation of sulfates and the subsequent repoisoning of the catalyst on rereduction. Considerably more research with both well-defined surfaces and supported metals should be encouraged in this important area of regeneration by O_2.

The removal of sulfur in either H_2 or a sulfur-free reactant mixture may also have potential as a regeneration technique in steam reforming.

Although the rate of desorption of H_2S is very slow at 450-500°C (106), it should increase significantly at higher temperatures (800-900°C) as the adsorption becomes significantly more reversible (see Table A-2). This is apparently the basis of a patent for regeneration of sulfur-poisoned methanation catalysts (114). Of course, this technique may not find general application because of reactor system temperature restrictions and/or catalyst sintering problems. It does, however, merit additional investigation.

VII. EXPERIMENTAL CONSIDERATIONS

Although the discussion of previous work illustrates valuable techniques and approaches, not much has been said to this point regarding the details of experimental problems in the investigation of sulfur poisoning. Most of the difficulties occur because of: (a) strong adsorption, which results in nonuniform poisoning of the catalyst, (b) choice of apparatus materials that adsorb or react with sulfur compounds, or (c) choice of experimental conditions, such that heat- and mass-transport limitations, disguise the true effects of poisoning.

Because sulfur adsorbs so strongly and rapidly, it tends to distribute with complete coverage at the entrance to the bed (108) and on the outside of catalyst particles, in a manner typical of shell poisoning (106). Hence, sulfur is very nonuniformly distributed in a partially poisoned catalyst; some areas are completely poisoned and other areas are not poisoned at all. Thus great care should be exercised in describing the surface coverage and experimental results obtained for a partially poisoned catalyst. For this reason, it is safer to infer effects of poisoning from comparison between fresh catalysts and completely poisoned catalysts. It is also advisable to avoid P_{H_2S}/P_{H_2} values that are large enough to cause bulk metal sulfide formation, since this introduces additional complications. Much of the previous work is suspect for this very reason.

The choice of materials for controlled atmosphere studies is crucial. Most metals adsorb, desorb, or react with sulfur compounds, depending on the experimental conditions. At very low P_{H_2S}/P_{H_2} values (<1 ppm), desorption of H_2S from any metal, and adsorption/desorption effects of Pyrex® are serious problems (116). Quartz and Teflon® are the preferred materials at these low H_2S concentrations (28, 116).

Many of the previous investigations of the effects of sulfur poisoning on catalytic activity were carried out at high conversions in a large bed of pellets. Unfortunately, the resulting nonuniform distribution of sulfur on the bed and catalyst pellets combined with heat- and mass-transport

limitations for the reaction to disguise the true effects of poisoning. Fowler and Bartholomew (29) demonstrated that under such conditions, reaction rates over partially poisoned methanation catalysts are about the same as for the fresh catalysts and that the true effects of poisoning on activity and selectivity are observed only under reaction-limited conditions at low conversions.

Experimental and theoretical surface-science techniques (12) have considerable potential for investigating the nature of metal-sulfur bonds at the surface. Auger and LEED spectroscopies have already proven themselves as useful techniques for investigating the structure of absorbed sulfur on metals and such phenomena as surface reconstruction. One of the most promising tools for investigating the effects of sulfur on metal crystallite structure in real catalysts is extended x-ray adsorption, fine-structure spectroscopy (EXAFS).

Adsorption/desorption studies of H_2S on supported and unsupported metals (27, 28) can now be carried out conveniently with the recent development of automated chromatographic analysis using flame photometric detectors with extremely high sensitivity for sulfur. The desorption technique developed by Oliphant et al. (27) appears to be the most accurate, convenient technique for generating adsorption isotherms.

Fitzharris and Katzer (116) have developed Pyrex® and quartz CSTR reactors which enable convenient, direct study of sulfur-poisoning kinetics and effects on activity and selectivity during reaction on metal films (117-119) and monolithic catalysts (120, 121). Bartholomew and co-workers (29, 122) have also developed quartz and Pyrex® differential fixed-bed reactors for similar studies on catalyst powders, pellets, and monoliths.

In addition to the careful choice of experimental conditions and reactor materials, the choice of well-defined catalyst systems is important. Investigator-prepared catalysts, the physical and chemical properties of which have been carefully determined by a number of techniques, are preferred.

VIII. CONCLUSIONS AND RECOMMENDATIONS

A. Conclusions

1. Metal-sulfur bonds at the surface are significantly stronger than the corresponding metal-sulfur bonds in bulk metal sulfides. Heats of H_2S adsorption on metals are 20-40% larger than heats of formation of the bulk sulfides.

2. Adsorption of H_2S on metals occurs dissociatively over a wide range of temperatures and coverage. During initial stages of H_2S adsorption on nickel, sulfur resides in the high coordination sites, with each sulfur atom being bonded to 3 or 4 nickel atoms; however, as the sulfur coverage is increased, the surface restructures, with each sulfur atom being bonded to 2 nickel atoms. Further restructuring of the surface and adsorption of sulfur occurs at relatively high H_2S concentrations and temperatures.

3. Sulfur poisons the adsorption of H_2 and CO on most metals; however, CO adsorption on nickel may be increased at sufficiently high pressures because of the formation of $Ni(CO)_4$. No data are available on the effect of sulfur on CH_4 adsorption.

4. Sulfur-poisoning threshold levels range from 1 to 20 ppm H_2S for conventional steam-reforming catalysts, depending on the outlet temperature. The few available data suggest that poisoning occurs by a simple blockage of the surface for further adsorption of reactants. The poisoning process is somewhat reversible at high outlet temperatures. Sulfur is distributed mainly in the front of the bed and on the outside of catalyst pellets at near-threshold sulfur concentrations.

B. Recommendations for Further Work

This discussion of previous work has focused on several fundamental questions. Some of these questions could not be addressed because of the present lack of information. For example, how are metal-sulfur bonds affected by metal crystallite size and metal-support interactions?

Can sulfur-poisoned catalysts be successfully regenerated? Since no reported investigation has considered adsorption of H_2S on Co, Pd, or Ru, or the effects of sulfur poisoning on the adsorption of methane, and since only two studies have considered the poisoning of catalysts during steam reforming, additional research in these areas is highly recommended. Other specific needs for further research were addressed at various appropriate points earlier in this section.

REFERENCES

1. Maxsted, E.B., Adv. Catal. 3, 129 (1951).

2. Madon, R.J., and Shaw, H., Catal. Rev.-Sci. Eng., 15, 69 (1977).

3. Pauling, L., "The Chemical Bond," 4th edition, Cornell University Press, Ithaca, New York, 1966.

4. Kishi, K., and Roberts, M.W., J. Chem. Soc. Far. Trans. I, 71, 1715 (1975).

5a. Goddard, W.A., III, Walch, S.P., Rappe, A.K., Upton, T.H., and Melius, C.F., J. Vac. Sci. Technol. 14, 416 (1977).

b. Walch, S.P., and Goddard, W.A., III, Surface Sci. 72, 645 (1978).

6. Grimley, T.B., J. Vac. Sci. & Technol. 8, 68 (1971).

7. Rosenqvist, T., J. Iron Steel Inst. 176, 37 (1954).

8. Kirkpatrick, W.J., Adv. Catal. 3, 329 (1951).

9. Elliott, R.P., "Constitution of Binary Alloys, First Supplement, McGraw-Hill, New York, 1965.

10. Barin, I., and Knacke, O., "Thermochemical Properties of Inorganic Substances," Springer-Verlag, N.Y., 1973.

11. Foroulis, Z.A., ed. "High Temperature Metallic Corrosion of Sulfur and Its Compounds," The Electrochem. Soc., Corr. Div., New York, 1970.

12. Boudart, M., Cusamano, J.A., and Levy, R.B., New Catalytic Materials for Liquefaction of Coal. Electric Power Research Institute Report RP415-1, Oct. 30, 1975.

13. Shatynski, S.R., Oxidation of Metals 11, 307 (1977).

14. Thomas, C.L., "Catalytic Processes and Proven Catalysts," pp. 149-151, Academic Press, N.Y., 1970.

15. Bartholomew, C.H., and Fowler, R.W., Proceedings of the 3rd International Conference of the Chemistry and Uses of Molybdenum, August 19-23, 1977, Ann Arbor, Mich.

16. Saleh, J.M., Kemball, C., and Roberts, M.W., Trans. Farad. Soc. 57, 1771 (1961).

17. Den Besten, I.E., and Selwood, P.W., J. Catal. 1, 93 (1962).

18. Blyholder, G.D., and Bowen, D.O., J. Phys. Chem. 66, 1288 (1962).

19. Rostrup-Nielsen, J.R., J. Catal. 11, 220 (1968).

20. Richardson, J.R., J. Catal. 21, 130 (1970).

21. Perdereau, M., and Oudar, J., Surface Sci. 20, 80 (1970).

22. Oudar, J., Bull. Soc. fr. Mineral. Cristallogr. 94, 225 (1971).

23. Blyholder, G.D., and Cagle, G.W., Environ. Sci. Tech. 5, 158 (1971).

24. Rudajevova, A., Pour, V., and Regner, A., Coll. Czech., Chem. Comm., 38, 2566 (1973).

25. Rochester, C.H., and Terrell, R.J., JCS Faraday I, 73, 596 (1977).

26a. Ng, C.F., and Martin, G.A., C.R. Acad. Sc. Paris, 284, 589 (1977).

b. Ng, C.F., and Martin, G.A., J. Catal. 54, 384 (1978).

27. Oliphant, J.L., Fowler, R.W., Pannell, R.B., and Bartholomew, C.H., J. Catal. 51, 229 (1978).

28. McCarty, J., Wentrcek, P.R., Wise, H., and Wood, B.J., Annual Report to DOE, Contract No. 76-C-03-115, Dec. 1978.

29. Fowler, R.W., and Bartholomew, C.H., I & EC Prod. Res. & Devel., 18, 339 (1979).

30a. Demuth, J.E., Jepsen, D.W., and Marcus, P.M., Surface Science 45, 733 (1974).

b. Demuth, J.E., Jepsen, D.W., and Marcus, P.M., Phys. Rev. Letts 32 (21), 1182 (1974).

31. Van Hove, M., and Tong, S.Y., J. Vac. Sci. Tech. 12, 230 (1975).

32. Andersson, S., and Pendry, J.B., J. Phys.-C: Solid State Phys. 9, 2721 (1976).

33. Fisher, G.B., Surface Science 62, 31 (1977).

34. Hagstrum, H.D., and Becker, G.E., J. Chem. Phys. 54, 1015 (1971).

35. Demuth, J.E., and Rhodin, T.N., Surf. Sci. 45, 249 (1975).

36. McCarroll, J.J., Edmonds, T., and Pitkethly, R.C., Nature 223, 1260 (1969).

37. Edmonds, T., McCarroll, J.J., and Pitkethly, R.C., Nederlands Tijd. Voor Vacuumtechniek 8, 162 (1970).

38. Edmonds, T., McCarroll, J.J., and Pitkethly, R.C., J. Vac. Sci. & Technol. 8, 68 (1971).

39. Vahrenkamp, H., Lichtman, V.A., and Dahl, L.F., J. Am. Chem. Soc. 90, 3272 (1968).

40. Domange, J.L., Communication Presented at the Colloquium on Physical Chemistry of Surfaces, May, 1973 (Brest. F.).

41. Thapliyal, H.V., and Blakely, J., J. Vac. Sci. Technol. 15, 600 (1978).

42. Windawi, H., and Katzer, J.R., Surface Science 75, 1761, (1978).

43. Martin, G., and Imelik, B., Surf. Sci. 42, 157 (1974).

44. Bonzel, H.P., Surf. Sci. 27, 387 (1971).

45. Joyner, R.W., McKee, C.S., and Roberts, M.W., Surf. Sci. 27, 279 (1971).

46. Roberts, M.W., Nature 188, 1020 (1960).

47. Hobert, H., Schimerstoffe Schiverungsteel 36, 15 (1969).

48. Neff, L.D., and Kitching, S.C., J. Phys. Chem. 78, 1648 (1974).

49. Saleh, J.M., Roberts, M.W., and Kemball, C., Trans. Faraday Soc. 58, 1642 (1962).

50. Benard, J., Catal. Rev. 3, 93 (1969).

51. Oudar, J., Conference on Catalyst Deactivation and Poisoning, Lawrence Berkeley Laboratory, Berkeley, Calif., May 24-26, 1978.

52a. Cabane-Brouty, F., and Oudar, J., Compt. Rend., 258, 5428 (1964).

b. Cabane-Brouty, F., and Oudar, J., Compt. Rend., 259, 4003 (1964).

53. Cabane-Brouty, F., J. Chim. Phys. 62, 1045, 1056 (1965).

54. Bernard, J., Oudar, J., and Cabane-Brouty, F., Surf. Sci. 3, 359 (1965).

55. Oudar, J., Compt. Rend. 249, 91 (1959).

56. Benard, J., Bull. Soc. Chim. France, 203 (1960).

57. Domange, J.L., and Oudar, J., Compt. Rend., 265, 35,951 (1967).

58. Domange, J.L., and Oudar, J., Surf. Sci. 11, 124 (1968).

59. Roberts, M.W., and Ross, J.R.H., Trans. Faraday Soc. 62, 2301 (1966).

60. Brill, Von R., Schaefer, H., and Zimmerman, G., Br. Bunsinges, Phys. Chem. 72, 1218 (1968).

61. Huber, M., and Oudar, J., Surf. Sci. 47, 605 (1975).

62. Biberian, J.P., and Huber, M., Surf. Sci. 55, 259 (1976).

63. Grabke, H.J., Peterson, E.M., and Srinivasan, S.R., Surf. Sci. 67, 501 (1977).

64. Legg, K.O., Tona, F., Jepsen, O.W., and Marcus, P.M., Surf. Sci. 66, 25 (1977).

65. Kawai, T., Kunimori, K., Kondow, T., Onishi, T., and Tamaru, K.,

66. Peralta, L., Berthier, Y., and Oudar, J., Surf. Sci. 55, 1999 (1976).

67. Kikuchi, T., and Ishizuka, K., J. Res. Inst. Catal. Hokkaido Univ. 26, 7 (1978).

68. Fisher, G.B., Surf. Sci., in press.

69. Schmidt, L.D., and Luss, D., J. Catal. 22, 269 (1971).

70. Somorjai, G.A., J. Catal. 27, 453 (1972).

71a. Bonzel, H.P., and Ku, R., J. Chem. Phys. 58, 4617 (1973).
b. Bonzel, H.P., and Ku, R., J. Chem. Phys. 59, 1641 (1973).

72. Bertheir, Y., Perdereau, M., and Oudar, J., Surf. Sci. 36, 25 (1973).

73. Heegemann, W., Meister, K.H., Bechtold, E., and Hayek, K.H., Surf. Sci. 49, 161 (1975).

74a. Fischer, T.E., and Keleman, S.R., Surf. Sci. 69, 1 (1977).
b. Fischer, T.E., and Keleman, S.R., J. Vac. Sci. Technol. 15, 607 (1978).

75. Bertheir, Y., Oudar, J., and Huber, M., Surf. Sci. 65, 361 (1977).

76. Domange, J.L., Oudar, J., and Benard, J., "Growth Mechanism and Structure of Adsorption Layers." Molecular Processes on Solid Surfaces. McGraw-Hill, Inc., 1968.

77. Bartholomew, C.H., Annual Technical Progress Report to ERDA, FE-1790-4, May 6, 1975.

78. Chung, K.S., Master's Thesis, Brigham Young University, 1976.

79. Stowell, D.E., Master's Thesis, Brigham Young University, 1976.

80. Pannell, R.B., Chung, K.S., and Bartholomew, C.H., J. Catal. 46, 340 (1977).

81. Pannell, R.B., Ph.D. Dissertation, Brigham Young University, 1978.

82. Uken, A.H., and Bartholomew, C.H., Manuscript in Preparation, Oct. 1979.

83. Bartholomew, C.H., and Pannell, R.B., Preprints of the Amer. Chem. Soc. Petr. Chem. Div., Houston, March 23-28, 1980.

84. Rendulic, K.D., and Winkler, A., Surf. Sci. 74, 318 (1978).

85. Garland, C.W., J. Phys. Chem. 63, 1423 (1959).

86. Crell, W., Hobert H., and Knappe, B., Z. Chem. 10, 396 (1968).

87. Rochester, C.H., and Terrell, R.J., J.C.S. Faraday I. 73, 609 (1977).

88a. Rewick, R.T., and Wise, H., Preprints ACS Div. of Petr. Chem. 22(4), 1324 (1977).
b. Rewick, R.T., and Wise, H., J. Phys. Chem. 82, 752 (1978).

89. Rhodin, T.N., and Brucker, C.F., Solid State Commun. 23, 275 (1977).

90. Erley, W., and Wagner, H., J. Catal. 53, 287 (1978).

91. Bartholomew, C.H., and Gardner, D.C., Presentation at Advances in Catalysis I, Snowbird, Ut., Oct. 3-5, 1979.

92. Milliams, D.E., Pritchard, J., and Sykes, K.W., Sixth International Congress on Catalysis, London, July 1976, Paper A-32.

93. Holloway, P.H., and Hudsen, J.B., Surf. Sci. 33, 56 (1972).

94. Bayer, J., Stein, K.C., Hofer, L.J.E., and Anderson, R.B., J. Catal. 3, 145 (1964).

95. Kishi, K., and Roberts, M.W., J.C.S. Faraday I, 71, 1715 (1975).

96. Argano, E.S., Randhava, S.S., and Rehmat, A., Trans. Faraday Soc., 65, 552 (1969).

97. Jackson, S.D., Thomson, S.J. and Webb, G., Radiochem. Radioanal. Letters 28, 459 (1977).

98. Grabke, H.J., Paulitschke, and Srinivason, S.R., 8th International Symposium on the Reactivity of Solids, p. 12, June 14-19, 1976, Gothenburg, Sweden.

99. Bottoms, W.R., and Lidow, D.B., J. Electrochem. Soc.: Solid-State Sci. & Technol. 122, 119 (1975).

100. Pichler, H., Adv. Catal. 4, 326 (1952).

101. Morita, S., and Inoue, T., Int. Chem. Eng. 5, 180 (1965).

102. Morita, S., and Inoue, T., Kogyo Kagaku, Zasshi 68, 659 (1965).

103. Bridger, G.W., and Chinchen, G.C., "Hydrocarbon Reforming Catalysts" in "Catalyst Handbook," Wolfe Sci. Books, London, 1970.

104. Rostrup-Nielsen, J.R., "Steam Reforming Catalysts," Teknisk Forlag A/S, Copenhagen, 1975.

105. Rostrup-Nielsen, J.R., J. Catal. 31, 173 (1973).

106. Bartholomew, C.H., Weatherbee, G.D., and Jarvi, G.A., J. Catal., 60, 257 (1979).

107. Tomita, T., and Kitagawa, M., "A New Reforming Process of Heavy Hydrocarbons," Presented at the European Meeting of Chemical Engineering, Frankfurt, Germany, June 23, 1976.

108. Gikis, B.J., Isakson, W.E., McCarty, J.G., Sancier, K.M., Schechter, S., Wentrcek, P.R., Wood, B.J., and Wise, H., "Sulfur Poisoning of Catalysts: A Study of Activity Decay in Methanol Synthesis and Fischer-Tropsch Catalysis," Final Report to ERDA, PERC-0060-8, Sept. 30, 1977.

109. Riesz, C.H., Dirksen, H.A., and Kirkpatrick, W.J., "Sulfur Poisoning of Nickel Catalysts," Institute of Gas Technology Research Bulletin No. 10, September, 1951.

110. Rostrup-Nielsen, J.R., J. Catal. 21, 171 (1971).

111. Sickafus, E.N., Surf. Sci. 19, 181 (1970).

112. Pieters, W.J., Freel, J., and Anderson, R.B., U.S. Patent No. 3,674,707 (1972).

113. Schoofs, R.J., Nordhausen, L.J., and Dugdale, L.A., U.S. Patent No. 4,026,821 (1977).

114. Dobashi, H.H., U.S. Patent No. 4,065,484 (1977).

115. Katzer, J.R., Private Communication.

116. Fitzharris, W.D., and Katzer, J.R., Ind. Eng. Chem. Fundam. 17, 130 (1978).

117. Fitzharris, W.D., and Katzer, J.R. submitted to J. Catal., 1979.

118. Agrawal, P.K., Katzer, J.R., and Manogue, W.H., Presentation at the Sixth North American Meeting of the Catalysis Society, Chicago, March 18-22, 1979.

119. Agrawal, P.K., Katzer, J.R., and Manogue, W.H., Presentation at the ASC/CSJ Chemical Congress, Honolulu, April 1-6, 1979.

120. Bartholomew, C.H., and Erekson, E.J., submitted to Ind. Eng. Chem. Fundam., 1979.

121. Bartholomew, C.H., Quarterly Report to DOE, FE-2729-8, Oct. 5, 1979.

122. Bartholomew, C.H., Final Report to ERDA, FE-1790-9, Sept. 6, 1977.

APPENDIX B

I INTRODUCTION

Deactivation of supported metal catalysts by carbon or coke is a serious problem in steam reforming, methanation, and other important catalytic processes. Its effects are generally threefold: (1) fouling of the metal surface, (2) blockage of catalyst pores and voids, and (3) disintegration of the catalyst support. Since loss of catalytic activity and physical destruction of the catalyst by carbon deposits can occur rapidly (within hours or days), control of these effects is of major technological and economic importance.

The high degree of interest in these problems is evident from the fairly extensive literature dealing with carbon deposition and coke formation on metals and metal catalysts, summarized in recent reviews (1-7). Progress in understanding carbon formation and needs for further research are documented reasonably well in the most pertinent of these literature surveys (5-7). Nevertheless, it is clear that some old and even some new concepts regarding carbon deposition need to be revised and/or updated in light of even more recent data. Moreover, new directions of research have just recently come to view.

The purpose of this section is to survey briefly the previous work with carbon deposition on metals; emphasized are research areas in which significant progress has been and/or could be made. As in the section on sulfur poisoning, this discussion focuses on several important, basic questions which should reveal the present state of understanding and needs for further investigation:

1. What are the mechanisms by which carbon and coke are deposited? What is the rate-determining step?

2. What are the chemical, physical, and morphological properties of various carbonaceous materials formed in the decomposition of CO and hydrocarbons on metals?

3. How do catalyst and gas-phase compositions influence the rate of carbon formation and the amount ultimately deposited?

4. How do metal crystallite size, surface structure, and metal-support interactions affect the rate of carbon formation and the nature of the species deposited?

5. How can the unfavorable consequences of carbon deposition be avoided? Which methods of regeneration are most practical and result in the least damage to catalysts?

Because this document is directed at problems connected with steam reforming, the ensuing discussion in this section will emphasize work with nickel catalysts and surfaces.

II CARBON AND COKE FORMATION

A. Morphology of Carbon and Coke

The definitions of carbon and coke are somewhat arbitrary and by convention related to their origin. Carbon is a product of CO disproportionation, while coke is produced by decomposition or condensation of hydrocarbon on metals. Nevertheless, actual coke forms may vary from high-molecular-weight hydrocarbons such as condensed polyaromatics to carbons such as graphite, depending on the conditions under which the coke was formed and aged (Figure B-1). Formation of carbon deposits via CO (see Figure B-2) may involve the production and transformation of various carbon forms (8), e.g., atomic (C_α), amorphous, vermicular (C_β), bulk nickel carbide (C_γ), and crystalline, graphitic (C_c), the structures and reactivities of which are summarized in Table B-1. Recent investigations (9-21) of the structure and bonding of carbon on well-defined nickel surfaces by low-energy electron diffraction (LEED) and Auger electron spectroscopy (AES) confirm the presence of "dispersed" or atomic carbon stable below 325°C (sometimes referred to as a surface nickel carbide) and polymerized carbon stable above 325°C. For example, Kelley and co-workers(21) investigated the nature of dispersed carbon formed by dissociation of CO at 325°C on Ni(100) using AES, concluding that the adsorbed carbon is "carbidic" in nature. This carbon was easily removed by hydrogen at the same temperature; however, on heating in vacuum at significantly higher temperatures, the surface carbon apparently diffused into the bulk. However, decomposition of CO on the Ni(100) crystal at 425°C produced a carbon with an AES spectrum characteristic of graphite forms. McCarty and Wise (8) have demonstrated that C_α is converted to C_β at temperatures above 325°C and C_β to C_c at even higher temperatures, according to the scheme shown in Figure B-2.

Several studies of carbon deposition on nickel powders, foils, and single crystals (5, 7, 22-30) show direct evidence of low-density filamentous (amorphous) and high-density, crystalline graphitic forms, such as platelets (30) observed after treatment in carbonizing atmospheres at temperatures above 550°C. It should be emphasized that, at high temperatures, amorphous carbons may convert to more graphitic forms in terms of their

TABLE B-1

Forms and Reactivities of Carbon on Nickel

	Structural type	Designation	Temperature formed, °C	Peak temperature for reaction with H_2, °C	Ref.
1.	Atomic (dispersed, surface carbide)	C_α	200-400	200	8
2.	Vermicular (polymeric, amorphous)	C_β	300-1000	400-600	6-8
	a. Filaments				
	b. Fibers				
	c. Whiskers				
3.	Nickel carbide (bulk)	C_γ	150-250	275	8
4.	Graphitic (crystalline)	C_c	500	550-850	5-8
	a. Platelets		550		28
	b. Films				

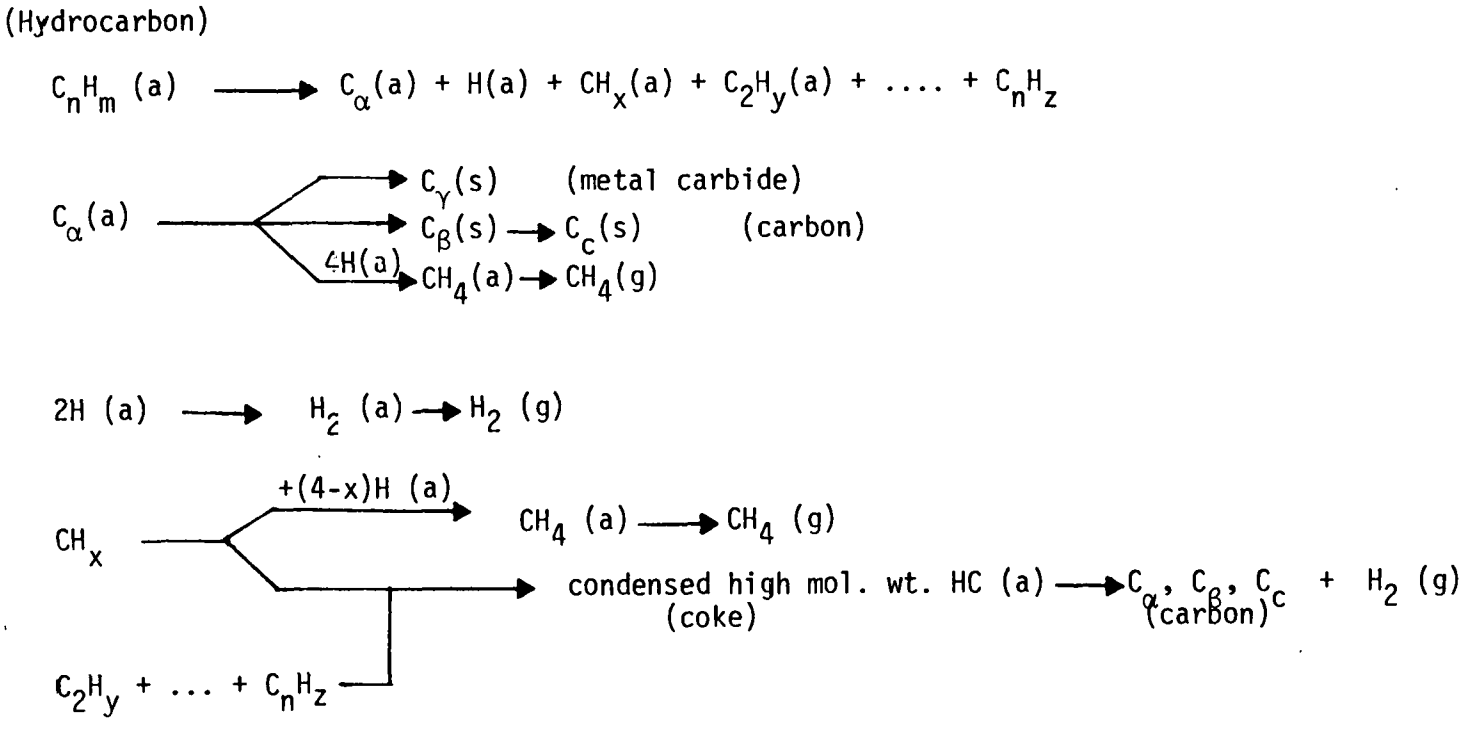

Fig. B-1. Formation and transformation of coke on metal surfaces (a, g, and s refer to adsorbed, gaseous, and solid states, respectively; gas-phase reactions are not considered).

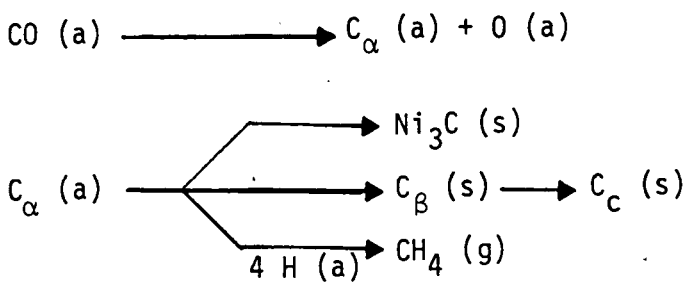

Fig. B-2. Formation, gasification, and transformation of carbon on nickel (a, g, and s refer to adsorbed, gaseous, and solid states, respectively).

reactivity and even crystallinity, while retaining their overall vermicular structure (7, 8, 21, 29). The kinetics and mechanisms of formation and transformation will be discussed later in this section.

B. Thermodynamics

1. Carbon Formation. Equilibrium calculations (4, 25, 31, 32) can be used to estimate the amount of solid carbon in equilibrium with gaseous CO, H_2, CH_4, CO_2, and H_2O for fixed values of O/H ratio, temperature, and pressure in any reaction system involving mainly these six species, such as in methanation or steam reforming. Calculations are typically based on equilibrium constants for the following three independent reactions:

$$CO + 3H_2 \rightleftharpoons CH_4 + H_2O \qquad \text{Methanation } (\Delta H = -206 \text{ kJ/mole}) \qquad \text{(B-1)}$$

$$CO + H_2O \rightleftharpoons H_2 + CO_2 \qquad \text{Shift } (\Delta H = -41 \text{ kJ/mole}) \qquad \text{(B-2)}$$

$$2CO \rightleftharpoons C + CO_2 \qquad \text{Boudouard } (\Delta H = -172 \text{ kJ/mole} \qquad \text{(B-3)}$$

Other carbon-forming reactions involving the six species above, such as methane decomposition, $CH_4 \rightleftharpoons C + 2H_2$, are not independent since they result from a combination of Reactions B-1, B-2, and B-3. From the above-described equilibrium calculations, it is possible to plot the interface between carbon-forming and carbon-free regions on a C-H-O ternary diagram and thus estimate the carbon-forming potential for given process conditions. This is illustrated in Figure B-3, in which the equilibrium carbon deposition boundaries are shown for amorphous (25, 31) and graphitic (33) carbons at 450°C and 1.4 atm. Points A and B correspond to reactant gas compositions of $H_2O/CH_4 = 0.1$ and $H_2O/CH_4 = 2.0$, respectively. Since point A lies above the boundary lines for both carbons, there is a predicted tendency to deposit carbon. For the composition represented by Point B, however, no deposition of carbon is expected, as this point is clearly below the boundary lines for both carbons. It should be emphasized that,

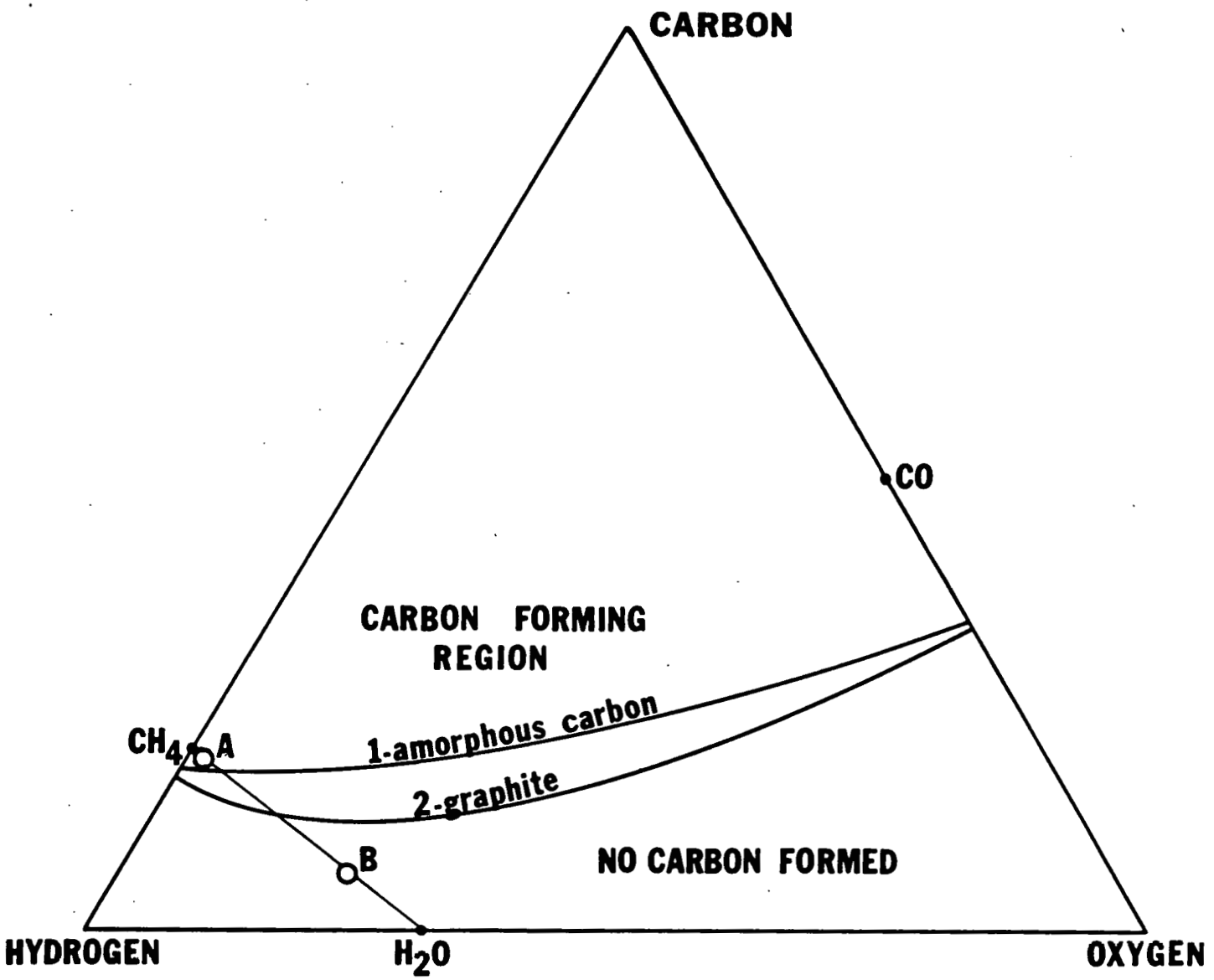

Fig. B-3. Equilibrium C-H-O diagram showing carbon isotherms at 450°C and 1.4 atm for graphite and amorphous carbons. Points A and B correspond to compositions of H_2O/CH_4 = 0.1 and H_2O/CH_4 = 2.0, respectively. Point A is in the region above the isotherms where carbon is predicted to form. Carbon formation is not expected at Point B because it lies below the isotherms for carbon formation.

although the presence of carbon is predicted for composition A, formation may not actually occur unless the system is at equilibrium. Since near-equilibrium conditions obtain in methanation and steam-reforming reactions at 400 and 850°C, respectively, ternary diagrams such as Figure B-3 are useful for estimating the amount of carbon formed under these conditions. Major deviations from predicted equilibrium isotherms may occur if the product gas contains other gaseous species (e.g., C_2^+ hydrocarbons) than the above-mentioned five. Moreover, Rostrup-Nielsen (25) states that in steam reforming, coke may be formed because of poor activity or selectivity of the catalyst under steady-state conditions, for which the equilibrium composition is predicted to form no carbon. In addition, if the surface temperature of the catalyst is higher than that of the bulk gas, carbon could form on the catalyst surface when no carbon formation is predicted on the basis of the bulk gas temperature (4).

Whalen (4) has discussed the effects of temperature, pressure, composition, and carbon type on equilibrium carbon deposition isotherms. The carbon-forming boundary is apparently more sensitive to carbon fraction than any other variable. Addition of water or hydrogen decreases the propensity to form carbon. Formation of amorphous carbon from H_2/CO mixtures is more likely to occur with increasingly higher temperatures and pressures, whereas formation of graphitic carbon from H_2O/CH_4 mixtures is more likely at low pressures and very high temperatures. Although formation of "nonideal" (amorphous) carbon permits carbon-free operation over a wide range of compositions (see Figure B-3), the deviation of experimentally obtained equilibrium constants for amorphous carbon from those for graphite becomes smaller with increasing temperature (25) as the amorphous carbon becomes more graphitic. In the range of 400-600°C, however, the deviations from graphite are significant; they also increase significantly with decreasing metal crystallite diameter. Rostrup-Nielsen (25) attributes these deviations to the higher surface energy and structural disorder of the small-diameter filaments formed on small crystallites. This geometrical effect is consistent with data obtained for single-crystal nickel (22, 23) and shows the strong influence of crystal orientation. Indeed, carbon was formed in the Boudouard reaction on Ni(111) but could not be detected on Ni(100) and (110)! That this effect is mainly geometrical

is emphasized by the experimental observations of Rostrup-Nielsen (25), which show catalyst composition, supports, promoters, and alloys to have negligible influence on the thermodynamics of carbon formation. Nevertheless, the kinetics of carbon formation are clearly influenced by these factors, as will be demonstrated later in this section.

The practical application of the above thermodynamic information to steam-reforming and methanation processes is illustrated as follows. Since the equilibrium carbon formed in steam reforming at 600-850°C is mainly graphitic in terms of its reactivity (rather than structure) and since typical steam-reforming catalysts contain relatively large metal particles, thermodynamic data for graphite are more applicable to this process, particularly at the reactor outlet. On the other hand, the carbons formed in methanation (250-450°C) and at the steam-reformer inlet (400-500°C) are clearly amorphous, and the thermodynamic data show significant deviations from graphite, especially in the case of well-dispersed methanation catalysts having average crystallite diameters in the range of 4-6 nm.

2. Carbon Adsorption on Nickel.

The binding energies of carbon atoms on various single crystal surfaces of Ni, Pd, and Pt have been determined by Blakely and co-workers(15-18, 34, 35) through LEED and AES studies of equilibrium segregation of carbon dissolved in the metal. Some of their results are summarized in Figure B-4. Carbon is endothermically dissolved in Ni with an energy of solution relative to graphite of 41.8 kJ/mole. Segregration of dispersed carbon to the surface of Ni(100) is energetically favorable, and releases 40.2 kJ/mole. Since the dispersed carbon adsorbed on Ni(100) at low coverage has a heat of formation of only 1.6 kJ/mole relative to graphite, it remains stable at low coverages over a fairly wide range of temperature. Segregation of dispersed carbon to the Ni(111) surface was not observed by Blakely et al., presumably because the energy of adsorbed carbon on Ni(111) is greater than that for C dissolved in Ni; this is illustrated in Figure B-4 by a dotted line at an arbitrary value

above 41.8 kcal/mole. Blakely et al. have provided data for carbon segregated to a number of other stepped surfaces, showing the stability of the dispersed, adsorbed carbon to be favorable relative to carbon dissolved in Ni. Apparently the binding of carbon atoms to step sites is stronger than on smooth planes. Their results also show (see Figure B-4) that dissolved carbon is unstable relative to graphite on Ni(111), suggesting that formation of graphite occurs preferentially on the (111) surface. This may explain the earlier observations by Leidheiser et al. (22, 23) of carbon formation on the (111) but not on the (100) and (110) faces of Ni. The facts that the energetics of carbon adsorption vary with crystallite surface steps and planes and that the energy of filamentous, amorphous carbon[1] is expected to be higher than for graphite (see Figure B-4) may account in part for the deviations in equilibrium constants observed for amorphous carbon relative to graphite. More research of this kind with other catalysts, e.g., promoted Ni, Fe, and Co systems, would be valuable.

In the section dealing with sulfur poisoning, evidence for a sulfur-induced reconstruction of the surface was documented. Can adsorbed carbon also cause rearrangement of the metal surface? Although very few data are available in this regard, they tend to support such a possibility. For example, Thapliyal and Blakely (18) provide evidence for faceting of stepped Ni(111) planes by adsorbed graphite to (111) and (110) planes at high carbon coverages. They conclude that adsorbed carbon enhances the attractive interaction among steps to cause faceting. Sulfur adsorbates on the other hand tend to inhibit step coalescense on similar stepped surfaces of Ni. This difference in behavior may account for the different effects of carbon and sulfur on activity/selectivity properties in a number of reactions.

[1] The energy level shown for amorphous carbon in Figure B-4 is arbitrary. Although it clearly has a higher energy than graphite, the actual energy level depends on the vermicular structure. The energy level probably increases with decreasing filament diameter (see Ref. 25).

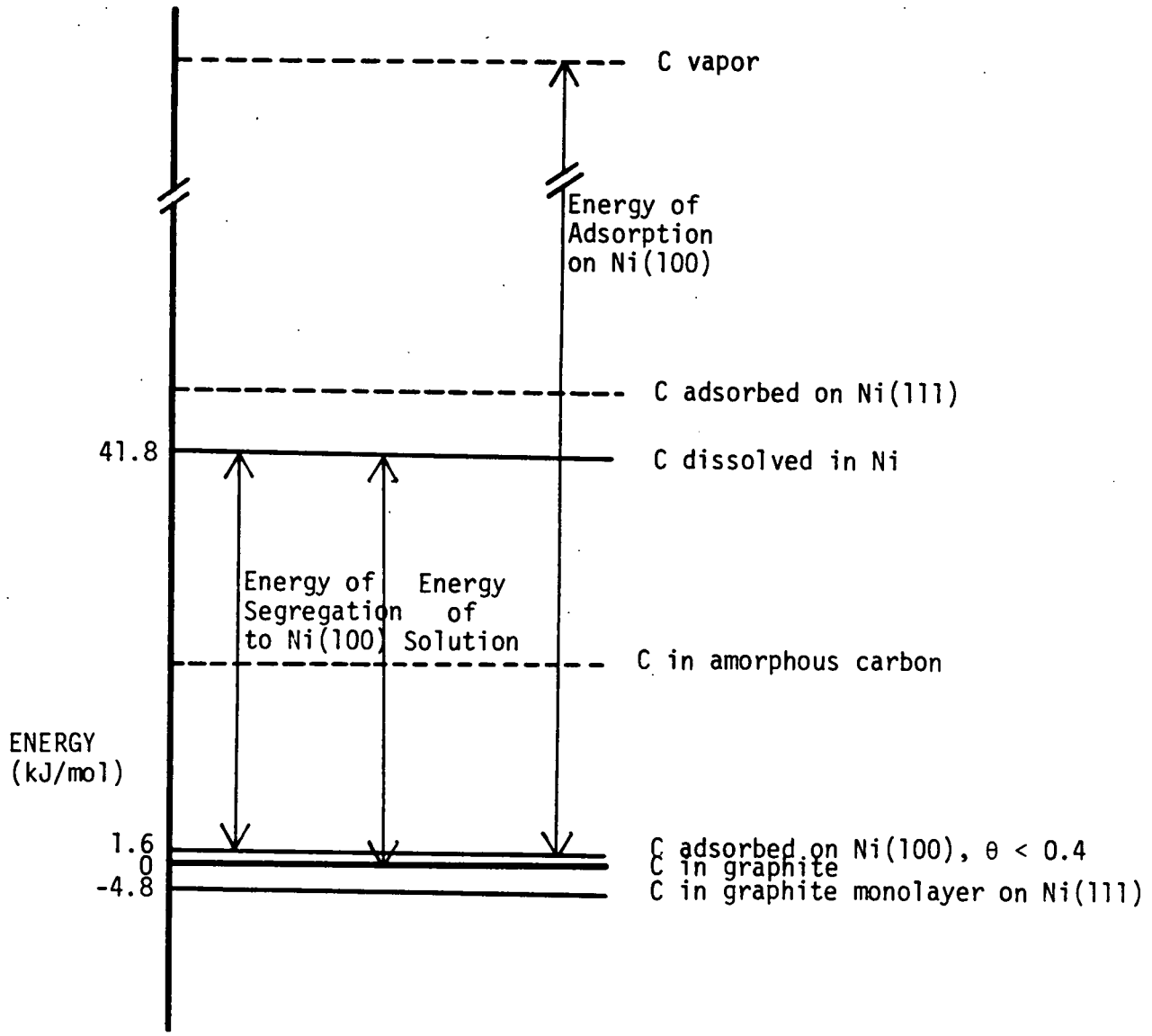

Fig. B-4. Energies of adsorbed carbon species relative to carbon in graphite.

C. Kinetics and Mechanisms

1. Disproportionation of Carbon Monoxide

The stoichiometry of CO disproportionation of the Boudouard reaction is shown by Equation B-3. The forward reaction is exothermic and is favored at temperatures below 700°C. Measurable rates of carbon formation occur in the presence of Co, Fe, and Ni catalysts above 350°C. Recent investigations (7, 36) indicate the decreasing order of activity to be Fe, Co, and Ni, although each metal has a different optimum temperature of operation (7, 37). The form of carbon deposited depends on reaction conditions. In the lower-temperature range, 350-600°C, filamentous carbons predominate (7, 24, 25, 37), while at 700°C and above, platelet graphite is observed (7, 30, 27, 38).

The kinetics of CO disproportionation has received relatively little attention; in fact, only two comprehensive kinetic studies of Ni catalysts (both gravimetric) have been reported (39-41) and to our knowledge, none of other metal catalysts. Tøttrup (39) investigated the reaction on Ni/η-Al_2O_3 in the temperature range of 280-500°C; Gardner and Bartholomew (40, 41), on γ-Al_2O_3 -supported Ni and Ni bimetallics from 300 to 450°C. In both investigations, an induction period of 0.5 to 5 hours was observed, during which no measurable weight increase occurred and after which the rate of carbon deposition passed through a maximum, reaching a steady state within the next 1-2 hours (see Figure B-5). The rate of carbon formation is zero to first-order in CO and quite sensitive to temperature, apparent activation energies ranging from 100-130 kJ/mole. Gardner and Bartholomew found the specific steady-state rate of multilayer filamentous carbon formation (on a Ni-site basis) to be reasonably high but nevertheless about one order of magnitude less than for methanation of CO under comparable conditions. Recent data from Goodman et al. (42) indicate that the turnover number (rate per site per sec) for formation of atomic carbon on Ni(100) at coverages less than a monolayer is about the same as for methanation of CO; their reported activation energy of 105 kcal is also the same as for methanation, within experimental error. Thus, the rate of formation of atomic

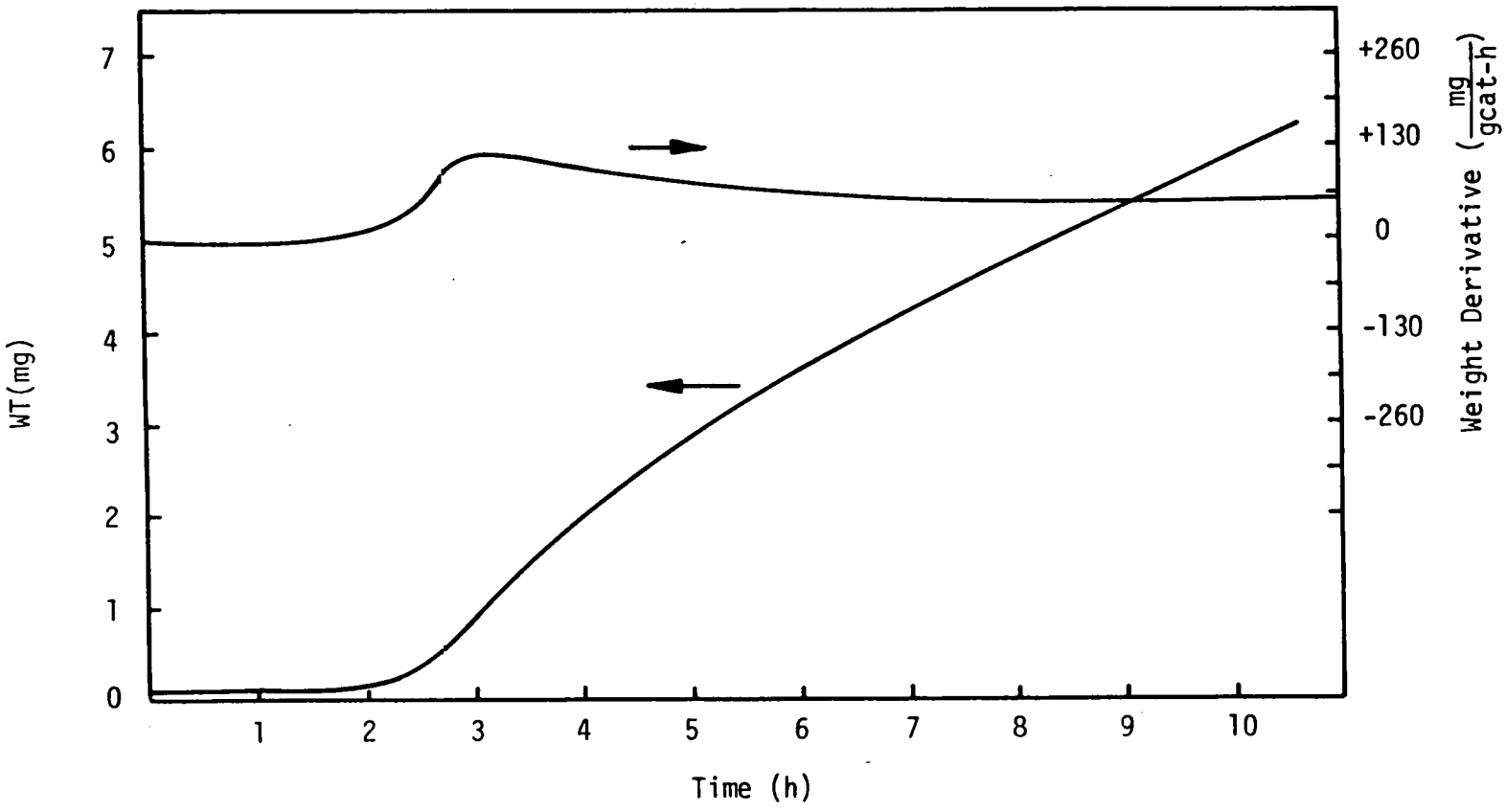

Fig. B-5. Weight and weight derivative as a function of time during the Boudouard reaction at 648 K (P_{CO} = 9.0 kPa and P_{N_2} = 80.6 kPa).

carbon on Ni at low coverages is apparently significantly greater than that of filamentous carbon formed in relatively massive quantities.

A mechanism for carbon formation on Ni consistent with these previous studies is shown in Figure B-2. The rate-determining step at low coverages is presumably the dissociation of CO. The atomic carbon thus formed is transformed to a polymeric form C_β, according to kinetics reported by McCarty and Wise (8). The proposed mechanism by which the filaments of C_β are formed has been discussed in great detail by Trimm (6) and by Baker and Harris (7). Briefly, it entails (a) the dissolution of adsorbed carbon atoms in the metal crystallite, (b) diffusion through the metal, and (c) precipitation of carbon atoms at the rear of the metal particle to form a polymeric carbon filament. Thus, the metal particle is lifted off the support and is moved outward on top of the growing filament. This process continues until the metal particle becomes encapsulated with inactive carbon. The observed induction period for filamentous carbon formation is explained by this mechanism; that is, a certain induction period is required for dissolution, precipitation, and separation of the metal crystallite from the support.

The nature of the driving force and the rate-determining step for the formation of carbon filaments are matters of some controversy. Rostrup-Nielsen and Trimm (5) suggest that the driving force is a concentration gradient of carbon (atoms presumably) across the metal particle, the activity of carbon being lower at the growing filament/metal interface. Harris and Baker (7), on the other hand, argue that the reaction is driven by the temperature gradient due to the exothermicity of CO dissociation. The advantages and disadvantages of both mechanisms have been discussed at some length (5, 67). Since some hydrocarbon decomposition reactions are endothermic, the actual process may require a combination of concentration and temperature driving forces.

The rate-determining step in formation of filaments is believed to be the diffusion of carbon through the metal, since the sum of the activation

energy for diffusion of carbon through Ni (43) of 84 kJ/mole, plus the heat of solution of carbon in Ni (44) of about 42 kJ/mole, is near the observed activation energy for carbon formation of 130 kJ/mole. An alternative mechanism is surface migration of adsorbed carbon atoms or CO molecules to carbon filament/metal interface (5, 45). However, since data from Massaro and Peterson (43) indicate that surface diffusion on a Ni foil is negligibly small in the temperature range of 350-700°C, the concept of surface diffusion of carbon itself may not be reasonable. Experimental evidence for a metal carbide intermediate (6, 7, 27) in carbon formation supports the bulk migration model.

2. Decomposition of Hydrocarbons.

Trimm (6) and Baker and Harris (7) have reviewed in some detail previous studies of the kinetics and mechanisms of carbon formation from decomposition of various hydrocarbons on Co (46), Fe (46), and Ni (6, 46-51). Generally, rates of formation of carbon decrease in the following order: acetylenes, olefins, paraffins (6, 51). For example, Rostrup-Nielsen (49) shows that during steam reforming at 500°C ($H_2O/C = 2$), the coking rate for ethylene on $Ni/MgO \cdot Al_2O_3$ is a factor of 10^4 greater than that for n-butane and 200 times greater than that for n-heptane. Rates of carbon formation from benzene and toluene are orders of magnitude greater than that from CO (6).

Kinetic data for carbon formation on Ni catalysts in the temperature range of 350-600°C are summarized in Table B-2. Reaction orders are generally zero for both hydrocarbons and H_2, although the order for hydrocarbons may increase to 1-2 at temperatures above 650°C (6). Activation energies for acetylene and olefin decomposition on Ni range from 125 to 139 kJ/mole. Since these values of E_{act} are so very near those observed for CO disproportionation, the same mechanism (formation of filamentous carbon) and rate-determining step (i.e., diffusion of carbon through the metal) are believed to operate (5-7). Indeed, the filamentous carbons formed by decomposition of these unsaturated hydrocarbons are very similar in structure to those observed in CO disproportionation (5-7, 27, 29, 52). For

TABLE B-2

Kinetic Parameters for Steady-State Carbon Formation on Nickel-Containing Catalysts[a]

Hydrocarbon gas	Catalyst	T, °C	Reaction orders RH	Reaction orders H_2	E_{act}, kJ/mole	Ref.
C_2H_2, C_2-C_4 olefins	Ni	375-525	0	0	138±17	46-47
C_2H_2	Ni	--	--	--	145	48
C_3H_6	Ni foil	375-525	0	0	138±4	50
	Ni/Al_2O_3	350-450	0	0	125±8	
	Ni/kieselguhr	350-450	0	0	125±8	
C_2H_6	Ni/Al_2O_3	350-475	≠0	≠0	199	6
C_6H_{14}	Ni/Al_2O_3	350-525	--	--	139	6
Benzene	Ni/Al_2O_3	475-600	-0.36	-0.9	201	6
Toluene	Ni/Al_2O_3	475-600	0	0	151	6
n-Heptane	$Ni/MgO{\cdot}Al_2O_3$	450-550	0	0	167	49[b]

[a] In most of these experiments, sufficient H_2 was present to prevent encapsulation.

[b] Under conditions representative of steam reforming with H_2O = 2.0; not really comparable with the other data because it includes the gasification process.

decomposition of paraffins and light aromatics on metals, the overall rate of carbon formation is slower (than for acetylenes and olefins) and is controlled by the rate of surface reaction (6); activation energies are also larger (see Table B-2).

Although catalytic decomposition of methane to form filamentary carbon has been reported (25, 29, 53, 54b), Baker et al. report that their attempts to produce it from very pure methane failed (7, 55). Baker and Harris (7) suggest that hydrocarbon impurities and/or the production of unsaturated hydrocarbon products over a long test period may account for the previous observations of carbon filaments from methane. They argue that since methane decomposition is endothermic, there is no temperature driving force to sustain its decomposition, unless oxygen or other hydrocarbons are present. If methane does not form carbon, then the carbon formed in steam reforming of methane must originate from decomposition of CO formed by the reverse methanation reaction (Equation B-1).

Beside the formation of filamentous carbon and very similar activation energies, there are several other chacteristics of the kinetics of carbon formation from hydrocarbons which appear to be general features. One of these is the form of the weight-versus-time curve illustrated in Figure B-5; this curve is for CO disproportionation, but it is also applicable to hydrocarbon decomposition, with perhaps one slight modification. After steady state is reached, the rate of carbon formation may, after a period of time, drop off because of widespread crystallite encapsulation, lending an S shape to the curve. This behavior, however, is usually not observed if a small amount of either H_2 or H_2O is present.

A second feature common to carbon formation from hydrocarbons is the form of the Arrhenius plot over a wide range of temperature, illustrated by the data for 1-butene on Ni in Figure B-6. At relatively low temperatures (400-550^{o}C) typical Arrhenius behavior is observed, with activation energies ranging from 100 to 200 kJ/mole (see Table B-2). However, at moderate temperatures (550-650^{o}C), negative temperature coefficients are observed, and finally at high temperatures (above 650^{o}C) positive

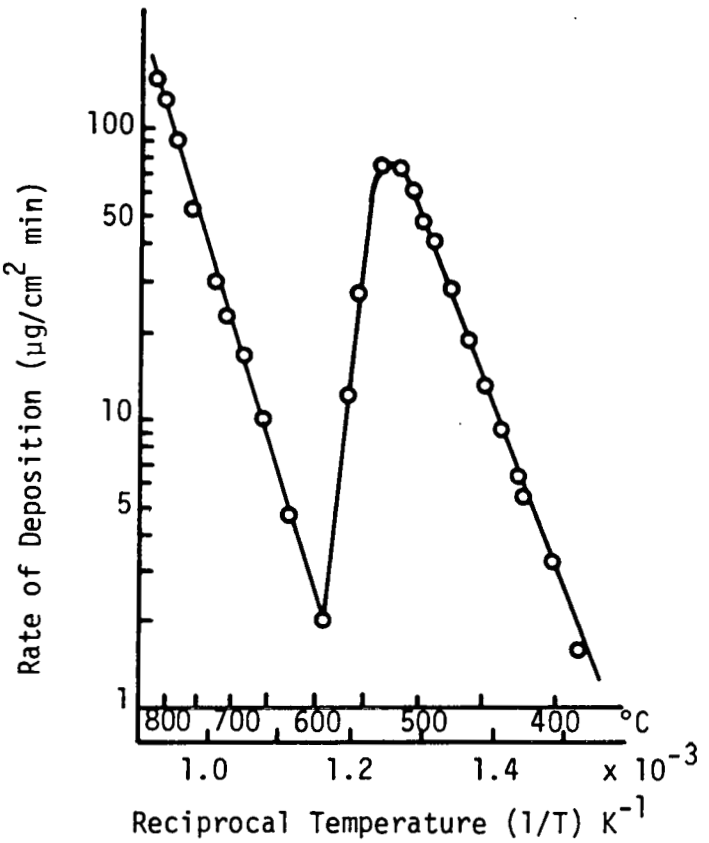

Fig. B-6. The temperature dependence of carbon deposition on Ni foil. Butene-1 = 100 Torr; H_2 = 25 Torr (Ref. 51).

temperature coefficients are once more observed (presumably because of the onset of cracking on the support and in the gas phase). The possible basis for the negative activation energy at moderate temperatures has been discussed in some detail by Rostrup-Nielsen and Trimm. They believe it is best explained by adsorption effects, i.e., a decline in surface concentration of reactants with increasing temperature. Although these authors discount other possibilities, most notably gasification of the adsorbed carbon by H_2 or H_2O, or self-poisoning by a film of graphite (54a) or polymer (56, 57), these are nevertheless also plausible explanations. It is obvious that more careful research is needed to settle this controversy.

However, a more urgent need is the study of complex precursors from decomposition of hydrocarbons which lead to coke and carbon formation. Because only a few previous studies (7, 58-61) have been made, this seems to be another area for further research.

3. Effects of Hydrogen and Water

The presence of either H_2 or H_2O can very substantially reduce or eliminate altogether the formation of carbon or coke deposits in either methanation or steam reforming. The mechanism by which this occurs is simple. Adsorbed H_2 or H_2O react with, and thus remove, atomic carbon and/or coke precursors formed by dissociation of CO or decomposition of hydrocarbons to form CH_4, CO, and H_2 (8, 40, 41, 49). If sufficient H_2 or H_2O is present, the surface residence time of active carbon forms and coke precursors will be short. Thus, there is little transformation of these species to more inactive forms according to the schemes in Figures B-1 and B-2, and the formation of condensed hydrocarbons and amorphous and graphitic carbons is minimized. This is well illustrated by data from the studies of Gardner and Bartholomew (40, 41) of carbon deposition during methanation and from the investigation of Rostrup-Nielsen (49) of coking under steam-reforming conditions.

Gardner and Bartholomew (40, 41) found that massive formation of filamentous carbon did not occur over a period of 24 hours on a 14% Ni/Al_2O_3 catalyst tested at temperatures from 350 to 450°C (1 atm) in a carefully purified mixture of N_2-diluted H_2 and CO (the H_2/CO ratio was varied from 0.5 to 3.0). However, if the H_2/CO ratio was lowered to less than 0.25, massive formation of carbon occurred within a few minutes; moreover, once initiated, the deposition continued at relatively high rates, even at H_2/CO ratios ranging up to 4.0. Nevertheless, the overall rate of carbon formation (after initiation) at 400°C, $H_2/CO = 3$, was a factor of 20 lower than that under equivalent conditions in the absence of H_2, indicating substantial gasification of carbon intermediates even after the deposition had begun (see Figure B-7). More important, however, these results demonstrate that, if sufficient H_2 is present initially (and other gaseous impurities are absent), carbon deposition does not occur, even over a long period of time and over a wide range of process conditions.

Rostrup-Nielsen (49) reported similar observations in regard to coking under steam-reforming conditions of 500°C, 1 atm, and $H_2O/C = 1.3$ to 2.0. For example, he noted that the residence time of coke precursors is greater and that coking rates are much larger in the absence of steam. His results suggest that the best steam-reforming catalysts are active for adsorption of both hydrocarbons and steam, i.e., achieve an even balance between rates of formation of coke precursors and gasification by adsorbed water. Catalysts with enhanced ability to adsorb steam delay the formation of coke and also lower the rate of formation once it is initiated.

Both studies demonstrate the importance of investigating carbon-deposition kinetics under reaction conditions in the presence of H_2 and H_2O. Previous investigations in which the formation of carbon and coke and their gasification were carried out separately have little general application to real reaction systems entailing both reactions, because

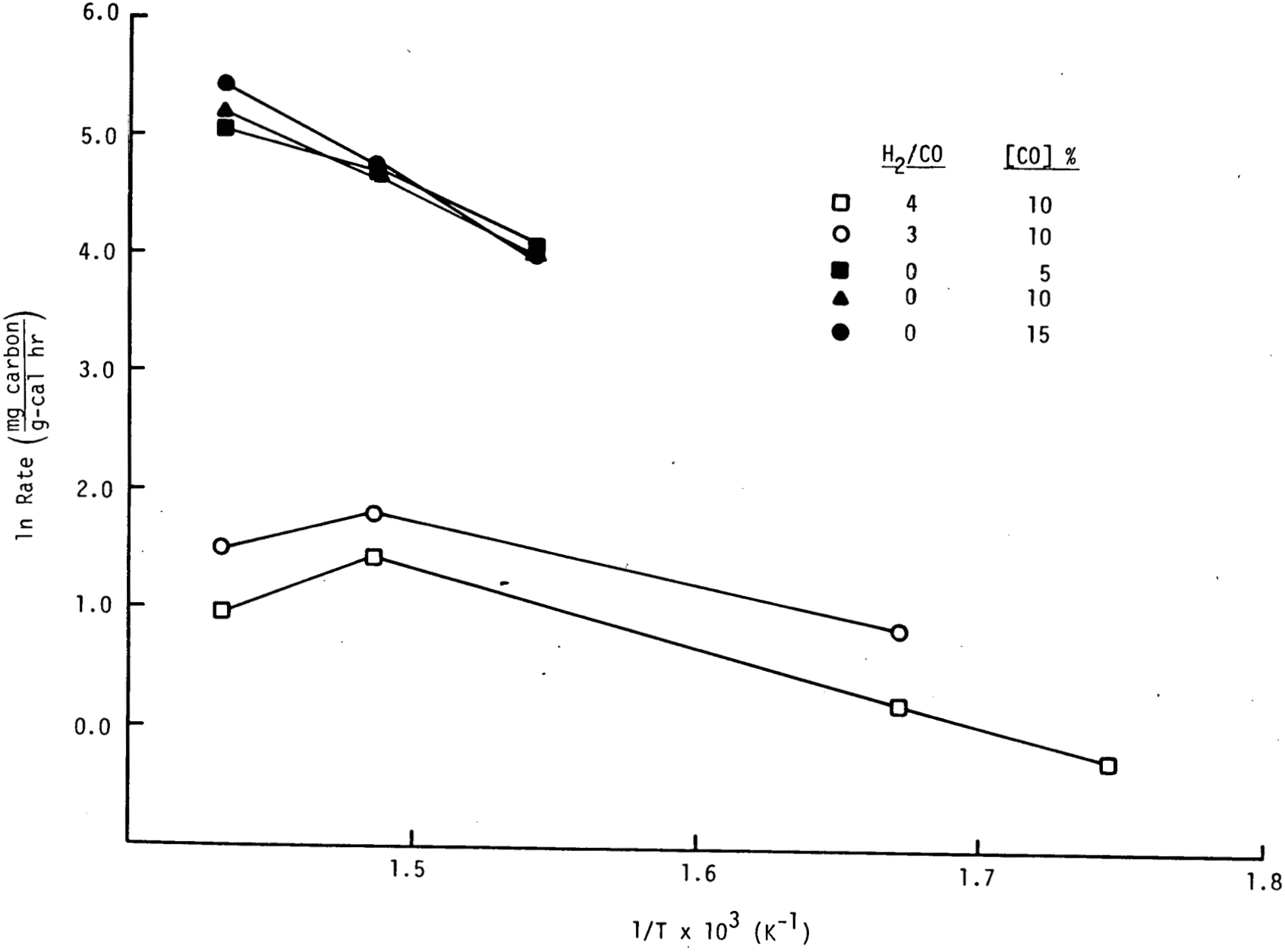

Fig. B-7. Rates of carbon formation from CO in the absence and presence of H_2 (Refs. 40, 41).

the carbonaceous deposits are transformed to unreactive and unrepresentative carbon deposits. An important exception to this was the temperature-programmed reaction study of McCarty and Wise (8), in which representative carbon forms were carefully deposited at low coverages and then quantitatively hydrogenated. The need for additional quantitative studies of the formation and gasification of carbon and coke precursors and of carbon formation under reaction conditions cannot be overemphasized.

4. Effects of Promoters and Poisons

Promoters that enhance the adsorption of H_2 or H_2O and/or the rate of gasification of carbon or coke by H_2 or H_2O should, in principle, minimize the deposition of carbon. Gardner and Bartholomew (40, 41) found that the rate of carbon deposition on Ni/Al_2O_3 in methanation was increased by addition of Mo and decreased by addition of Pt (see Table B-3). Rostrup-Nielsen (49) observed that formation of coke in steam reforming was delayed and occurred at lower rates on Ni catalysts promoted with alkali or supported on MgO. This effect was attributed to enhanced steam adsorption and more efficient gasification in the presence of these promoters. The better selectivity of urania-promoted catalysts has also been related to the ability of urania to enhance steam adsorption and gasification (62). Catalysts containing Ni-Cu, Co, and Pt produced no coke but also demonstrated negligible activity in ethane reforming, presumably because they did not dissociatively adsorb hydrocarbons (49). Ru and Rh catalysts, however, showed very high reforming activity, while producing no coke. This was attributed to reduced mobility and/or solubility of carbon in the metal which retards nucleation.

Two poisons, S and $Fe(CO)_5$, are known to affect the deposition of carbon in methanation and steam reforming, although the precise nature of their influence is not clear from the somewhat scarce, contradictory literature on this subject.

TABLE B-3

Turnover Numbers for Carbon Formation of Alumina-Supported Ni and Ni Bimetallics during Methanation (P_T = 1 atm, P_{CO} = 0.09 atm, H_2/CO = 3).

Catalyst, wt%	Average metal crystallite diameter, nm	N_C (s^{-1}) x 10^3 350°C	425°C
3% Ni/Al_2O_3	4.4	0.32	2.9
14% Ni	6.2	0.37	0.9
15.7% Ni/0.5% Pt	12	0.18	1.9
2.5% Ni/3% MoO_3	9.2	2.7	19

Kelley et al. (21) observed deactivation of a Ni(100) crystal for methanation by ppm quantities of $Fe(CO)_5$ that deposited Fe on the surface, and by diffusion of S from the bulk Ni. In both cases, the deactivated surface was covered with a "graphitic" carbon after the reaction. Gardner and Bartholomew (40, 41) found that by carefully purifying the gases of $Fe(CO)_5$ and S compounds, carbon formation on Ni/Al_2O_3 could be avoided over a wide range of methanation conditions. Two recent papers (63, 64) indicate that S enhances the transformation of C_α to C_β on Ni/Al_2O_3, either by catalyzing the α to β transition (63) or by preventing the dissociative adsorption of H_2, thereby poisoning hydrogenation of C_α (64) and causing it to build up and polymerize. Thus S does not completely prevent dissociative adsorption of CO in Ni but rather changes the selectivity in methanation to hydrogen-poor products that coke and carbon the surface.

In apparent contradiction to the results obtained under methanation conditions, Rostrup-Nielsen (49) reported that carbon formation did not occur on a S-poisoned $Ni/Al_2O_3 \cdot MgO$ catalyst under steam-reforming conditions. This, he explained, was because of a blockage of the Ni surface. A possible explanation for this apparent contradicition is that, whereas dissociate adsorption of CO can take place on a S-poisoned Ni surface, dissociative adsorption of hydrocarbons is not possible. Additional research on how S affects the adsorption of hydrocarbons and deposition of carbon should be encouraged.

5. Effects of Surface Structure, Particle Size, and Support

Effects of surface structure (6, 22, 23, 30, 65-68) and metal crystallite size (7, 25, 40, 41, 69) on the rate of carbon formation have been observed in several previous studies. Coke formation occurs at different rates on different metal crystal faces (67, 68), the order of activity depending on the extent of deposition (6). Formation of filamentous carbon is apparently favored on the (111) steps and on the (111) face of Ni (22, 23), and in general on rough surfaces (66),

and it is less favored on single crystals containing no grain boundaries (66). Induction periods are shorter for supported catalysts relative to foils, suggesting that nickel particles must be separated from the foils for measurable rates of carbon formation to occur. According to these data, the formation of carbon should be favored on small particles having a higher frequency of rough planes, and indeed that is the case (25, 69). Data in Table B-3 (40, 41) show that the carbon deposition rate during methanation is greater on smaller particles of Ni on Al_2O_3. Admittedly this could be either a particle-size effect or a support (metal-loading) effect.

The influence of metal-support interactions on the rate of carbon formation has received very little attention. Figueiredo and Trimm (50b) found that Al_2O_3 and kieselguhr supports had little effect on the rate of carbon deposition from propylene (see Table B-2), except that hydrogen changed the kinetics for the unsupported Ni but had no effect on the supported catalysts. In comparing the formation of carbon on Ni/Al_2O_3 and Ni/TiO_2, Bartholomew, et al. (70) found that the rate of carbon formation from CO on Ni/TiO_2 was negligible under conditions for which the rate was very significant on Ni/Al_2O_3. Moreover, very little filamentous carbon was observed in electron micrographs of Ni/TiO_2, whereas copious amounts were observed in the micrographs for Ni/Al_2O_3. This result suggests that strong metal-support interactions may significantly lower the rate of carbon formation. In view of the potential importance of these results, further research into metal-support interactions should have a high priority. Since carbon deposition often results in a transfer of Ni particles from a ceramic to a carbon support, the study of the properties of Ni supported on high-surface-area filamentous carbon should also be of great interest.

III. DEACTIVATION BY CARBON DEPOSITS

At the beginning of this section we mentioned three ways in which carbon deactivates catalysts. The extent and nature of deactivation by one or a combination of these modes depends on reaction conditions; temperature and H_2/CO or H_2O/C ratios are apparently the most critical factors. For example, in steam reforming there is a critical H_2O/C ratio (for a given temperature and hydrocarbon feed), above which coking does not occur (71). At low temperatures (<375°C) condensed polymers, and at high temperatures (>650°C), graphitic carbon encapsulate the metal surface (26, 72). However, in the temperature range of 375-650°C, encapsulation of the metal does not occur; thus, filamentous carbon formed in steam reforming at these temperatures does not cause a loss of intrinsic catalyst activity (26, 49, 71, 72). In fact, it may result in increased specific activity because of a redispersion of the Ni on the carbon support (26, 72).

Nevertheless, formation of copious amounts of filamentous carbon can bring about other forms of deactivation, namely plugging of catalyst pores and reactor voids (49, 71) and destruction of catalyst pellets (49, 71, 73). Rostrup-Nielsen concluded that pore mouth poisoning by carbon was responsible for decreased activity of reforming catalysts tested in a pilot plant (49). If sufficient carbon is allowed to accumulate in the pores, the strong carbon filaments can actually break up catalyst pellets into a fine powder (49, 71, 73). Carbon and catalyst powders can thereby plug the voids and cause channeling, decreased conversion, and ultimately plugging of the reformer tubes (49).

One other possible mode of deactivation should be mentioned—namely formation of metal carbides having lower activities than the metals. The importance of such carbides is still open to question. Coad and Riviere (11) reported that bulk metal carbides are unstable above 300°C, but Lobo (46) and Moayeri and Trimm (72) have identified their presence

in catalysts exposed to coking environments. Whether metal carbides are involved in filament growth, or are formed during cooling or when filament growth has ceased, is also open to question (7). The role of metal carbides is clearly an area needing further investigation.

Although a number of empirical power-law models including the Voorhies Correlation (74) have been developed for coking on cracking catalysts, these models are not applicable to carbon deposition on the supported metal catalysts used in methanation and steam reforming (49). There are two fundamental differences between the two kinds of catalysts which explain this: (1) the mechanism of carbon formation on metals involving a linear weight increase with time (see Figure B-5) is different from that on acid supports, and (2) the various types of carbon formed on metals may or may not lower intrinsic activity (e.g., in steam reforming, amorphous filaments do not, and graphite films do).

Even so, since carbon filaments plug and break up the catalysts, their formation is undesirable. A relatively simple model of carbon filament formation would involve two kinetic parameters from gravimetric measurements under reaction conditions over a range of temperatures (e.g., 500-600^{o}C) and reactant partial pressures: (1) induction time and (2) the zero-order rate constant (49). In addition, if the results were to be accurate, the effects of heat and mass transport would need to be inputted to a two-dimensional model, such as that developed by Rostrup-Nielsen (71) for steam reforming.

Deactivation by graphite films at temperatures above 650^{o}C might be modelled with a general power-law rate expression according to Levenspiel (75), although the intrusion of cracking reactions in the gas phase and on the support at very high temperatures adds considerable complexity.

The need for realistic, accurate models of metal catalyst deactivation by carbon is apparent.

IV. REGENERATION OF CATALYSTS

In spite of its obvious importance, regeneration of coked catalysts has received relatively minor scientific attention. Future requirements for processing heavy fuels will undoubtedly stimulate more activity in this area. Nevertheless, carbon deposition, like sulfur poisoning, is more easily prevented than cured, because the "cure" entails process interruptions and possible damage to the catalyst. Thus, it is preferable if steam-reforming catalysts can be developed which interfere with the deposition of carbon by promoting the immediate removal of coke precursors via gasification. Once coked, however, the alternatives for removing the carbon are twofold: (1) gasification with H_2 or H_2O or (2) controlled oxidation with oxygen or oxygen-containing compounds.

Removal of coke by H_2 of H_2O has been reviewed in some detail by Trimm (6). Gasification by steam of coke (presumably C_β) deposited by pyrolysis of hydrocarbons on Ni occurs at significant rates between 500 and 700°C, once the encapsulating material has been removed. The rates are comparable with those of the diffusion of carbon through Ni, which suggests that the backdiffusion of carbon is rate-determining. In accordance with earlier discussion, gasification rates are enhanced by alkali and other oxide promoters. That the rate of carbon gasification by steam also depends on the reactivity of carbon is confirmed by Rostrup-Nielsen (49). He observed that freshly formed fibrous carbon was easily removed by a large excess of steam (presumably at 500°C), but a flake-like coke produced in reforming over a few hundred hours was not so removed. However, a few percent air added to the steam above 450°C caused complete decoking of all samples.

Gasification of amorphous carbon by H_2 is slower than with steam (6). The rate-determining step appears to be a surface reaction of carbon and hydrogen atoms, rather than diffusion of carbon through Ni (6, 76).

The rate of gasification apparently increases with increasing temperature up to about 700°C, above which the rate decreases with increasing temperature. Nashiyama and Tamai (77) have suggested that the negative activation energy results from the approach of the reaction to equilibrium, although the suggestion by Rewick et al. (78) of a thermal restructuring of carbon to a less active form is equally reasonable.

The removal of coke from nickel with CO_2 at 625°C has also been reported (6, 79). As with H_2, it also apparently entails dissociative adsorption and a surface reaction with carbon.

Moeller and Bartholomew (80) recently studied the oxygen regeneration of nickel methanation catalysts deactivated under carbon-forming reaction conditions at 450°C. A mild treatment in O_2 at 300°C over a period of 15-30 minutes restored complete activity. However, chemical analysis showed a 7% loss of nickel following the regeneration treatment, which suggests that some of the nickel crystallites were lost from the catalyst as the carbon was burned off. If in fact Ni is lost, the outlook for repeated regeneration in O_2 is poor.

Although the above-mentioned studies establish that carbon removal by O_2, H_2O, H_2, and CO_2 is possible, the effects of these exothermic or high-temperature treatments on a metal surface area were, with only one exception, not determined. The need for additional careful study of the effects of these treatments on metal and support surface areas and metal content is clear.

V. EXPERIMENTAL CONSIDERATIONS

Much of the previous carbon deposition work may be subject to question because (a) the gases were not carefully purified of iron carbonyl, sulfur compounds, and organic impurities, all of which affect the rate of carbon formation; (b) conditions were poorly chosen in the case of mechanistic or deposition studies (i.e., they included heat/mass-transport limitations or conditions not representative of the process of interest); and/or (c) catalyst or surface properties (e.g., surface area and composition) were not carefully characterized before and after formation of carbon. For example, in their study of hexane steam reforming Bett et al. (81) attempted to identify the precursor to carbon formation by means of gas-phase analysis of products in an integral reactor operating over the range of 500-750°C, to which was fed laboratory-grade hexane (no further purification). The ethylene observed in the product, which they hypothesized to be a carbon precursor, may have been formed by gas-phase cracking at 750°C. Moreover, the carbon formed may have been due to olefin impurities in the hexane feed. Fortunately, these workers did examine the filamentous carbon formed by electron microscopy.

Electron microscopy, AES, LEED, and temperature-programmed reaction spectroscopy have proven themselves as very useful techniques for investigating the structure and reactivity of carbons on metals (6-8, 13, 15-18, 21). Gravimetric analysis (5-7, 40, 41, 49) is invaluable in the investigation of carbon deposition and gasification rates, as is the more specialized but very powerful technique of controlled-atmosphere electron microscopy (7).

Promising techniques for investigating coke precursors and characterizing surface carbons include high-resolution energy loss, infrared, and Raman spectroscopy; for the investigation of catalytic phases (e.g., carbides, small particles) controlled-atmosphere Moessbauer spectroscopy and EXAFS are recommended. The use of single-pellet (82),

mixed-flow, recirculation, and single-pass differential reactors, coupled with careful gas-phase analysis, should facilitate the identification of coke and carbon precursors. Again, as mentioned in connection with sulfur poisoning, the careful choice of well-defined catalyst systems and surfaces is critically important.

VI CONCLUSIONS AND RECOMMENDATIONS

A. Conclusions

1. Carbons and cokes vary in their structure and reactivity. Atomic carbon (C_α) formed by dissociative adsorption of CO and hydrocarbons is transformed to low-density filaments (C_β) and to graphitic carbon (C_c) at progressively higher temperatures.

2. Filamentous carbon is formed in steam reforming by the decomposition of both CO and hydrocarbons. Apparently, the rate-determining step is the diffusion of atomic carbon through the metal crystallite to the back side, where it precipitates to form C_β filaments.

3. The presence of H_2 and/or H_2O is desirable in preventing carbon formation. Alkali, oxide promoters, and noble metals lower the deposition rate by enhancing adsorption of water, increasing the rate of gasification by H_2, or lowering the solubility of carbon in the metal.

4. Carbon deposition is sensitive to surface structure, occurring at faster rates on small particles. Strong metal-support interactions may decrease carbon formation.

5. Removal of coke and carbon with steam and oxygen appears to be practical; however, the effects on surface area and catalyst life are unknown.

B. Recommendations for Further Work

Several fundamental questions were presented at the beginning of this section which we have attempted to address throughout this discussion of previous work. We attempted to identify specific needs; also additional questions were raised. For example, what are the precursors

in coke formation? Can strong metal-support interactions reduce carbon formation on nickel while maintaining high activity for steam reforming? Some of the most promising areas for future work are in the study of deposition and gasification rates, noble-metal-promoted nickel catalysts for steam reforming, and the structures and reactivities of polymeric substances formed in coking during reaction. We also agree with Baker (6) that additional research is needed to understand the region of negative temperature coefficients and to determine the stoichiometry of hydrocarbon decomposition reactions through analysis of gas-phase products.

REFERENCES

1. Hofer, L.J.E., in Catalysis, Vol. 4 (P.H. Emmett, ed.), Reinhold Publishing Co., New York, 1956, p. 373.

2. Donald, H.J., An Annotated Bibliography, Mellon Inst. Res., 1956.

3. Palmer, H.B., and Cullis, C.F., in Chemistry and Physics of Carbon, Vol. 1 (P.L. Walker, Jr., ed.), Marcel Dekker, Inc., N.Y., 1965, p. 265.

4. Whalen, M.J., "Carbon Formation in Methanators," Final Report to ERDA, FE-2240-10, July 1976.

5. Rostrup-Nielsen, J., and Trimm, D.L., J. Catal. 48, 155 (1977).

6. Trimm, D.L., Catal. Rev.-Sci. Eng., 16, 155 (1977).

7. Baker, R.T.K., and Harris, P.S., in Chemistry and Physics of Carbon, Vol. 14 (P.L. Walker, Jr., ed.), Marcel Dekker, Inc., N.Y., 1979, p. 83.

8. McCarty, J.G., and Wise, H., J. Catal. 57, 406 (1979).

9. Ertl, G., in "Molecular Process on Solid Surfaces" (E. Drauglis, R.D. Cretz, and R.I. Jaffee, Eds.), pp. 155-157, McGraw-Hill, N.Y., 1969.

10. Pitkethly, R.C., in "Chemisorption and Catalysis," pp. 107-113. Inst. Petroleum, London, 1970.

11. Coad, J.P., and Riviere, J.C., Surf. Sci. 25, 609 (1971).

12. Dalmai-Imelik, G., Bertolini, J.C., and Rousseau, J., Surf. Sci. 27, 379 (1971).

13a. McCarty, J., and Madix, R.J., J. Catal. 38, 402 (1975).

b. McCarty, J.G., and Madix, R.J., J. Catal. 48, 422 (1977).

14. Zuhr, R.A., and Hudson, J.B., J. Vac. Sci. Tech. 14, 431 (1977).

15. Blakely, J.M., Kim, J.S., and Potter, H.C., J. Appl. Phys. 41, 2693 (1970).

16. Shelton, J.C., Patil, H.R., and Blakely, J.M., Surf. Sci. 43, 493 (1974).

17a. Isett, L.C., and Blakely, J.M., J. Vac. Sci. Technol., 12, 237 (1975).

b. Isett, L.C., and Blakely, J.M., Surf. Sci. 47, 645 (1975).

c. Isett, L.C., and Blakely, J.M., Surf. Sci. 58, 397 (1976).

18. Thapliyal, H.V., and Blakely, J.M., J. Vac. Sci. Technol. 15, 600 (1978).

19. Zuhr, R.A., and Hudson, J.B., Surf. Sci. 66, 405 (1977).

20. Demuth, J.E., Chem. Phys. Lett. 45, 12 (1977).

21. Kelley, R.D., Goodman, D.W., Madey, T.E., and Yates, J.T., Jr., Presentation at the Conference on Catalyst Deactivation and Poisoning, May 24-26, 1978, Berkeley, CA.

22. Leidheiser, H., and Gwathmey, A.T., J. Amer. Chem. Soc. 70, 1206 (1948).

23. Kehrer, V.J., and Leidheiser, H., Jr., J. Phys. Chem. 58, 550, 1954.

24. Hofer, L.J.E., Sterling, E., and McCartney, J.T., J. Phys. Chem. 59, 1153, 1955.

25. Rostrup-Nielsen, J.R., J. Catal. 27, 343 (1972).

26. Trimm, D.L., Inst. Chem. Eng. 54, 119 (1976).

27. Renshaw, G.D., Roscoe, C., and Walker, P.L., J. Catal., 22, 394 (1971).

28. Baker, R.T.K., Barber, M.A., Harris, P.S., Feates, F.S., and Waite, R.J., J. Catal. 26, 51 (1972).

29. Baird, J., Fryer, J.B., and Grant, B., Nature 233, 329 (1971).

30. Grenga, H.E., and Lawless, K.R., J. Appl. Phys. 43, 1508 (1972).

31. Dent, F.J., Moignard, L.A., Eastwood, A.H., Blackburn, W.H. and Hebden, D., Trans. Inst. Gas Eng., 1945-1946, p. 602.

32. White, GA., Roszkowski, T.R., and Stanbridge, D.W., Hydrocarbon Proc., July 1975, p. 130.

33. Joint Army-Navy-Air Force Thermochemical Table, 2nd Ed., June 1971.

34. Hamilton, J.C., and Blakely, J.M., J. Vac. Sci. Technol. 15, 559 (1978).

35. Blakely, J.M., Presentation at the Conference on Catalyst Deactivation and Poisoning, May 24-26, 1978, Berkeley, CA.

36. Walker, P.L., Jr. and Thomas, J.M., Carbon 8, 103 (1970).

37. Baukloh, W., Chatterjee, B., and Das, P.P., Trans. Indian Inst.

Metals 4, 271 (1950).

38. Renshaw, G.D., Roscoe, C., and Walker, P.L., Jr., J. Catal. 18, 164 (1970).

39. Tøttrup, P.B., J. Catal. 42, 29 (1976).

40. Gardner, D.C., and Bartholomew, C.H., Publication in preparation, 1979.

41. Gardner, D.C., Master's Thesis, Brigham Young University, 1979.

42. Goodman, D.W., Kelley, R.D., Madey, T.E., and White, J.M., Paper in Preparation, 1979.

43. Massaro, T.A., and Peterson, E.E., J. Appl. Phys. 42, 5534 (1971).

44. Wada, T., Wada, H., Elliott, J.F., and Chipman, J., Metal Trans. 4, 2199 (1971).

45. Baird, T., Fryer, J.R., and Grant, G., Carbon 12, 591 (1974).

46. Lobo, L.S., Ph.D. Dissertation, University of London (1971).

47. Lobo, L.S., and Trimm, D.L., Nature 234, 15 (1971).

48. Tesner, P.A., Robinovich, E.Y., Rafalkes, I.S., and Arefieva, E.F., Carbon 8, 435 (1970).

49. Rostrup-Nielsen, J.R., J. Catal. 33, 184 (1974).

50a. Figueiredo, J.L., Ph.D. Dissertation, University of London, 1975.

b. Figueiredo, J.L., and Trimm, D.L., J. Appl. Chem. Biotechnol. 28, 611 (1978).

51. Lobo, L.S., Trimm, D.L., and Figueiredo, Proceedings of the Vth International Congress on Catalysis, 1972, 1125.

52a. Edmonds, T., and Pitkethly, R.C., Surf. Sci. 15, 137 (1969).

b. Edmonds, T., and Pitkethly, R.C., Surf. Sci. 17, 4509 (1969).

53. Evans, E.L., Thomas, J.M., Thrower, P.A., and Walker, P.L., Carbon 11, 441 (1973).

54a. Macek, J., Luka, S., and Malecha, J., Chim. Ind., Genie Chem. 150, 517 (1972).

b. Macek, J., Knizek, P., and Malecha, J., Carbon 16, 111 (1978).

55. Baker, R.T.K., Harris, P.S., Henderson, J., and Thomas, R.B., Carbon 13, 17 (1975).

56. Mosely, F., Stephens, R.W., Stewert, K.D., and Wood, J., J. Catal. 24, 18 (1972).

57. Bhatta, K.S.M., and Dixon, G.M., Trans. Faraday Soc. 63, 2217 (1967).

58. Harris, P.S., Baker, R.T.K., and Buch, R.A., Carbon 11, 531 (1973).

59. Sterligov, O.D., and Olfer'eva, R., Kinetics and Catalysis 8, 407 (1967).

60. Frennet, Cat. Rev.-Sci. Eng. 10, 37 (1974).

61. Wolf, E., and Peterson, E.E., Submitted to J. Catal., 1979.

62. Bhatta, K.S.M., and Dixon, G.M., Ind. Eng. Chem. Prod. Res. Develop. 8, 324 (1969).

63. Ablow, C.M., McCarty, J.G., Wentrcek, P.W., and Wise, H., paper submitted to J. Catal., 1979.

64. Bartholomew, C.H., and Gardner, D.C., Paper Presented at Advances in Catalysis I, Snowbird, UT, Oct. 3-5, 1979.

65. Beeck, O., Adv. Catal. 11, 151 (1949).

66. Bernardo, C., and Trimm, D.L., Carbon 14, 225 (1976).

67. Kahn, D.R., Peterson, E.E., and Somorjai, G.A., J. Catal. 34, 294 (1974).

68. Cunningham, R.E., and Gwathmey, A.T., Adv. Catal. 9, 25 (1957).

69. Baker, R.T.K., Harris, P.S., Thomas, R.B., and Waite, R.J., J. Catal. 30, 86 (1973).

70. Bartholomew, C.H., Gardner, D.C., and Mustard, D.G., Paper in Preparation, 1979.

71. Rostrup-Nielsen, J., Chem. Eng. Prog., Setp. 1977.

72. Moayeri, M., and Trimm, D.L., J. Appl. Chem. Biotechnol. 26, 419 (1976).

73. Kiovsky, J.R., Preprints of the ACS Division of Petr. Chem. 22 (4), 1300 (1977).

74. Voorhies, A., Jr., Ind. Eng. Chem. 37, 318 (1945).

75. Levenspiel, O., "Chemical Reaction Engineering," John Wiley & Sons, Inc., 1972.

76. Baker, R.T.K., Paper presented at Advances in Catalysis I, Snowbird, Utah, Oct. 3-5, 1979.

77. Nishiyama, Y., and Tamai, Y., Carbon 14, 13 (1976).

78. Rewick, R.T., Wentrcek, P.R., and Wise, H., Fuel 53, 274 (1974).

79. Bernardo, C., Ph.D. Dissertation, University of London, 1978.

80. Moeller, A.D., and Bartholomew, C.H., Preprints of the Amer. Chem. Soc. Fuels Chem. Div., Houston, March 23-28, 1980.

81. Bett, J.A.S., Christner, L.G., Hamilton, R.M., and Olson, A.J., Preprints Amer. Chem. Soc. Petr. Chem. Div., 22(4), 1290 (1977).

82. Hegedus, L.L., and Peterson, E.E., J. Catal. 28, 150 (1973).